Investigations Into Infrared-Selected Variable Stars

Author:
Calum MORRIS

Supervised by:
Prof. Philip W. Lucas
SECOND SUPERVISOR
Dr. Jan Forbrich

Centre for Astrophysics Research
Physics, Engineering and Computer Science
University of Hertfordshire

Submitted to the University of Hertfordshire in partial fulfilment of the requirements of the degree of Doctor of Philosophy.

July 2023

Abstract

The diversity seen in the infrared variable sky is vast, and understudied when compared to variability in the optical regime. Utilising near-infrared (NIR) colours and amplitudes can be a powerful tool in the classification of the various members of this population, made easier in combination with spectroscopy. Understanding the demographics of NIR variables is key when considering pre-main sequence stellar evolution, because high-amplitude variability in YSOs can trace eruptive behaviour, which in turn is crucial in understanding the 'protostellar luminosity spread problem'. Eruptive YSOs were traditionally thought to encompass two categories, FU Orionis (FUors) and EX Lupi (EXors), the former having higher amplitude bursts on the order of centuries, and the latter with smaller, possibly repeating events on time-frames between months and years. More recent work has established a much broader zoo of observable eruptive behaviours, which warrant further investigation. For example eruptive events lead to rapid increases in the temperature of the disk environment and thus drastically alter the chemical conditions within the disk, which would then impact planet formation (Cieza et al., 2016, see).

Using the widely spaced epochs of the UKIDSS Galactic Plane Survey (UGPS), in concert with the 2 Micron All-Sky Survey (2MASS), stellar variability can be detected on a variety of timescales. Probing the long term behaviour of these variables can be accomplished with the $\approx$20 epochs (covering 12 years at present) of MIR photometry from the WISE and NEOWISE missions, and thus can be used to identify candidate eruptive variable YSOs. In so doing both the rates of eruptive behaviour in class I and class II YSOs (younger and older systems respectively), and the overall demographics of variability in these systems can be inferred.

We used a combination of K-band spectroscopy and long-duration mid-infrared light curves to determine the classification of 29 'likely' YSOs (and 1 candidate AGB star). These were selected on the basis of confirmed large amplitude K-band variability in addition to a projected membership of a local star forming region. We find 2 stars display features consistent with a FUor classification, 1 to have an EXor like spectrum, likely associated with a long duration outburst, and 6 other young stars with emission spectra and large outbursts (and thus could be EXors in quiescence). In addition to these candidate eruptive variables (EVs), we also find 4 'dippers' with a range of variability timescales, from $<$1 year to $>$10 years. Finally we note that 4 stars are now of uncertain classification, after their spectra and near-infrared colours showed similarity to D-type symbiotic stars (albeit only two have clear 13CO absorption lines, which are associated with this class of evolved star). Following this we construct an expectation value for the prevalence of eruptive variables within a sample of YSOs, given previously observed high amplitude variability, finding a value of 14^{+7}_{-2}%. This compares to the $\approx$10% found for YSOs more generally (from a sample of known Spitzer colour selected YSOs - see below), and thus

demonstrates that known variable YSOs may be more likely to be eruptive. The value of eruptive candidates then rises if we include 6 further EXor candidates, which lack recent eruptions.

We then examine a less-biased sample, again using both UGPS photometry and NEOWISE time-domain light-curves to identify further EV candidates. This sample was constructed from the sample of Cygnus-X YSOs from Kryukova et al. (2014), and includes all stars in the the above catalogue that have a single UGPS detection and a NEOWISE or unWISE counterpart. The resulting analysis provided an expectation value for EVs of $10^{+2}_{-1}\%$, in line with previous predictions. Two unexpected results from this work were the lack of detection of the long duration 'dippers' (as mentioned earlier), and the discovery of 5 YSOs with high amplitude, long duration bursts (on the order of a decade).

Investigating some of the unclassified (or mis-classified) members of the Lucas et al. (2017) sample, led to the discovery of a new short-period intermediate polar (IP), of novel type. We utilised a thorough multi-wavelength observing strategy covering x-ray imaging, optical spectroscopy, and multi-colour optical photometric monitoring. This combined with existing archive data from IGAPS, PANNSTARRS and Gaia, led us to conclude that we had discovered a new IP with a NIR-bright SED, likely a result of a very complete disk, as can be interpreted from the H I line ratios.

Finally, three stars with NIR/WISE colours that were neither entirely YSO, nor AGB-like were analysed with a range of archival and VVV/X data, to place an estimate on their true classification. Three independent distance methods were trialled on one of these stars (GPSV3 from Contreras Peña et al. (2014a)), which allowed us to make the conclusion that the star is likely some form of O-rich AGB star in the galactic halo. The three distance measures trialled were as follows: Mira period-luminosity relation derived fluxes used in an empirical AGB flux-distance relation, NIR-fitted proper motion based kinematic distances, and spectroscopically confirmed radial velocity distances. Applying the same Ishihara et al. (2011a) empirical measurements to the other two stars (GPSV15 & GPSV34), gives a similar classification, which given the similarity of their light curves could be expected.

Declaration

I declare that no part of this work is being submitted concurrently for another award of the University or any other awarding body or institution. This thesis contains a substantial body of work that has not previously been submitted successfully for an award of the University or any other awarding body or institution.

The following parts of this submission have been published previously and/or undertaken as part of a previous degree or research programme:

1. In Charper 2 the Gemini/NIFS spectra were reduced by Carlos Contreras-Pena as part of their PhD Thesis. Further analysis is presented here through the inclusion of additional MIR light curves from the WISE mission.
2. Chapter 4.1 to 4.5: this has been published as Morris et al., 2022, *Monthly Notices of the Royal Astronomical Society*, **514**, 6002.

Except where indicated otherwise in the submission, the submission is my own work and has not previously been submitted successfully for any award.

Acknowledgements

I'd first like to extend my heartfelt thanks to my supervisor, Professor Philip Lucas, for guiding me through my studies. Both helping me to mature as a scientist, and for providing all the help, support and time I needed to complete not just the science we needed to do, but also the science that I wanted to do. I'm aware of how privileged of an opportunity that is at my career stage, and I will always appreciate it. I'd also like to thank my co-supervisor Dr Jan Forbrich, for always making time for me, no matter how busy you were with your own students, and for providing valuable insights for a number of my projects.

To Dr Zhen Guo I would like to express my deep gratitude, both as a mentor and close personal friend. Your presence during my studies has helped me to progress my science more than I can put into words. I'll always keep the memories of our observing runs, and our fun chats over dinner (and cocktails)!

To Ryan and Ben I need to say very little, you two are my best friends, and provided me with the happiness and the escapism I required, not just for our PhDs, but for a whole decade of laughs (and evenings with far too much alcohol)!

Then we come to my work family, the... denizens of that hive of scum and villainy, 2E50:

- To Marina: Thank you for being one of the kindest and most supportive friends that I could ever of had the pleasure of working with. I always appreciate you laughing at my terrible jokes, and generally putting up with all my nonsense! I'll be wishing you all the best for your career going forward, although I'm sure it'll be... unbe-WEAVE-able! Blagodarya ti Marina.

- To Matt: The most constant presence in my work day, thanks for friendship and chat, from the first day of my PhD, to the last. Thanks also for the repeated code, stats, and pool help, the first two will always be appreciated, the latter I'll probably forget, sorry coach!

- To Niall: Thanks for being a great research partner (or should I say, pardner'), and for using your skills to help make my work ten times easier, and probably Phil's for that matter! I'll be thankful for the laughs, music and chat, which if anyone asks, were *not* about dinosaurs, the ocean or Skyrim. It was about space, honest! I look forward to continuing our work over the coming years, provided PRIMVS doesn't become self aware and replace me...

- To Alex, Max & Thomas (aka Spriggs!): Thanks for helping me to feel so welcome when I started out, and for making our little office feel like the best place to work in the whole campus!

To my family, friends and colleagues:

- A massive thank you to my parents and my sister (and also Barney) for putting up with my continued insistence on being a student for as long as humanly possible. The support is immeasurable, even when what I do is ramble on about space while everyone else pretends to listen!
- I'd like to thank William Cooper for your continued friendship, and for being a fun and actually helpful version of stack exchange! Your help on my paper is greatly appreciated, and I apologise for introducing you to F1, right as it went downhill!
- To all of my friends that have stuck with me over the many years since we did our undergrads, I'd like to thank each and every one of you for being the best pals a lanky scientist could ask for!
- I'd like to thank the rest of my friends from the office: Tracey, Jaime, Kasia, Lizzie & all of the others that are too many to name here. Thanks for making the IC such a fun place to work!

To my collaborators, and to the various institutions, databases and funding agencies that made this work possible:

- I'd like to acknowledge the co-authors on my first paper: T. J. Maccarone, J. Strader, C. Britt, S. Swihart, & J. E. Drew.
- This work makes use of service mode data from the William Herschel Telescope: The WHT and its service programme are operated on the island of La Palma by the Isaac Newton Group of Telescopes in the Spanish Observatorio del Roque de los Muchachos of the Instituto de Astrofísica de Canarias.
- Use was also made of service mode on the Liverpool Telescope: The Liverpool Telescope is operated on the island of La Palma by Liverpool John Moores University in the Spanish Observatorio del Roque de los Muchachos of the Instituto de Astrofisica de Canarias with financial support from the UK Science and Technology Facilities Council.
- Elements of this work are based on observations obtained at the Southern Astrophysical Research (SOAR) telescope, which is a joint project of the Ministério da Ciência, Tecnologia e Inovações (MCTI/LNA) do Brasil, the US National Science Foundation's NOIRLab, the University of North Carolina at Chapel Hill (UNC), and Michigan State University (MSU).
- This research has made use of the SIMBAD database, operated at CDS, Strasbourg, France

- My work has been supported by STFC grant ST/S505419/1.

Contents

List of Figures

List of Tables

List of Abbreviations

AGB	**A**symptotic **G**iant **B**ranch
AML	**A**ngular **M**omentum **L**oss
CE	**C**ommon **E**nvelope
CTTS	**C**lassical **T** **T**auri **S**tar
CV	**C**ataclysmic **V**ariable
EV	**E**ruptive **V**ariable
EW	**E**quivalent **W**idths
EXor	**E** **X** Lupi-type star
FUor	**F** **U** Orionis-type star
IP	**I**ntermediate **P**olar
LTV	**L**ong **T**erm **V**ariable
mCV	**m**agnetic **C**ataclysmic **V**ariable
MIR	**M**id **I**nfra **R**ed
MNor	**M**cNeil's **N**ebula
MTV	**M**ultiple **T**imescale **V**ariable
NIR	**N**ear **I**nfra **R**ed
PDM	**P**hase to **D**ispersion **M**inimisation
PM	**P**roper **M**otion
PMS	**P**re **M**ain **S**equence
RV	**R**adial **V**elocity
SED	**S**pectral **E**nergy **D**istribution
SNR	**S**ignal to **N**oise **R**atio
STV	**S**hort **T**imescale **V**ariable
UV	**U**ltra **V**iolet
WD	**W**hite **D**warf

WTTS	**W**eak-line **T** **T**auri **S**tar
YSO	**Y**oung **S**tellar **O**bject

Telescopes & **Surveys**	
2MASS	**2** **M**icron **A**ll **S**ky **S**urvey
IPHAS	**I**NT **P**hotmetric **H** **A**lpha **S**urvey
LT	**L**iverpool **T**elescope
PanSTARRS	**P**anoramic **S**urvey **T**elescope and **R**apid **R**esponse **S**ystem
SOAR	**So**uthern **A**strophysical **R**esearch Telescope
UGPS	**U**KIDSS **G**alactic **P**lane **S**urvey
UKIDSS	**U**nited **K**ingdom **I**nfrared **D**eep **S**ky **S**urvey
UVEX	**U**ltra **V**iolet **Ex**cess Survey
UWISH2	**UKIRT** **W**ide-Field **I**nfrared **S**urvey for **H2**
VLASS	**V**ery **L**arge **A**rray **S**ky **S**urvey
VVV	**V**ista **V**ariables in the **V**ia Lactea
WHT	**W**illiam **H**erschel **T**elescope
WISE	**W**ide-Field **I**nfrared **S**urvey **E**xplorer
VPHAS	**V**ista **P**hotmetric **H** **A**lpha **S**urvey

Chapter 1

An Introduction to Variability in the Near-Infrared

1.1 Introduction

Stellar Variability has long since held the intrigue of astronomers, and the eclectic mix of observed behaviours provides a wealth of opportunity to study all aspects of stellar evolution. In the near-infrared wavelength range, much of the observed variability is driven by circumstellar material, either as discs or outflowing shells.

1.2 Overview of Pre-Main Sequence Evolution

The classical view (and currently accepted model) of low-mass star formation (Shu et al., 1987) posits that molecular cloud cores hierarchically fragment and collapse under gravity. These cores form from larger giant molecular clouds, which fragment into denser filamentary-like structures, in which gas is transported along to nodes where multiple filaments meet, and where most star formation will occur. The inner portion of the cloud core collapses faster than the outer areas, leading to a denser central 'core', with an envelope. Mass accretion then occurs at close to free-fall velocities, material from the envelope falling onto the core, eventually forming a more keplerian accretion disk. It is at this point the system is considered a 'protostar', often referred to as a Class 0 object, whose spectral energy distribution (SED) peaks towards the sub-mm regime, and thus is opaque to wavelengths shorter than the mid-infrared (MIR). Protostars

then become optically visible once the pre-stellar envelope collapses to form a disk (a cartoon diagram of the structure of such a system can be found in figure 1.1. The SED and its slope across the infrared, referred to as α (from Lada (1987)) takes the form:

$$\alpha = \frac{d\ log(F\lambda)}{d\ log(\lambda)}$$

Where λ is a wavelength in the range from 2μm to 25μm, although in practise this is done instead with photometry from 2MASS K-band to either Spitzer [7.8μm] $I4$ or WISE [22μm] $W4$ (originally used IRAS). The value can be used to categorise young stellar objects (YSOs) into evolutionary groups (Lada, 1987; Andre et al., 1993; Greene et al., 1994), and is described below (see also figure 1.2):

- **Class 0**: characterised by non-detection in the near-infrared (NIR), these stars are heavily embedded and thought to be far younger than the other groups.
- **Class I**: Sources with $\alpha > 0.3$, these are still optical non-detections, but are visible in the NIR. Their SED peaks at longer wavelengths (circa 100μm), with the flux dominated by re-emission from the star's envelope.
- **Flat-SED**: Added to the classifications by Greene et al. (1994), flat SED/spectrum sources act as an intermediate or transitional stage between class I and class II systems. It cannot be ruled out that disk inclination could also play a role here, by increasing line-of-sight reddening. These systems are considered to have $-0.3 \leq \alpha < 0.3$
- **Class II**: Defined as having $-1.6 < \alpha < -0.3$ this group contains both classical T Tauri stars (CTTS - Joy (1945)) and Herbig Ae/Be stars (Herbig), for stars below and above $2M_{\odot}$ respectively. Class II objects are optically visible, since the envelope has dissipated, although they still exhibit excess infrared emission from accretion disks. The inner disk area is linked to the young star via magnetic field lines, and it's through these that material continues to accrete (Shu et al., 1994).
- **Class III**: Stars with $\alpha \leq -1.6$, often referred to as weak line T Tauri stars (WTTS), have only a small IR excess. The excess being caused by emission from an optically thin accretion disk.

There are some caveats to this system of classification, stemming from its empirical nature. YSOs can have significant foreground reddening from their local environment as well as from

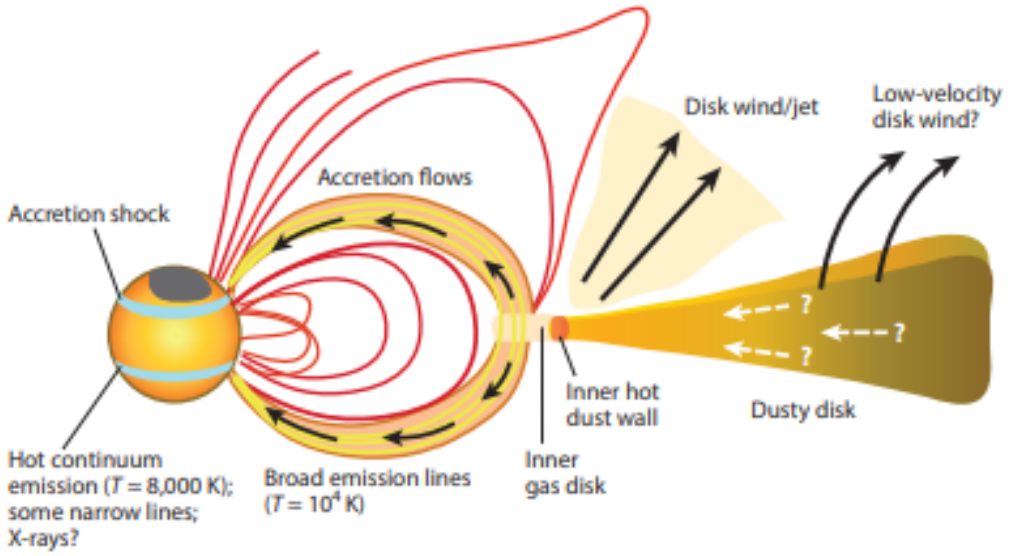

FIGURE 1.1: Cartoon displaying the typical structure of an accreting YSO. Figure reproduced from (Hartmann et al., 2016).

their disk geometry w.r.t their line-of-sight, both of which can inflate the measured value of α. Additionally photometric variations in the time domain can lead to significant changes in the SED slope of the system, which is especially notable given the wide sampling of the commonly used MIR surveys. It is for these reasons that the above groups are referred to as 'Stages' rather than 'Classes'.

Given the assumed timescale for PMS evolution of $\approx 10^5$yr the average accretion rate for a solar-type star should be on the order of $10^{-5}\mathrm{M}_\odot\mathrm{yr}^{-1}$. The calculated luminosity (L_{proto}) would then be of the order $50\mathrm{L}_\odot$ assuming a average mass of $0.5\mathrm{M}_\odot$ and radius of $3\mathrm{R}_\odot$, with the formulae being:

$$L_{proto} = L_{photospere} + L_{acc} \text{ where } L_{acc} = \frac{GM_*\dot{M}}{R}$$

Where L_{proto} is the total protostellar luminosity, $L_{photosphere}$ is the luminosity component from the young star itself, L_{acc} is the accretion luminosity, M_* is the protostellar mass, $\dot{M}$ is the mass accretion rate, R is the radius, and G is the gravitational constant. Various publications (such as Kenyon et al. (1990); Kenyon and Hartmann (1995)) noted that protostars in the Taurus-Auriga region were underluminous (for the region overall), the average observed luminosity being of order $1\mathrm{L}_\odot$. The above is referred to as the *protostellar luminosity problem*, and is now mostly considered solved (Offner and McKee, 2011), via the observed protostellar lifetimes

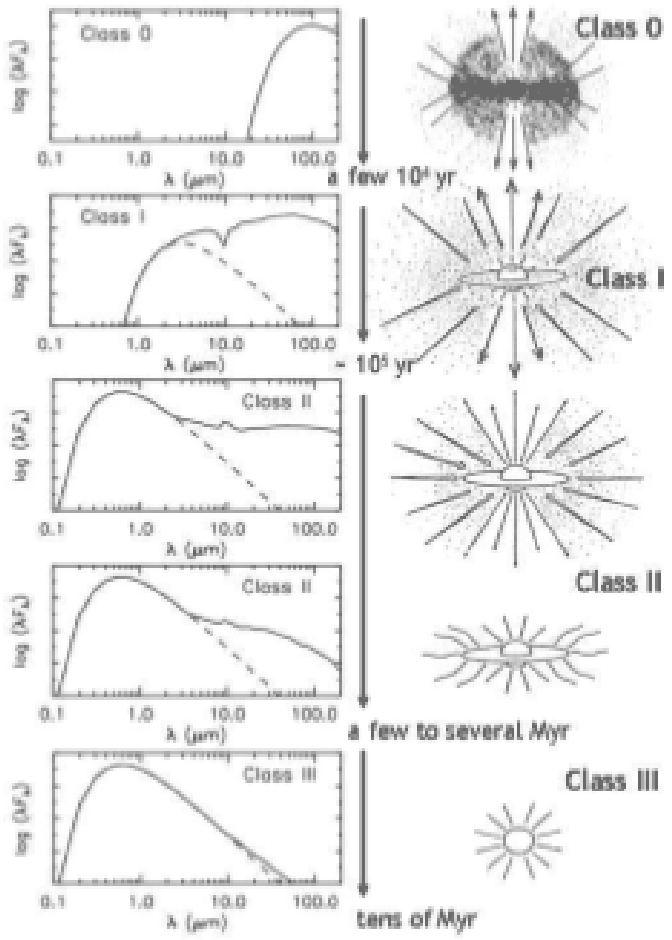

FIGURE 1.2: Cartoon displaying the SED features and rough physical layout of the various classes of YSO. Figure reproduced from (Wilking, 1989).

being adjusted to $\approx$ 5Myr for some cases, and the observed luminosities being increased.

Another solution proposed at the time was episodic accretion, wherein observed accretion rates can rapidly change over a range of days to centuries (reviewed by Audard et al. (2014)). Considering that systems could spend a statistically significant amount of time in a low accretion state (and corresponding low luminosity), before any period of sustained high mass transfer, the observed luminosity spread would be biased to the underluminous state (suggested in Protostars and Planets VI (Beuther et al., 2014)). Episodic accretion events, and their associate spread in colour and luminosity also provides a plausible explanation for the large spread of YSOs about Hayashi tracks on HR diagrams (Hayashi tracks are the paths followed by YSOs of a given mass, towards the MS on a Hertzsprung-Russel diagram), see Mayne and Naylor (2008). While the original *luminosity problem* is now considered solved (Fischer et al., 2017), the observed

luminosity spread (for YSOs) is too high to be explained from steady state accretion alone, now referred to as the *protostellar luminosity spread problem* (Fischer et al., 2022).

1.2.1 Eruptive Variable YSO Classification

Young stellar objects display a vast range of behaviours in the time domain, with episodic accretion events being among the highest amplitude and longest duration events (exceptions are extinction driven fading events such as those seen in V2492 Cyg, Kóspál et al. (2013a)). Classically episodic accretors were divided into FU Orionis & EX Lupi types, although more recently a larger spread of classifications has been used for these stars, discussed in more detail below:

- **FU Orionis (FUor)**: First described in Herbig (1977), FU Ori events are notable for sustained high amplitude bursts (see figure 1.3), with faster heating times compared to decay timescales on the order of (or above) 10s of years. The stars have absorption dominated spectra, consistent with a viscously heated disk, with a temperature that is inversely proportional to the observed wavelength. Most outbursts of this nature are more pronounced in optical wavelengths, likely owing to the systems being embedded enough to veil the system at lower wavelengths until the disk is sufficiently heated to become optically thin. Three stars provided the initial basis for the group, FU Ori, V1057 Cyg & V1515 Cyg, although there are some key differences between the stars: V1057 has a comparatively short decay timescale in comparison to the others and V1515 does not possess the rapid optical brightening (although it remains very high amplitude) of other early class members. FUors are normally spatially (where such information is available) kinematically associated with star forming regions, and/or Herbig-Haro outflows or other features like cometary nebulae. These last features might have played a more significant role in the FU-Ori Class - or some members within it - with recent research, such as by Cuello et al. (2023), suggesting multiple young stellar flyby events can cause the disc instabilities (and thus episodic accretion). This was carried out by simulating the disks of these systems and the associated accretion, and thus providing a useful replication of some FU Ori-like phenomena. This work built on the suggestions of Bonnell and Bastien (1992) that the large scale accretion changes of FU Ori events could be caused by binary interactions, in order to provide the necessary instability within the YSO disk to cause a collapse and free-fall of material onto the YSO. Spectrally FUors are relatively homogeneous when captured in outburst (see figure 1.4), featuring prominent absorption by warm 12CO and

water vapour absorption on top of a red continuum. Very rarely are any emission features seen, save perhaps for small Brackett γ lines (often with a P Cygni line profile), as seen in Connelley and Reipurth (2018). For many years the number of observed FUors was fairly stable, at around 35 circa 2018, however large surveys in the southern hemisphere - like VVV (Minniti et al., 2010) - have been able to provide a far larger sample of these systems, with a broad range of behaviours. Additionally, new photometric alert systems for transient-like phenomena, such as Gaia and ZTF (Gaia Collaboration et al., 2016a; Dekany et al., 2020) can provide similar insights for less embedded objects

- **EX Lupi (EXor)**: Categorised in (Herbig, 1989) EXors are noteworthy for their intermediate-term (on the order of between 10^2 & 10^3 days) outbursts of 2-5 magnitudes (in optical bands). The long-term behaviour of these systems is remarkably varied: some members show decades of quiescence in between stochastic bursts, while others (notably seen in Guo et al. (2022)) are remarkably periodic, with frequent bursts (as can be seen in figure 1.3). It is worth stating however that the periodic bursts of these sources may not be true EXor outbursts, and should be referred to as 'Pulsed Accretors'. During outburst an EXor has bluer colours (noticeably visible in $J-H$ & $H-K$) that predominantly move the star onto the classical T Tauri tracks, observed in Lorenzetti et al. (2012). The spectra of EXors are different depending on the current outburst status of the star, with quiescent sources having features unlike those seen in active ones (an example active EXor is provided in figure 1.4). Erupting sources have their inner disk dominate over the protostellar photosphere, and can be characterised by strong emission lines from the following sources:

  - Hydrogen recombination lines: in the NIR these are Paschen β & Brackett γ. These provide a tracer of mass accretion rate which can be as high as $10^{-7}\mathrm{M}_{\odot}\mathrm{yr}^{-1}$ (Aspin et al., 2010)
  - Molecular hydrogen lines: these lines are indicators of outflows, with the ratio between the S(1) and S(0) lines able to indicate the method of excitation, see Greene et al. (2010) for a detailed explanation.
  - Carbon monoxide: 12CO is visible in emission for all EXors in outburst, and gives the clearest indication of the source of the flux coming from the heated inner disk of the system.

  - Numerous metal lines: a number of metal lines including (but not limited to) Na, Fe, Ca and Si, which are commonly seen in young stellar photospheres, although in absorption for non-outbursting sources.

  For quiescent/ dormant EXors the spectrum will often reflect a that of a typical YSO, of similar age and mass. Hence some stars like the prototypical EX Lup will have a typical CTTS spectra with photospheric absorption lines, while others will retain the redder spectrum of an accreting Class I or flat-spectrum star with faint emission lines. The observed variability has all the tracers of enhanced magnetospheric accretion, with an observed 2-3 order of magnitude increase in flux from quiescence to outburst (Sipos et al., 2009). Given the high amplitude of EXors across multiple wavebands, these stars can be readily detected with multiple facilities, although there is still a bias towards the faster rising and higher amplitude optical sources.

- **V1647 Ori (MNor)**: Recently more eruptive YSO candidates are being discovered with mixed photometric and spectroscopic properties (EXor-like spectra, and FUor shaped light curves) and variation on intermediate timescales, originally noted in the system V1647 Ori (Aspin et al., 2009). These objects are often referred to as MNors, after the nearby McNeil's nebula (Contreras Peña et al., 2017), with other early members including Gaia19bey (Hodapp et al., 2020) and V346 Nor (Kóspál et al., 2020). Recent work by Guo et al. (2021) has further constrained these objects, to prevent the group becoming a catch-all for unusual YSOs in general. This requires stars to undergo outbursts with timescales longer than classical EXors, and comparable to that of FUors.

- **Long Term Variables (LTVs)**: Referred to as *protostellar outbursts (infrared)* in some literature, LTVs are currently understudied because of their combination of long rise times (on the order of 10^3+ days) and highly embedded nature. The work of Guo et al. (2021) identified a small number of these sources, noting they possessed emission line spectra. This behaviour could be linked to that seen in PGIR 20dci (Hillenbrand et al., 2021), which spent a decade slowly brightening before a much larger FUor-like outburst.

- **Multiple Timescale Variables (MTVs)**: First documented in the work of Guo et al. (2020), MTV's are emission-line objects that are characterised by variation on sub-100 day timescales in addition to unrelated changes on the order of years. The most significant aspect are the short timescale spectral variations, notably in the Brackett γ and molecular

hydrogen emission features. The spectral changes are thought to be as a result of short-term changes in accretion rate and material ejection (via outflows). Long-period changes are not though to be different to the LTVs discussed above.

In addition to the eruptive objects, variability can be detected as a result of changes in extinction, both from intrinsic and extrinsic sources. In most cases these can be disentangled from eruptive variables through their colour differences in faint and bright states: extinction dominated variables will get redder as compared to a typical TTS in their faint stage, while eruptives will get bluer in their bright phases. The two key types of extinction dominated YSOs are detailed below:

- **'Dippers'**: Stars characterised by either short or intermediate duration (order of days to several months) dips in their light curves, across optical, NIR and MIR wavelengths (Cody and Hillenbrand, 2010; Morales-Calderón et al., 2011a). The behaviour was formalised within multiple works, including Bouvier et al. (2007a); Kóspál et al. (2011); Rice et al. (2015). Positing that the observed extinction can be a result of an optically thick accretion stream/column passing in front of the line of sight, or magnetically induced warps in the inner disk (for the longer duration dips). Recent work such as Guo et al. (2021) has noted that dippers can have high accretion rates, and thus have EXor-like emission spectra, making classification more challenging without full coverage of a light curve.
- **'Faders'**: Extinction events that last for years or more are also referred to as RW Aur or UX Ori type systems, depending on if the system is redder or bluer whist fading, respectively. The large amplitude fades are a result of disk geometry, with either large asymmetries in the outer regions of the disk, or possible warping with respect to the line of sight (Bouvier et al., 2013a). Additionally changes in the thickness of the inner-disk can also cause a long duration increase in extinction, and reproduce the observed fading behaviour (Covey et al., 2021).

1.3 Non-YSO IR variables

In most cases non-YSOs can be identified in large NIR surveys with relative ease, with the eclipsing binaries (EBs) and AGB stars displaying different colours and periodicities to YSOs. Generally evolved objects are redder in the NIR and bluer in the MIR, and EBs have an obvious

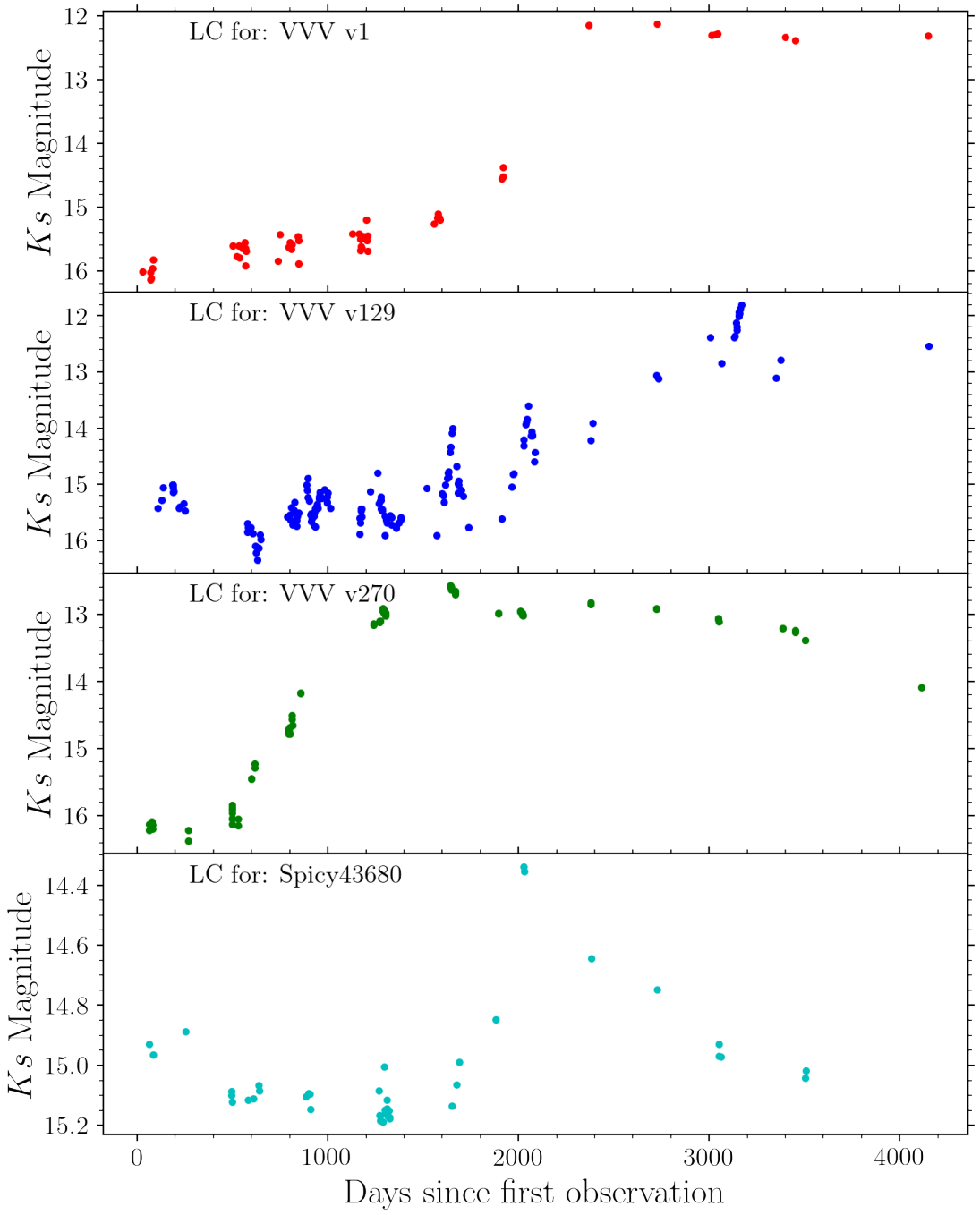

FIGURE 1.3: VVV *Ks* light curves for an archetypal FUor (VVV v1 - red), an MTV (VVV v129 - blue), an MNor (VVV v270), and an EXor (Spicy 43680). All reproduced with permission from Guo et. al. (Sub.). Repeating outbursts are shown for v129, in conjunction with a long term brightening trend. The above is similar to the behaviour seen in LKHα225 (Hillenbrand et al., 2022). VVV v270 has a light curve with morphology similar to that of a FUor, but has the characteristic spectrum of an EXor outburst.

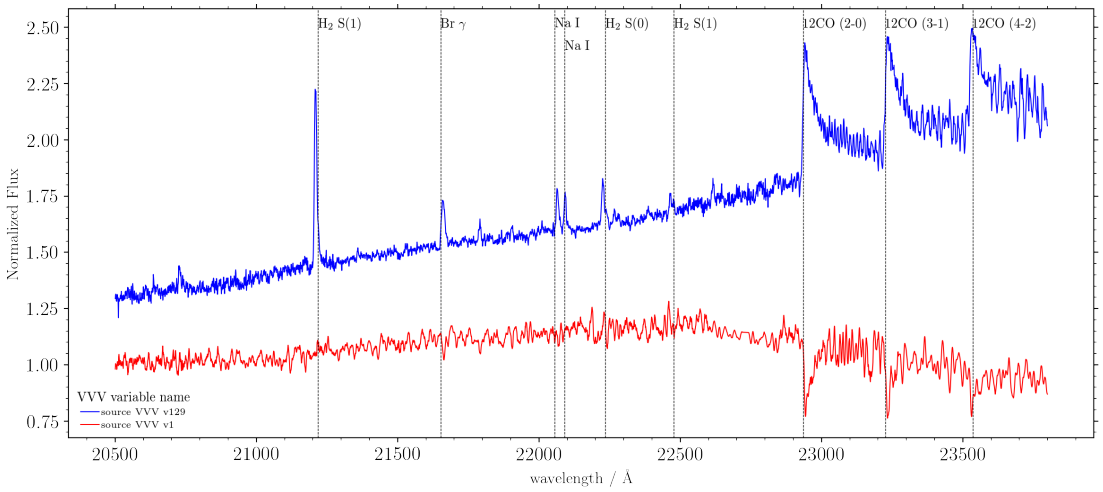

FIGURE 1.4: Magellan/FIRE NIR spectra (K band shown here) for the same stars as in figure 1.3. The EXor (blue) has many of the emission features expected in this class of star, with 3 H_2 lines, the Brackett γ H I line and hot 12CO lines. Additionally a number of photospheric lines can be observed such as the sodium doublet at 2.21μm. The FUor (red) has the broad water absorption features present in the continuum post 2.25μm, as well as cool 12CO absorption lines.

double peaked light curve that makes them easy to distinguish. This is however a somewhat simplistic viewpoint, and there are a variety of objects that can occupy similar regimes to pre-main sequence stars, and thus require new methods to identify.

1.3.1 Evolved High Amplitude IR Variables

Asymptotic giant branch stars are considered to be one of the more common objects in the IR variable sky, which also dominate in the optical regime (see Samus et al. (2010)). NIR variability in this group is either as a result of excessive photospheric carbon (elevated to the surface during a dredge-up event) for carbon rich stars (C or S-type), or from pulsations leading to circumstellar shells in O-rich stars, like Miras. The AGB phase occurs for all stars at with a zero-age main sequence (ZAMS) mass of $<8M_{\odot}$, although given how long of a process stellar evolution is for low mass stars, no star under $0.8M_{\odot}$ has yet reached the AGB. The fundamental structure of an AGB star is of an inert C/O core, surrounded by twin shells of He and H. The lower helium shell burns on the surface of the C/O core, and once this shell is depleted Hydrogen burning will then occur in the outer shell. Said hydrogen burning will then produce helium, and thus replenish the He shell, restarting the process (this process is called a thermal pulse). Burning on the surface of the convective core is the cause of the third dredge up event and provides the basis for much of the chemical enrichment (for elements produced by nucleosynthesis) of the

ISM (see Karakas and Lattanzio (2014) for a review). The chemical enrichment comes about through the mass loss that is associated with the AGB phase, and occurs for both the lower mass (at ZAMS) carbon rich stars, as well as the $>4M_{\odot}$ oxygen rich AGBs. Mass loss on the AGB is driven by low surface gravity of the stars, which with relatively low masses and stellar radii on the order of $\tilde{1}00R_{\odot}$s, means the outer layers of the star are very loosely bound against radiation pressure or shock acceleration. Mass loss solely through winds would not generate the kind of high amplitude variability that is often seen in AGB stars, so a method needs to exist that will allow large volumes of material to be ejected in a single event. The interplay between stellar pulsations and shocks can provide stellar material with enough additional kinetic energy for the escape velocity to be easily breached with the remaining radiation pressure. This process can be said to induce 'levitation', with the stellar pulsations inducing sound waves that propagate through the stellar envelope, providing the additional kinetic energy required to overcome the gravitational potential energy, inducing mass loss.

The observed variability is not always the result of the pulsation of the star, but can be related to extinction from optically thick material produced in the dredge-ups that exist between hydrogen and helium shell burning phases. This is more common for carbon rich (lower mass) AGB stars of the C or S-type, with pulsation driven variability more common in O-rich stars like Miras. Given that AGB stars are extremely bright objects, most would be over-saturated in IR deep-sky surveys, hence those found likely being at the low-end of the luminosity scale or at large distance (see chapter 6). Variability in these stars is of long duration, often periodic, from 300 to 1500+ days (Whitelock et al., 2008), and in the case of Miras the period is linked to the luminosity. A final note is for the carbon-rich R Coronae Borealis (R Cor Bor) stars, which produce aperiodic variability caused by the production of thick dust shells, leading to large variance at optical wavelengths. Their spectra can be quite similar to that of a YSO, but will lack hydrogen features, and often show helium in emission (this because RCBs are hydrogen-deficient stars), see the recent spectral atlas by Karambelkar et al. (2021). For further information on the various mass loss inducing mechanisms observed here, see the review (and references therein) by Höfner and Olofsson (2018).

Certain main sequence stars can also display IR variability, associated with material ejection: the broad group of B(e)/[e] stars. 15-20% of the population of main-sequence B-type stars are associated with the Be phenomena: the presence of hydrogen emission lines from a viscous disk of ejected material, produced by a rapidly rotating massive star. There comprises a loose grouping of objects which display this phenomena (best described by the review of Rivinius

et al. (2013), and references therein), albeit through different methods. Classical B(e) stars are the most common, but are infrequently detected in the IR, and usually lack disks thick enough for the production of a meaningful IR excess. Some can still be detected in this wavelength regime however, as evidenced by the star GPSV13 from Contreras Peña et al. (2014a), as well as 6 others observed by this author, from the same UGPS selection. B[e] stars are a distinct group that have forbidden lines of various metals (including O and Fe) also present in emission (see Lamers et al. (1998)).For B[e] stars IR excesses are more common and the method of excitation is rarely well constrained. The group has been known to contain anything from supergiant stars, to symbiotes, to Herbig Ae/Be stars, and thus can lead to stars at many locations on NIR Colour-Colour diagrams. A final noteworthy member of the Be stars are those of the FS Canis Majoris (FS CMa) type, which consist of many previously unclassified B[e] stars (formalised in the work of Miroshnichenko and Zharikov (2015)). These are characterised by strong IR excess (peaking in the MIR), and emission lines an order of magnitude stronger than seen in classical B(e) stars (Miroshnichenko et al., 2008). Current consensus on these stars indicates that they are likely binary systems, with a cool companion, which can often be seen in the NIR spectrum. On the whole Be stars have variability on a range of timescales, with short period luminosity changes from rotation contrasting with the much longer timescale for decretion disk production and destruction, with intermediate period variability being observed from disk warping.

White dwarf binaries are another group of variable sources that can be detected in the IR. Ordinarily considered to be optical/X-ray sources, the presence of circumstellar disks around cataclysmic variables including dwarf novae, as well as dusty shells in certain symbiotic and white dwarf X-ray binaries (WD-XRBs) can lead to an observable IR excess. These systems are characterised by complex light-curves, often with short-period components relating to fast orbital and rotation periods. These are often found in combination with repeating high-amplitude variability associated with companion variability (such as Mira-like pulsation), thermonuclear runaway (in the case of classical novae), or accretion rate changes (as in dwarf novae).

1.3.2 Cataclysmic variables

Cataclysmic variables (CVs) are interacting white dwarf (WD) binary systems, which comprise of a WD accreting from a low mass main sequence (MS) companion, usually of the M-type. For strongly magnetic white dwarfs, accretion from the MS companion is either direct via magnetic field lines, or magnetospheric from a keplerian accretion disk, in systems referred to as Polars

and Intermediate-Polars (IPs) respectively. The large magnetic field strengths found in the WDs of Magnetic CVs (mCVs) are thought to be produced as a result of their evolution as common envelope (CE) binaries (Ivanova et al., 2012). Known as the 'Fossil Field Scenario' (Braithwaite and Spruit, 2004), this stipulates that a powerful dynamo is created by the rapidly rotating WD with the common envelope, which is fed by the stratification of oxygen and carbon in the core of the WD. As the oxygen sinks to the centre, the carbon rises and in concert with other metals, generates a magnetic field in a similar fashion to that seen in terrestrial planets. This necessity for a CE evolutionary path to generate the observed magnetic field strengths (on the order of $\sim$1 MG) can explain the observed lack of detached magnetic WDs in the field.

Magnetic CV systems will evolve over time, with a reduction in the orbital period as a result of a loss of angular momentum (AML) from magnetic braking and gravitational radiation. The standard model of CV evolution is described in Rappaport et al. (1982, 1983), which provides a reasoning for the 'period gap', the name given to the lack of observed CVs with orbital periods between 2 and 3 hours. Mass accretion occurs only when the Roche-lobe of the donor is in contact with the WD, and at orbital periods of $\approx 3\ hr$ this ceases due to the donor becoming fully convective. A fully convective donor will contract, and thus break contact with the Roche-lobe, which will in turn stop AML via magnetic braking, leading further evolution to rely on AML from gravitational radiation. During this stage of GR driven evolution the systems are not observable as CVs, and hence define the 'period gap', wherein no binaries of this type should be detected. At periods less than two hours, the Roche-lobes will reconnect and mass transfer will begin again. There is a point at which the AML induced period reduction is reversed, referred to as the minimum period, P_{min}. Calculated to be at 80 minutes (Knigge et al., 2011), it represents the point at which the thermal timescale of the companion star increases at a faster rate than it's own mass loss:

$$\frac{GM_c^2}{L_c R_c} \sim \tau_{kh} > \tau_{\dot{M}_c} \sim \frac{M_c}{\dot{M}_c}$$

Where G is the gravitational constant, τ_{kh} is the Kelvin-Helmholtz timescale, $\tau_{\dot{M}_c}$ is the mass accretion timescale, M_c is the companion star mass, L_c is the companion star luminosity, R_c is the companion star radius, and $\dot{M}_c$ is the mass accretion rate from the companion to the WD primary.

The implication is that this change causes the radius of the companion star to increase and thus the radius of the binary orbit increases too. Stars that are in this regime are called 'period bouncers'.

At this juncture it is important to explain the distinction between polars and IPs: the magnetic field of an IP is not large enough to synchronise the spin of the white dwarf to the orbital period of the companion (Schreiber et al., 2021), whereas this is the case for Polars. The second result from the smaller magnetic field is that the keplerian accretion disk is not destroyed, only disrupted, thus creating different observable characteristics for the two groups. See the spectral sample of Oliveira et al. (2019) for examples from both groups.

- **Intermediate Polars**: IPs have highly variable light curves, usually with optical amplitudes of <1 magnitude, with detectable periods in the range from minutes to the order of 1 or 2 hours. The most easily detectable variability is associated with the spin of the WD, tracing the hotspot at the base of the accretion column. Their spectra present multiple ionisation lines of hydrogen, helium and metals such as carbon and nitrogen all in emission. These lines are especially broad owing to the spread of velocities found within the accretion column and disk. The shift in the peak of the line can be used to identify the orbital period of the companion star, although this can also be found from the X-ray light curve.

- **Polars**: Polars have variability of similar type to that shown in IPs, although of a higher amplitude (between 1 and 2 magnitudes). Given that both the spin and orbital periods are synchronous, the timescales of variability will have a lower limit at $\approx$80 minutes, corresponding to the minimum period of a CV (see Knigge et al. (2011) for an semi-empirical calculation of this value). Owing to the lack of an accretion disc in these systems, the detected emission lines are far narrower, and often double-peaked, as a result of the large magnetic field of the WD.

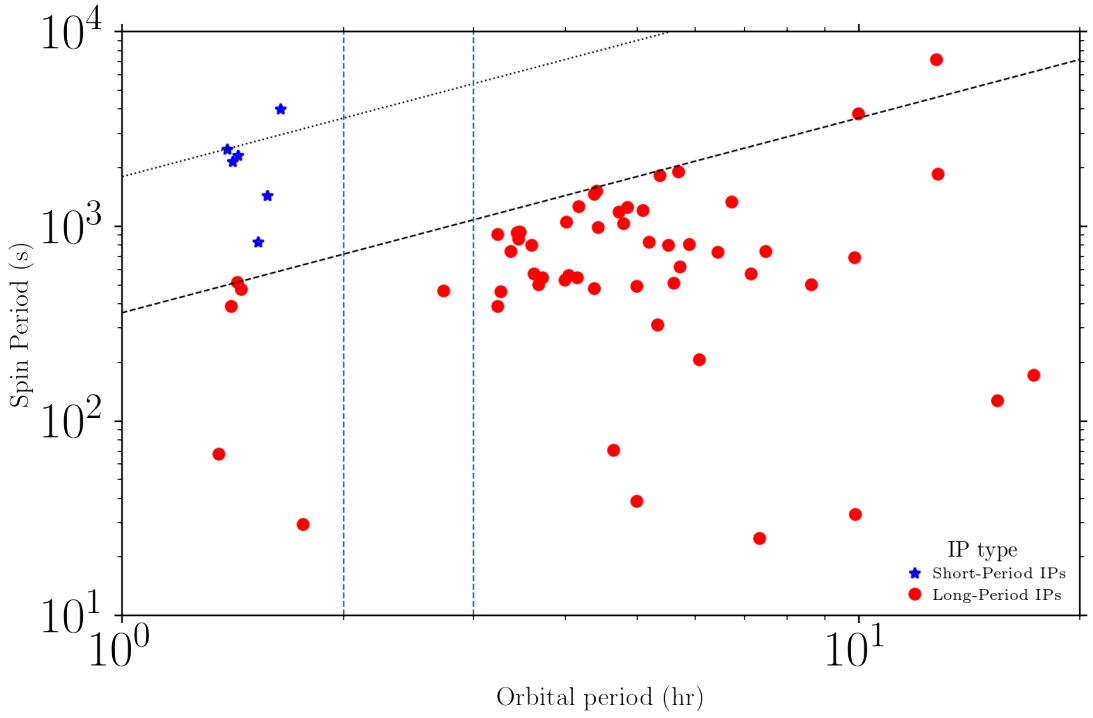

FIGURE 1.5: Orbital period versus spin period diagram for a large selection of intermediate-polars (data from K. Mukai's 'The Intermediate Polars' webpage[1]). Most systems are on or below at spin/orbit ratio of 0.1 (red), with a small subgroup (the so called 'short-period IPs') at a ratio of around 0.5 (blue). These two regimes are denoted by the black dashed and dotted lines, respectively. The vertical lines indicate the 'period gap', where classically IP's should not be found (save for 'period bouncers').

1.3.3 Symbiotic Stars

Whilst most WD binaries are not particularly bright in the IR, symbiotic stars are an exception, owing to the companion star being of a giant classification. The first examples of the type, CI Cyg and AX Per, were discovered long before their nature could be determined (Merrill and Humason, 1932), the binarity required to observe features associated with a red giant and also massive stars not being fully understood. These systems have extended orbital periods (as compared to CVs) often between 1 and 4 years, with the mass transfer either occurring due to Roche-lobe overflow (as in CVs) or from the enhanced stellar wind of the AGB star, which is more common among systems containing a Mira-type companion. Symbiotes can be put into three overarching groups based upon the presence and temperature of any observed dust: S, D', and D-types. S-types have no observed dust emission, D'-types have low temperature dust emission, and D-types which display warm or hot dust emission. It's the D-type systems that are of interest in this work, because the evolved star in the system is generally considered to be

[1]Located at https://asd.gsfc.nasa.gov/Koji.Mukai/iphome/iphome.html

either a Mira or Carbon star, both of which are IR bright variable stars in their own right. The addition of a hot (sometimes burning) WD moves the peak of the SED towards the optical, which in turn moves the stars to the left of the NIR/MIR CC diagram, into the area also inhabited by some YSOs. Thus spectroscopy can be used to distinguish these objects, although UV or X-ray imaging can also be used. The spectral features of these stars are similar to field red giants and carbon stars, with the addition of emission lines from helium and highly ionised oxygen (see Munari (2019) for a short review on the topic).

1.4 Motivations

Given the zoo of objects in the infrared variable sky, reliable classification methods are a requirement in the era of large surveys. For the traditionally NIR/MIR colour selected YSOs, this has further relevance, notably for embedded systems whose membership of star-forming regions cannot be determined through optical measurements of parallax & proper motion (such as by Gaia). Exploring the population of high amplitude variables associated with star formation, will thus allow for greater insight into the varied behaviours seen in early PMS evolution. Specific attention is paid to the prevalence and diversity of eruptive variables. Additionally the various interlopers in this NIR colour-space can be identified (via follow-up spectroscopy and mult-wavelength photometry), allowing for their more reliable extraction in future work. The primary goals of this work then become:

- To investigate the proportion of high amplitude variable YSOs that show evidence of eruptive variability, and of which sort.
- Test the effectiveness of using long duration MIR light curves to identify eruptive candidates, as compared to the higher sampling rate NIR VVV/X survey.
- Are there previously undiscovered classes of embedded objects that can be identified with our stellar variability and IR-based selection methods?
- What methods can be used to identify non-YSO interlopers from samples of objects within known star-forming regions, if the sources are too embedded or optically faint for Gaia?

This thesis is structured into the following chapters: In chapter 2 the incidence and characteristics of eruptive variability in near-infrared selected YSOs will be investigated in regard to

their NIR spectra and MIR light curves. Chapter 3 will expand on the previous section through the search for additional eruptions via the selection of known YSOs within the Cygnus-X star forming region. Chapter 4 discusses the classification of a NIR selected short-period variable star of novel type, through a comprehensive multi-wavelength study featuring both new and archival data. Chapter 5 details the investigation into the unclassified non-YSO members of the sample of Lucas et al. (2017). This will focus on 3 AGB star candidates of unusual type, via literature comparison, as well as astrometric and period fitting. Finally chapter 7 will offer concluding remarks from the findings of the thesis, and reflecting upon the science goals discussed previously.

Chapter 2

Data and Methods

2.1 Archival Data

Throughout this body of work several publicly available data sets will be used, and this section will serve as an introduction to those works.

2.1.1 2MASS

The 2 Micron all Sky Survey (2MASS, Skrutskie et al. (2006a)) covered the entire sky in J, H & K bands (with $\approx 1''$ resolution), utilising the 1.3m IR telescopes at Mt. Hopkins Observatory in the USA and CTIO in Chile. In this thesis we use 2MASS photometry to both extend the time baseline offered by our UGPS data, as well as providing a indication of a source's NIR colour change where J & H bandpass data is available.

2.1.2 UGPS

The UKIRT Galactic Plane Survey (UGPS) (Lucas et al., 2008) surveyed ~ 1470 deg^2 of the northern galactic plane twice (three in some regions), across widely spaced epochs between 2005 and 2014. The survey utilised three NIR filters: J, H & Ks (with only a single epoch observed with the former two filters), with a resolution of $0.75''$.

2.1.3 VVV/X

The Vista Variables in the Via Lactea (VVV) (Minniti et al., 2010) survey utilises the 4.1m Vista telescope at the Paranal observatory in Chile. It surveyed the southern galactic plane with up to 5 filters ($Z, Y, J, H\&Ks$) across more than 70 epochs covering a $\sim$ 10 year time baseline.

2.1.4 NEOWISE, ALLWISE & UnTimely

The Wide-Field Infrared Survey Explorer (WISE) is a 40cm MIR space telescope, with 4 filters: 3.6μm $W1$, 4.5μm $W2$, 12μm $W3$, & 22μm $W4$. The ALLWISE data release consists of the original WISE All-sky Data Release, as well as the later NEOWISE post-cryo reactivation survey. NEOWISE surveys the whole sky up to 3 times per year, with each observing block consisting of 10-20 individual scans. For most stars the spread in the measured fluxes across the scans is far higher than the stated photometric errors, and thus the photometry used in this thesis is calculated differently. For each epoch the photometry from the individual scans were then cleaned to remove points with a high psf error. Additionally those points with either *w1snr* or *w2snr* <5 were subject to cuts first used in Koenig and Leisawitz (2014):

$$w1rchi2 < \frac{w1snr - 3}{7} \tag{2.1}$$

$$w2rchi2 < (0.1 \times w2snr) - 0.3 \tag{2.2}$$

Following this data processing, the median was found for each epoch, with the stated error given as the error on the mean from the single scans. All WISE light curves in this work feature both the original WISE epochs, and the NEOWISE observations up to and including the early 2023 data release. Additional quality control cuts were in place, removing data points that were 'moon_masked', or that had a number of blends 'nb' greater than 3, or 1 without active deblending ('na' = 1). In Addition no data was used where 'qual_frame' was less than 5.

2.1.5 Spitzer Surveys

The sources within the region covered the Cygnus-X Spitzer Legacy Survey (Beerer et al., 2010), have their photometry included with the MIR WISE light curves. Given that the Spitzer IRAC 3.5μm ($I1$) & 4.5μm ($I2$) have subtly different bandpasses to $W1$ & $W2$, I apply a correction

to the IRAC photometry in this work. This set of corrections was first used in the work of Antoniucci et al. (2014), and entails the following:

$$\mathrm{I1}_{cor} = m_{I1} - 0.27489 * (m_{I1} - m_{I2}) + 0.07146 \mathrm{I2}_{cor} = m_{I2} - 0.1422 * (m_{I1} - m_{I2}) - 0.01855 \tag{2.3}$$

Where m_{I1} & m_{I2} are the apparent magnitudes for $I1$ and $I2$ respectively.

2.1.6 IPHAS, VPHAS+

The INT/VISTA Photometric H Alpha survey(s) (IPHAS/VPHAS - Barentsen et al. (2014); Drew et al. (2014a)) were northern/southern sky surveys in 3 filters: r,i & $H\alpha$. The surveys made use of the 2.5m Isaac Newton Telescope on La Palma for IPHAS and the 4m VISTA telescope for VPHAS. In this work IPHAS data is instead taken from the latest IGAPS release (Monguió et al., 2020), which also contains the u bandpass data from UVEX. VPHAS data is taken from DR2 where available (via Vizier) and from DR4 (via ESO) otherwise. VPHAS+ DR4 data is acquired through a $2''$cross match to the co-ordinates of the desired sources (in the case where this occurs the co-ordinates are taken from Virac-2β, by Smith et al. in prep). The full catalogue for the fourth data release is not yet completed, so the individual tile's catalogues are queried instead.

2.1.7 Gaia

The Gaia mission (Gaia Collaboration et al., 2016b) has surveyed the entire sky in a broad G-bandpass filter, that can also generate colour information ($BP - RP$) in addition to very low resolution spectra. In this work I employ a cross-match radius of $2''$between Gaia itself and UGPS, and this makes use of either the up-to-date DR3 or the previous eDR3 releases. For quality control cuts, I limit to those Gaia sources with a `ruwe` (reduced unit weighted error) of < 1.4, which will limit results to the most certain targets. This cut is additionally beneficial because it is an 'indexed column', meaning that it is able to be quickly scanned within the Gaia database, making the retrieval of data more efficient. Gaia will lack detections for some of the more optically faint (i.e class I YSOs) sources, but the distances of less embedded sources in the same region of sky will still be reliable.

2.2 Photometric Methods

Throughout this work I have used a consistent set of photometric procedures, which can be repeated when necessary. As such a breakdown of said methods for both data reduction and cross-matching is provided below.

2.2.1 Survey Cross-Matching

Combining multiple catalogues at different wavelengths necessitates matching the relevant science target to it's counterpart in other surveys. In this work I adopt a consistent set of parameters for cross-matching, which are described below:

- For matching between NIR and optical catalogues I require a counterpart within $0.5''$. Where multiple candidates exist within this radius, the nearest to the science target's position is selected, but both images are overlaid and visually inspected to confirm that the target is not blended in either.
- Matching to MIR catalogues (with typically lower resolution than in the NIR) is taken with a wider radius than to the other catalogues, at $1''$. Given the low resolution of WISE data, photometric blends are far more common, so higher resolution *Spitzer* catalogues are used to confirm that observed WISE flux is attributed to the relevant NIR science target.

2.2.2 Data Reduction

Photometric data reduction was carried out using my own pipeline within `python`, and making use of the `photutils` package (Bradley et al., 2023). For the case of time-domain datasets, such as those in chapter 5 the methodology was as follows:

- All frames were bias subtracted, a median flat field was produced (and dark subtracted), and divided into each science frame.
- If the science/standard frames lacked WCS information in the header, then all frames were mapped onto the first frame for each target in chronological order. This process made use of the `astroalign` package, wherein the first image in sequence has a plate solution acquired from 'astrometry.net'.

- Computation of the photometry was either carried out through simple aperture photometry (utilising `photutils.aperture`) for uncrowded fields, or psf photometry (with `photutils.psf`) for crowded fields. PSF photometry made use of the `photutils` interpretation of `iraf`'s `DAOPhot`, with fit itself using a Levenson-Marquardt least squares regression algorithm.

- The science frames are then flux calibrated with a known photometric standard, with it's own measured flux retrieved with the same method described above.

- A final calibration was made to account for small changes in the sky conditions over the course of the observations on a single target. This entails running photometry on five non-variable stars (confirmed via Simbad) in the frame, and fitting a linear trend across all epochs. The correction to the science target is then taken as the median of the differences between the trend and the measured flux for all five calibrators (at each epoch).

Chapter 3

Spectroscopic Classification of Eruptive YSOs in the Near-Infrared

3.1 Introduction

The intricacies of pre-main sequence evolution are not yet well understood, with the 'proto-stellar luminosity problem'(Fischer et al., 2017) indicating the challenge of estimating stellar parameters when large scale changes in mass accretion occur. Changes in accretion rate are detectable via stellar variability, and for younger (or more embedded) YSOs, this can be well studied in the infrared.

Spectroscopy can be used to disentangle the physical mechanisms behind the observed variability; the presence and ratios of different atomic and molecular lines can inform various physical properties, such as accretion method, rate, and wind behaviour (Kenyon and Hartmann, 1995; Hillenbrand, 1997). Thus motivation is provided to investigate a sample of known variable YSOs in order to explore both the frequency of individual eruptive events as well as variation within each class of EV YSO, discussed in chapter 1. The discovery of eruptive YSOs with mixed spectral characteristics (loosely dubbed as MNors, Contreras Peña et al. (2017); Fehér et al. (2017); Green et al. (2013)), increases the need to provide counterpart time-domain data. For targets in the northern hemisphere most multi-epoch data is in the optical regime, so for younger YSOs the MIR NEOWISE survey, with 20 (at time of writing) epochs, covering a baseline of over a decade, provides the best infrared coverage. Some investigations into YSO variability have been carried out in this wavelength range (see Scholz et al. (2013); Rebull et al.

(2014); Contreras Peña et al. (2020)), but few outbursts have been first detected in this range. However more recent samples and discoveries (such as Lucas et al. (2020b,a)) are showing the potential of NEOWISE to unveil high-amplitude or long duration outbursts for embedded and young objects. Bringing together the above methodologies for a single sample of NIR selected variables (the majority being 'likely' YSOs), allows for a comprehensive study of eruptive pre-main sequence behaviour, as well as providing the possibility of probing previously unstudied phenomena. This sample is drawn from Lucas et al. (2017), and builds on work done by Contreras Peña et al. (2014a); Contreras Peña (2015). This work is important in order to provide answers to the following questions:

- How common is eruptive variability in YSOs and what other variable events can be identified?
- What is the range in observed spectroscopic features and time-domain behaviour for young stars selected by Lucas et al. (2017), which demonstrate $>$1 magnitude variability in Ks?

The chapter will build on the work of Lucas et al. (2017); Contreras Peña et al. (2014a), which collectively located candidate eruptive YSOs in the northern galactic plane. Contreras Peña et al. (2014a) originally identified 45 high amplitude ($\Delta K < 1$ mag) variables with a majority of these being located in known star forming regions. This provided the capacity to estimate the fraction of the IR variable sky that would be dominated by YSOs. Additionally 4 Targets were subject to spectroscopic follow-up with Magellan/FIRE and Gemini/NIFS, which revealed them to be YSO-like (2 have since been reclassified as AGB stars, see chapter 6). The study of variability was expanded to the entirety of the northern galactic plane in Lucas et al. (2017), which revealed 618 high amplitude variable star candidates (with the same selection criteria as the previous study). This study identified 390 of these as YSOs, through NIR and MIR colours, in addition to spacial proximity to known tracers of star formation. In this chapter I will examine a subset of the aforementioned YSOs, with NIR spectroscopy and MIR light curves, with the aim of identifying the eruptive YSOs and locating those objects with multiple variable events.

This chapter is organised as follows: first a brief introduction to the observations and the target selection is offered (section 3.2), including an overview of the available archival data for the targets. The spectral sample will then be discussed in groups, based upon possible classifications or similarity to other members of the selection (either spectrally or photometrically), in section

3.3. The results will then be discussed in the wider context of eruptive variability in YSOs, and in comparison to similar surveys (section).

3.2 Observations and Data Reduction

By December 2013 the two epochs of the UKIDSS infrared survey (Lucas et al., 2008) had mapped a previously unprecedented amount of the northern sky in the J, H and K bands. The wide spacing of the epochs allowed for the acquisition of high-amplitude variable stars (with variations of at least 1 magnitude), especially for stars which change amplitude with rates on the order of months to years, making detections of FUor-like and EXor-like YSOs more likely. Lucas et al. (2017) completed a catalogue of 618 high-amplitude variables, of which approximately 60% are YSOs. These stars were cross matched with existing data from 2MASS (Skrutskie et al., 2006b), WISE (Wright et al., 2010), IPHAS (Drew et al., 2005; Barentsen et al., 2014) and the Spitzer GLIMPSE & GLIMPSE3D, MIPSGAL and Cygnus-X Legacy surveys (Benjamin et al., 2003; Churchwell et al., 2009; Rieke et al., 2004; Hora et al., 2007; Carey et al., 2009; Gutermuth and Heyer, 2015) where available, details can be found in chapter 2.

3.2.1 Target Selection

From the 390 'likely' YSOs of the Extreme infrared variables from UKIDSS Survey (Lucas et al. (2017)), those sources that were thought to be members of local and well-studied SFRs were listed for potential spectroscopic follow up. From this group 31 were observed across 3 programmes. These targets were selected on the basis that they were bright enough ($K < 14.5$) to be readily observed during each of the observing programmes. There was also a slight bias in favour of sources with larger K band amplitudes, in the sense that the most highly variable sources were included, if bright enough. However, sources with a wide range of amplitudes $1.00 < \Delta K_{all} < 2.45$ were observed, in order to better understand the photometric sample. The sources discussed further in this chapter are not the only 'likely' YSOs that met the criteria, but are those that had usable spectroscopic data. 15 of these are located in Cygnus-X, with a further 3 targets each in Aquila and Serpens and 10 others in other local infrared dark clouds. Thirty of these can be seen in Table 3.1, and the source numbers here will be used throughout this chapter (The reduction from 31 to 30 is due to one of the reduced spectra being unusable). The table provides an indication of the SED type via the spectral index, a measure of the slope from

2-24μm, wherein values ≥ 0.3 are treated as class I YSOs, and values below this (and above -0.3) are classified as 'Flat-Spectrum' sources. Sources where $W3$ and $W4$ were not available do not have a spectral index measurement.

Source Number	UGPS Designation	RA	Dec	J mag	H mag	Kc mag	Ko mag	ΔK mag	ΔK_{all} mag	Type (Lucas et al. (2017))	SED Class α
19	UGPS J043333.81+442630.4	68.391	44.442	18.26	16.14	14.17	12.44	1.73	1.87	YSO	Flat
123	UGPS J070045.78-032023.2	105.191	-3.340	18.40	16.58	14.57	12.67	1.90	1.90	YSO	I
136	UGPS J181707.12-115142.6	274.280	-11.862	16.86	15.44	14.15	13.15	1.00	1.00	YSO	Flat
142	UGPS J181809.25-115519.6	274.539	-11.922	18.25	17.04	16.37	15.36	1.00	1.00	YSO	-
144	UGPS J181933.65-112800.8	274.890	-11.467	16.43	15.19	14.47	16.41	1.94	2.44	YSO	I
152	UGPS J183629.82-024720.6	279.124	-2.789		19.60	14.41	16.25	1.84	1.84	YSO	I
196	UGPS J185559.84+074709.4	283.999	7.786	18.14	13.98	10.88	12.06	1.18	2.32	YSO	I
221	UGPS J190003.35+010528.7	285.014	1.091	19.46	16.47	14.19	16.27	2.07	2.07	YSO	Flat
236	UGPS J190147.07+011228.1	285.446	1.208	18.29	15.26	13.40	15.12	1.72	1.72	YSO	-
284	UGPS J192031.96+110151.2	290.133	11.031	14.58	13.34	12.49	11.47	1.02	1.02	YSO	-
321	UGPS J192926.46+175521.4	292.360	17.923	17.22	13.91	11.90	12.93	1.03	1.03	YSO	I
374	UGPS J195011.09+235557.9	297.546	23.933	18.62	16.47	14.39	12.37	2.02	2.32	YSO	I
420	UGPS J201228.83+365219.2	303.120	36.872	16.55	15.03	13.75	16.10	2.36	2.36	YSO	Flat
428	UGPS J201516.42+345341.5	303.818	34.895	18.72	16.96	15.44	13.36	2.08	2.08	YSO	Flat
433	UGPS J201613.49+415436.5	304.056	41.910	17.56	15.82	14.82	15.90	1.08	1.08	YSO	-
439	UGPS J201700.83+391953.8	304.253	39.332	16.45	14.65	13.36	14.61	1.25	1.25	YSO	Flat
441	UGPS J201924.83+410503.1	304.853	41.084	17.16	15.79	14.83	16.02	1.20	1.20	YSO	Flat
443	UGPS J202020.28+384209.3	305.084	38.703	16.11	15.06	14.37	15.47	1.10	1.80	YSO	-
446	UGPS J202038.91+405606.9	305.162	40.935	17.59	15.64	14.44	15.80	1.36	1.48	YSO	Flat
463	UGPS J202421.38+421605.6	306.089	42.268		14.50	11.88	12.89	1.00	1.56	YSO	I
465	UGPS J202448.50+391225.7	306.202	39.207	19.31	15.31	12.86	14.32	1.46	1.47	YSO	Flat
474	UGPS J202605.37+420933.0	306.522	42.159		18.23	15.38	16.89	1.51	1.51	YSO	I
476	UGPS J202632.19+410337.9	306.634	41.061	16.58	14.85	13.43	15.61	2.19	2.19	YSO	Flat
498	UGPS J203145.37+363015.5	307.939	36.504		16.58	12.65	14.63	1.98	1.98	AGB	-
500	UGPS J203205.29+424847.9	308.022	42.813	16.69	13.98	11.99	13.45	1.45	1.45	YSO	I
502	UGPS J203222.57+430910.5	308.094	43.153	18.12	15.74	13.99	16.20	2.21	2.21	YSO	I
510	UGPS J203451.05+410923.8	308.713	41.157	13.70	12.45	11.54	12.69	1.14	1.94	YSO	Flat
519	UGPS J203557.20+421408.6	308.988	42.236	15.48	13.64	12.24	13.62	1.38	1.88	YSO	-
533	UGPS J203930.60+425302.1	309.878	42.884	17.14	14.75	12.53	13.84	1.31	1.31	YSO	I
542	UGPS J204256.39+415458.1	310.735	41.916	15.57	14.47	13.95	12.62	1.34	1.46	YSO	Flat

TABLE 3.1: Target list for the spectroscopic sample, including both *Ks* epochs, and the contemporaneous *J* & *H* measurements (Kc indicates the epoch with contemporaneous photometry). Sources without SED classes lacked the $W3$ & $W4$ measurements needed to compute the α parameter. ΔK_{all} represents the maximum observed amplitude in the *K*-bandpass, including both UGPS and 2MASS photometry, ΔK includes only UGPS measurements.

3.2.2 Observations

Our targets were allocated time across 2 telescopes for near-infrared spectroscopy, with 16 being observed with Gemini/NIFS across the summers of 2013 and 2014 (with 8 done each time), and 16 (1 target is in both batches, and 1 IRCS spectrum not being used) being observed with Subaru/IRCS during July 2017. The NIFS spectra were originally part of the PhD thesis of Carlos Contreras-Peña (Contreras Peña, 2015), as mentioned in the declaration. Gemini North is an 8.1m telescope located on Mauna Kea, with NIFS as it's NIR spectrograph; it has a K band spectral resolution of 5290, a spatial resolution of 345kms^{-1}, with a pixel width of 0.04″. Of note is an unusual narrow artifact in a number of the spectra at $\approx 2.28\mu$m, originally thought to be related to Mg I, but is likely spurious owing to it not being seen in the spectra of YSOs taken with other instruments.

Our observations make use of the 8.2m NIR/Optical Subaru telescope, with our observations using the IRCS infrared spectrograph set up with a 52mas pixel scale, the K' filter and a slit width of 0.1″. This provides a resolution of 478.0μm across the K' filter, and a dispersion of 6.1Å per pixel. The targets were observed in two positions, following an A-B-B-A pattern to facilitate sky subtraction. Each target star was observed with a F-type telluric standard at similar airmass for later corrections. The conditions in Hawai'i at the time of observations (1/2 July 2017) were very good on the whole, with the seeing being 0.6" on average, although there did seem to be some issues with rapidly changing conditions on each night, which affected 4 pointings. One final point of note is that the laser-guided adaptive optics system on the telescope had malfunctioned in the preceding days before observation, and as a result it had to be deactivated for this run, which lowered the signal to noise ratio by a factor of 3-4.

3.2.3 Data Reduction

Data reduction was carried out solely in `iraf` using the `noao onedspec` and `twodspec` packages, with the data being cleaned, flat-fielded and sky-subtracted. Spectra were then extracted and wavelength calibrated. The calibration made use of the `identify, reidentify` & `refspec` commands, to apply the calibration spectrum of an argon lamp to the wavelength axis of all other spectra. The spectra of F-type standard stars were used to make the telluric corrections, with the stars weak photospheric absorption features removed by hand before they were divided into the science spectra. Finally the spectra were then cleaned (this being the removal of uncorrelated

noise in the spectrum) using `clean`. The reduced spectra have then been further improved using the `specutils` python package:

- Each spectrum was continuum subtracted, through the fitting of a polynomial (using `numpy.polyfit`), which ignored emission lines as well as the broad water absorption features.
- Further reduction in the noise was carried out using `specutils.manipulation.box_smooth`, which convolves the spectrum with a 1D box kernel. This process smooths the spectrum, and minimises the noise.

To calculate the equivalent widths for each of the spectral lines, I first fit a gaussian to each of the lines in the continuum subtracted spectrum. These fits made use of the `astropy Gaussian1D` model, which was then used as the default profile for the `specutils fit_lines` task. Each line was then passed to the `equivalent_width` routine to produce the final EW value. The 12CO molecular lines were instead fitted with a three component gaussian, where each part has a broader but lower amplitude initial guess than the one before it, to best mimic the shape of the first bandhead. The error on the EW widths is calculated from the equations of Vollmann and Eversberg (2006).

$$\sigma(W) = \sqrt{1 + \frac{\bar{F}_c}{\bar{F}}} . \frac{(\Delta\lambda) - W}{SNR} \tag{3.1}$$

where W is Equivalent width, $\bar{F}_c$ & $\bar{F}$ are mean fluxes for the continuum and line respectively, and $\Delta\lambda$ is the overall line width.

3.2.4 Archival Data

In addition to our spectroscopic data, I have generated light-curves for our targets using the combined WISE/NEOWISE surveys (Wright et al., 2010; Mainzer et al., 2014) (see chapter 2 for more information). These are available for 87% of the sample (27/30), and are constructed from the 3.4μm W1 and 4.6μm W2 bands across a $\sim$10 year time span. Light curves are produced with a `python` routine, finding the median magnitude at each of the wider ALLWISE/NEOWISE epochs, with the photometric error being plotted as the standard error on the mean from each observing block. This is carried out as opposed to using the stated errors because of the large photometric spread at short timescales not being consistent with the error ranges, a common issue with this dataset. Additionally the light curves contain Spitzer data (as taken from

Glimpse360, Whitney et al. (2011)), which have been colour corrected to bring the fluxes in line with similar WISE band passes, these corrections coming from Antoniucci et al. (2014).

3.3 Results

Looking at all of the data available for each target we can split our targets into multiple groups, which are described below:

- EX Lup-Type stars: characterised with an emission spectrum featuring 12CO, H I & H_2 (noting that the H_2 is seen in the embedded members of this class). In addition the star will have clear photometric evidence of an outburst. These outbursts can either be of the usual (order of months to 1 or 2 years) length, or of the much more extended duration, as noted by Contreras Peña et al. (2017); Guo et al. (2021).

- Quiescent EXor candidates: this grouping represents stars that have had an outburst of ≥ 2 mag (in order to distinguish them from short term variables), and spectra that have some emission features, notably those associated with magnetospheric accretion, but little to no emission of CO. Ideally these stars will also have bluer colours during outburst (if multiple epochs of colour information are available), mimicking behaviour seen in Lorenzetti et al. (2012).

- FU Ori candidates: distinguished from other sources by a combination of a large photometric outburst, combined with a spectrum with strong 12CO absorption lines. There is no longer a required timescale on the initial outburst, although the time taken to return to the initial luminosity should be high.

- Dippers: these are non-outbursting variable YSOs, characterised by a drop in flux, caused by extinction in one form or another. The events are generally thought to mean dips of longer than >1 year, such as is seen in the star AA Tau. Short duration dips are also common (and observed in AA Tau too), and it is thought that the extinction is as a result of a warp (magnetically induced) in the stars inner-disk region. See Bouvier et al. (2007b, 2013b) for detail on AA Tau specifically and the samples of dippers in YSOVAR (Morales-Calderón et al., 2011b) and the review of Rice et al. (2015) for a more general look at the class.

- Other non-outbursting YSOs: Any of the stars whose photometric or spectroscopic behaviour does not match with the definitions above is grouped here, and any previous eruptive behaviour cannot have it's initial cause determined. The stars are then loosely divided into two groups, those with emission spectra and those with absorption spectra. The initial cause of the variability in these stars is unknown, but given the lower amplitudes (≤ 1.5 mag in most cases), most are likely 'short-term variables', which dominate the number density of variable YSOs at these amplitudes (Contreras Peña et al., 2017).

Source Number	Classification	Eruptive?	Comments
236	FUor	Yes	Eruption seen in *Ks*-bandpass images, and the spectrum resembles others of this class
500	FUor	Yes	Eruption seen in *Ks*-bandpass images, and the spectrum resembles others of this class
463	EXor	Yes	Prominent emission line spectrum, with a >1 mag MIR outburst observed in 2022
533	EXor	Yes	NIR spectrum has a strong resemblance to that of EX Lupi, and has a confirmed H_2 outflow
123	EXor-Q	Possibly	Initial photometric outburst was >1.5 mag, spectrum has strong accretion signatures
144	EXor-Q	Possibly	Initial photometric outburst was >1.5 mag, spectrum has strong accretion signatures
374	EXor-Q	Possibly	Initial photometric outburst was >1.5 mag, spectrum has strong accretion signatures
428	EXor-Q	Possibly	Initial photometric outburst was >1.5 mag, spectrum has strong accretion signatures
476	EXor-Q	Possibly	Initial photometric outburst was >1.5 mag, spectrum has strong accretion signatures
446	Dipper	No	WISE LC has quasi-periodic fading events
465	Dipper	No	WISE LC has long term fading events
474	Dipper	No	WISE LC has long term fading events
152	Class I YSO	No	No obvious eruption is seen, spectrum is featureless
196	Class I YSO	No	No obvious eruption is seen, spectrum is featureless
221	Class I YSO	Possibly	Spectrum shows strong signs of a wind or outflow, Untimely LC has a 3 mag outburst.
321	Class I YSO	No	No obvious eruption is seen, spectrum is featureless
441	Class I YSO	No	No obvious eruption is seen, and the spectrum is dominated by absorption
502	Class I YSO	No	Does spectrally resemble a FUor, but combined 2MASS and UGPS photometry does not concur
19	FS YSO	No	No obvious eruption is seen, spectrum has faint emission features
433	FS YSO	No	No WISE LC, featureless spectrum, bluer NIR colours than class I YSOs
439	FS YSO	No	WISE LC shows no outbursts, spectrum is lacking any outburst signatures
142	Class II/FS YSO	No	No WISE LC, featureless spectrum, bluer NIR colours than class I YSOs
510	Class II YSO	No	Spectrally observed ongoing accretion with <1 mag photometric variation
519	Class II YSO	No	No observed eruptive behaviour in either the light curve or spectrum
542	Class II YSO	No	Spectrally observed ongoing accretion with <1 mag photometric variation
136	D-Type?	No	Unusual spectrum with mixed emission and absorption features including 13CO
284	D-Type?	No	Unusual spectrum with mixed emission and absorption features including 13CO
420	D-Type?	No	Unusual spectrum with mixed emission and absorption features including 13CO
443	D-Type?	No	Unusual spectrum with mixed emission and absorption features including 13CO
498	AGB	No	Prominent 13CO absorption, faint metal emission lines & no water absorption features

TABLE 3.2: Preliminary classifications of the YSOs in this sample, with a comment on their possible eruptive status and a brief summary of the associated evidence.

From this sample we find 1 likely outbursting EXor (with a long duration outburst), 6 Likely Quiescent EXors, 2 FUors, 4 'dippers' (2 of which show potentially periodic light-curves), and 12 other Non-outbursting YSOs. In addition 5 of the sources are now perceived to be evolved sources, with 4 dusty symbiotic star candidates, and 1 AGB star (Source 498). The breakdown of the sources in the spectral sample can be seen in table 3.2, with a brief description of the core characteristics from the NIR spectrum and MIR light curve (where present). Given the selection criteria (discussed earlier) the number of obvious eruptive sources is low (at 3), although the wide time gap between the UGPS observations and the Subaru/IRCS spectroscopy would make short duration eruptions hard to confirm. It should also be noted that spectral features associated with sodium are absent in the majority of spectra, which is unexpected considering the 2.20μm line is a common diagnostic tool in YSOs. A notable feature within the MIR light curves is the lack of repeated burst-like events, wherein only 1 source has showed a clear second brightening event.

In the sections below we will discuss the different members of each of the groupings laid out previously, with analysis of their NIR spectra and LCs (MIR and NIR from VVVx where available).

3.3.1 EXors and EXor-like Variables

The nature of the wide spacing between the NIR photometry and spectroscopy meant it was unlikely to find many that were still in a period of outburst; i.e classical EXors. However recent work by Guo et al. (2021) has shown that eruptive YSOs with mixed characteristics from both FUors and EXors are the most common. These stars are similar to the loose grouping of MNors (or V1647 Ori-like stars), but could more accurately be described as long-duration EXors (possibly as a new group within the MNor class). They can have long term outbursts, but maintain the accretion dominated emission spectra of an EXor-like star, and stars with these outbursts would still be detectable with the observation spacing used here.

Relevant to this discussion is the difficulty associated with disentangling long duration EXor-like events from 'dippers' with spectra and long duration light-curves alone. The 'dippers' found in Guo et al. (2021) had a range of spectra, but most often were emission dominated and red, with varying levels of 12CO emission and prominent molecular hydrogen features. This renders them similar to EXors, and the same is true of the majority of MTVs present in the aforementioned sample. It's important to note that the sources labeled as 'dippers' in the aforementioned paper,

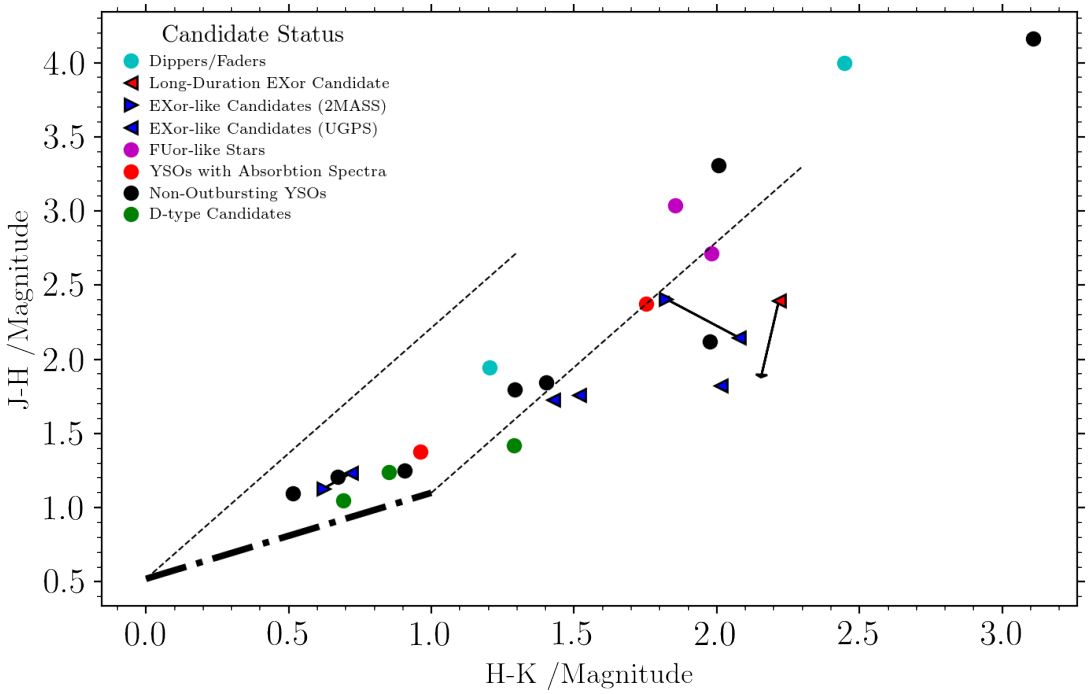

FIGURE 3.1: Contemporaneous J-H vs H-K colour-colour diagram for the variable star sample. Where available, 2MASS colours or lower limits are plotted for the outbursting sources, linked with arrows (not present if there was no 2MASS detection in any filter). There is a large overall spread for the different groups. Three candidate non-YSOs fall off the T-Tauri locus (black line), but are still mixed in with a selection of class I YSOs, illustrating the difficulty of disentangling the proposed D-type symbiotic systems using colour cuts alone. Linked data points indicate the trend in colour change (from 2MASS to UGPS) for the EXor candidate stars, discussed further in section 3.3.1.2. Dashed lines indicate the reddening vectors from 0 to 20 A_V.

may instead have been singular short term extinction events that were observed overlaid on a pre-existing long term accretion event, and thus were not 'dippers' in the traditional sense. Both of these groups will have lower amplitude events in the MIR as compared to the NIR selection, and thus we will be unable to rule these classifications out with confidence in this section, and would thus make excellent candidates for follow-up NIR photometric monitoring.

Source 533 was possibly in a period of sustained accretion when the spectrum was taken, while sources 19, 428, 443 and 519 were more likely in a quiescent phase. Sources 474 and 144 are both seemingly eruptive, with quasi-periodic behaviour, but don't spectrally resemble an EXor variable.

All equivalent widths are in Å				
Source Number	Brγ (2.16μm)	H_2 (2.12μm)	H_2 (2.22μm)	12CO (2.29μm)
19	-3.215 $\pm$ 0.501	-1.941 $\pm$ 0.209	n/a	n/a
123	-7.342 $\pm$ 0.827	-1.919 $\pm$ 0.361	-0.932 $\pm$ 0.261	n/a
136	-6.953 $\pm$ 0.151	n/a	n/a	19.609 $\pm$ 0.637
142	1.558 $\pm$ 10.36	-2.162 $\pm$ 1.023	-1.499 $\pm$ 0.674	n/a
144	-8.263 $\pm$ 0.127	n/a	n/a	3.359 $\pm$ 0.751
152	-2.224 $\pm$ 2.827	-1.442 $\pm$ 0.836	n/a	n/a
196	-1.49 $\pm$ 0.552	-3.497 $\pm$ 0.328	-1.706 $\pm$ 0.349	n/a
221	n/a	-1.201 $\pm$ 0.479	n/a	n/a
236	n/a	n/a	n/a	11.113 $\pm$ 1.172
284	-4.238 $\pm$ 0.204	n/a	n/a	7.168 $\pm$ 0.631
321	-1.954 $\pm$ 0.322	-1.484 $\pm$ 0.652	n/a	n/a
374	-6.06 $\pm$ 0.176	-2.988 $\pm$ 0.175	-1.672 $\pm$ 0.126	n/a
420	-1.369 $\pm$ 1.593	-8.107 $\pm$ 1.245	n/a	n/a
428	-6.728 $\pm$ 0.118	n/a	n/a	n/a
433	-1.874 $\pm$ 1.529	n/a	n/a	n/a
439	-5.703 $\pm$ 0.336	-1.257 $\pm$ 0.517	-0.748 $\pm$ 0.34	8.147 $\pm$ 1.167
441	n/a	n/a	n/a	7.922 $\pm$ 1.783
443	-8.015 $\pm$ 0.115	n/a	0.797 $\pm$ 1.846	3.587 $\pm$ 0.449
446	n/a	n/a	n/a	7.837 $\pm$ 1.142
463	-1.974 $\pm$ 0.577	-1.812 $\pm$ 0.156	n/a	n/a
463	-5.951 $\pm$ 0.2	-1.69 $\pm$ 0.22	n/a	n/a
465	-1.214 $\pm$ 8.713	n/a	n/a	n/a*
474	-2.322 $\pm$ 1.242	-1.21 $\pm$ 0.315	n/a	-4.08 $\pm$ 1.272
476	-23.118 $\pm$ -0.241	n/a	1.011 $\pm$ 6.209	n/a
498	n/a	-3.664 $\pm$ 1.928	n/a	11.256 $\pm$ 1.675
500	n/a	n/a	n/a	24.166 $\pm$ 0.933
502	n/a	n/a	n/a	n/a*
510	n/a*	n/a	n/a	n/a
519	-4.811 $\pm$ 0.277	n/a	n/a	3.004 $\pm$ 0.811
533	-6.88 $\pm$ 0.181	-3.356 $\pm$ 0.171	-1.039 $\pm$ 0.26	-6.626 $\pm$ 0.673
542	-3.273 $\pm$ 0.129	n/a	n/a	n/a*

TABLE 3.3: Measured EWs for important lines in the spectrum of YSOs. Containing hydrogen recombination, two molecular hydrogen and carbon monoxide lines. Many spectra had low S/N around the location of the 2.20μm sodium doublet, so this feature is not included here. Additionally lines marked with n/a* denote that the feature is present in the spectrum, but it is too noisy to accurately fit.

3.3.1.1 Source 533

533 resembles a traditional EX Lupi-type YSO, with its spectrum (Fig. 3.2) showing strong emission features in HI, H_2 and 12CO. The equivalent width for the HI Brackett γ line being -6.9*Å*, and the molecular hydrogen features being at -3.4*Å* and -1.0*Å* for the S(1) and S(0) transitions respectively.

The H_2 line ratio is likely very large, owing to the non-detection of the 2.24μm H_2 S(1) line. This could indicate a shock (Greene et al., 2010), and could be as a result of disk winds, which are now thought to be an important driver of disk evolution, and indicator of high mass accretion

rates (see the recent chapter of protostars and planets VII by Manara et al. (2022) for an in- depth review).

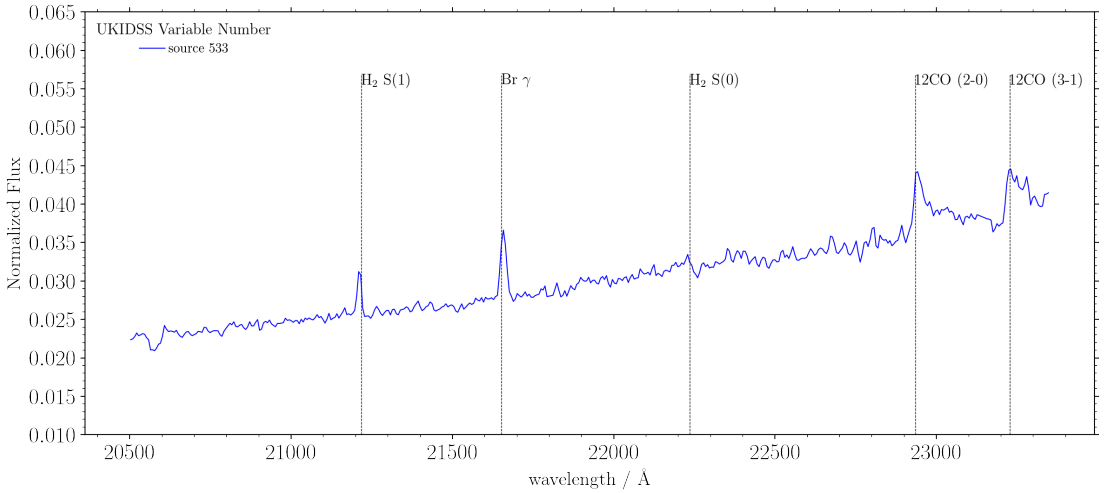

FIGURE 3.2: Subaru *Ks*-band Spectrum for the EXor-like source 533. The molecular hydrogen features tally with a known outflow, and the 12CO emission is seen with 2 bandheads.

The star has a molecular hydrogen outflow detected in the UWISH2 (photometric H_2) survey of the Cygnus-X cluster (Makin and Froebrich, 2018), and is the only star in this sample that appears in both UKIDSS and UWISH2. Whilst this proportion is lower than would be expected for eruptive YSOs, it can be partially explained by UWISH2 having detection problems for regions of K-band >6 mag. This is not uncommon for stars in the UKIDSS sample, which are mostly younger, class I sources.

The first UGPS measurement occurred in 2006, with the star at 12.5 ± 0.02 mag in K, before falling to 13.8 ± 0.02 at the second epoch in 2011. Compared to the 2MASS values (obtained in late 1998) the change in NIR colours is minimal, with $H-K$ at 2.1 in 1998 and 2.2 at the brightest observed point in 2006. Given that EXors traditionally get bluer during outburst (although the actual value of this change has a large variance), if this system is EXor like, we can infer that the initial observed eruption might be of longer duration than traditional systems, and was occurring for at least the first 8 years. EXor-like stars of this type are being more frequently observed (see the group of 'Long term emission line' sources from Guo et al. (2021)) but are currently under-studied.

The MIR light curves (Fig. 3.3) have limited long term variation, with a maximum amplitude of ≈ 1 mag across the full coverage, and of ≈ 0.6 mag within the regularly sampled NEOWISE data. The Subaru/IRCS spectral observation date is marked on the figure, and is close to the

brightest point, consistent with the high accretion rate suggested by the emission features. MIR colour change is slightly variable, becoming ≈ 0.2 mag more blue by the first NEOWISE epoch, whose photometry is commensurately brighter. This colour trend holds throughout the observed light curve, albeit at low levels.

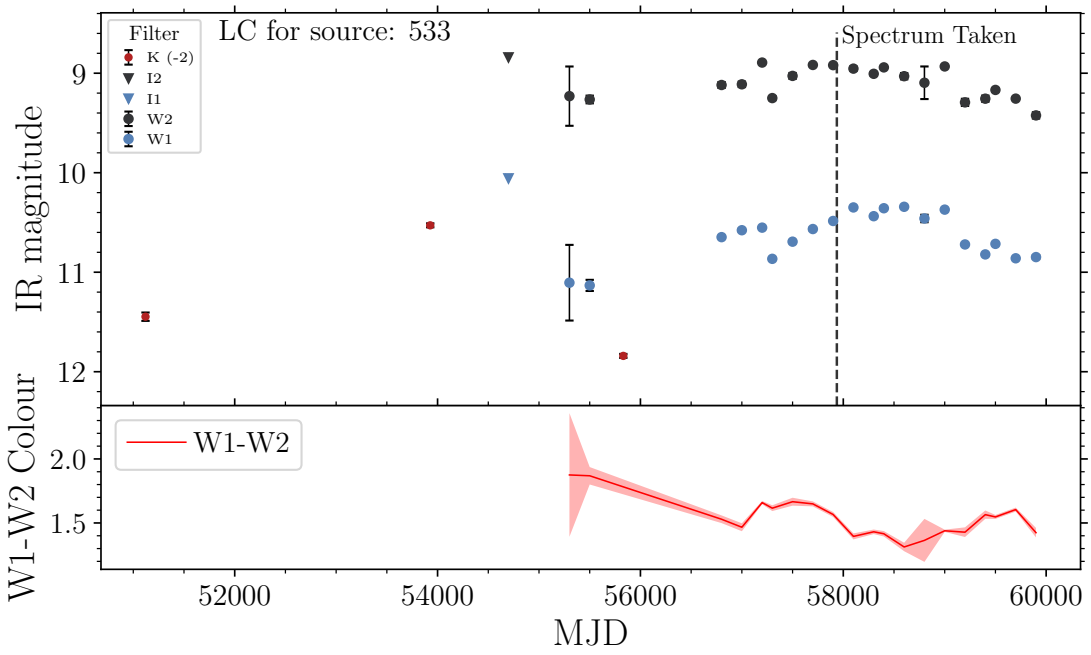

FIGURE 3.3: MIR light curve for Source 533. The NEOWISE data show no obvious outbursts, implying EXor-like eruptions have ceased. The detected variability is on the order of 0.5 magnitude, which is inline with general short-timescale variable behaviour for YSOs.

3.3.1.2 Quiescent EXors

Five of the six stars in this group displayed at least 2 magnitude increases in brightness in the original survey, either from the first to the second epoch of UKIDSS, or from 2MASS to UKIDSS epoch a (See black markers in Figs. 3.7 & 3.8 for the dates and fluxes). The amplitudes for these stars are higher than the approximate upper bound for short-term variability in YSOs (normally quoted as ≤ 1.5 mag, Contreras Peña et al. (2017)), hence there is a stronger chance that this group underwent EX Lup-type outbursts between the observations.

The more recent spectra however show only signs of continued accretion, via stronger than average Brackett γ equivalent widths, with fairly faint molecular hydrogen lines, and minimal or no CO in emission. The NIR colours ($J-H$ & $H-K$) for these sources provide an insight into the possible history of the objects, using the trends of EXors in outburst and quiescence

from Lorenzetti et al. (2012). Noting that both classical and non-standard EXors are on or above the classical T-Tauri locus during outburst, and redder in $H-K$ when quiescent. Whether or not this holds true for class I sources remains to be seen, but the information in figure 3.1 does appear to sustain the colour behaviour of outbursting/quiescent sources. All of the sources that have J-band data seem to follow this trend, sources that had their contemporaneous multi-colour photometry taken before or after the K-band variability are found to the right of the TT locus i.e are more red. It's worth mentioning that source 463 was not detected in J-band data, in either UGPS or 2MASS.

Sources 123, 374 and 463 have stronger hydrogen emission features, but still minimal CO emission and the spectra are too noisy to distinguish any sodium emission features. Source 463 (GPSV28) is an interesting case as it has two spectral epochs, with a 2015 spectrum displaying stronger H_2 than H I, but the reverse in the 2017 spectrum. This implies an increase in the accretion rate between the two observations, possibly corresponding to a 0.5 mag variation seen in the NEOWISE light curve.

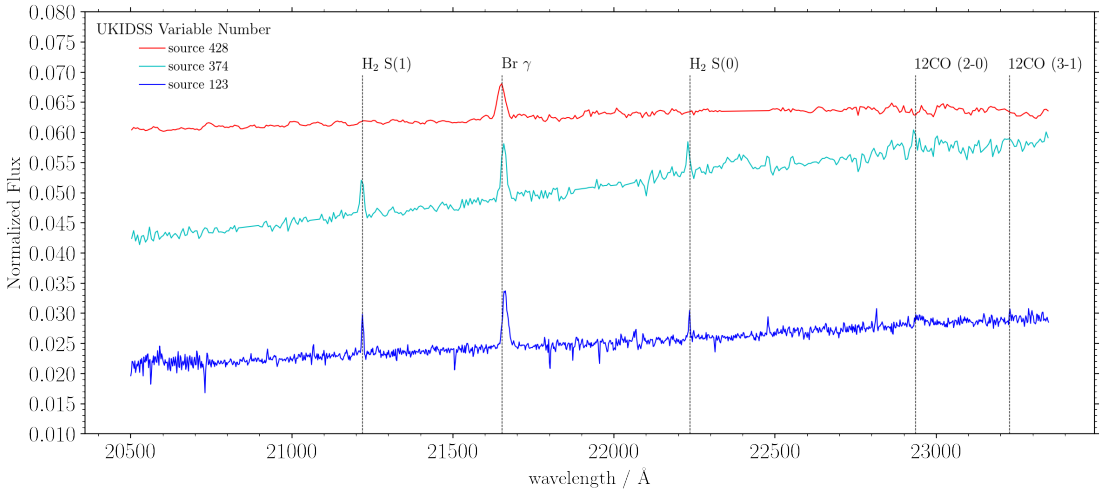

FIGURE 3.4: *Ks*-band spectra for three possible quiescent EXors. Source 123 contains weak 12CO emission but is otherwise similar to EXor-like variables, whereas any CO in source 374 is harder to confirm. Source 428 is dominated by Brγ, with no molecular hydrogen or 12CO visible in the spectrum.

All the stars in this group have similar MIR light curves (see Figs. 3.7 & 3.8), featuring repeated (often quasi-periodic) variation on the order of 0.5 mag. The $W1-W2$ colours are between 1 and 2, with source 144 as the only exception, with colours $W1-W2<1$ for the duration, and a vague S-shape variation over the past 8 years. Source 463 is also of note here, as the latest

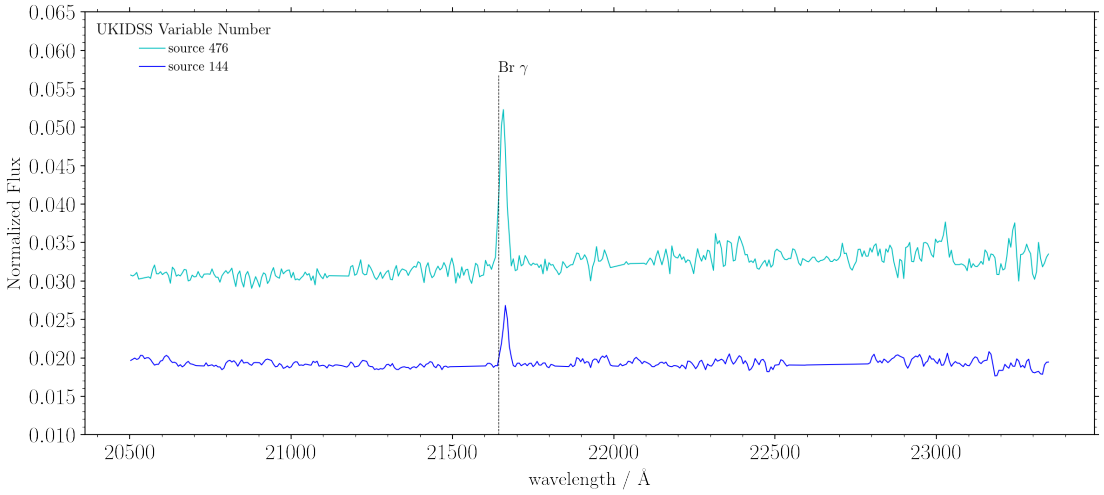

FIGURE 3.5: IRCS *Ks*-band spectra for two sources dominated by emission from the Brγ hydrogen recombination line.

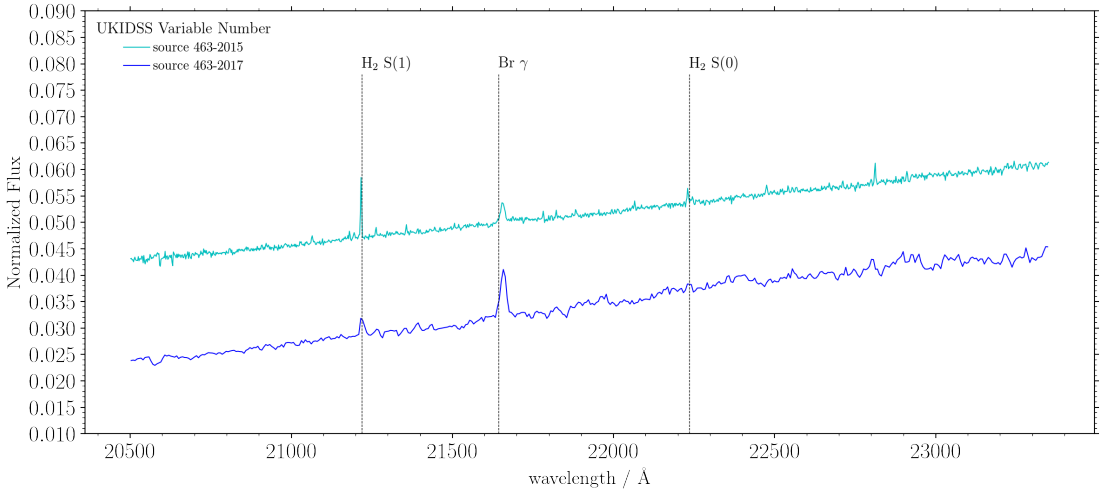

FIGURE 3.6: *Ks*-band spectra for source 463 across two epochs: 2013 with Gemini/NIFS and 2017 with Subaru/IRCS. The most notable change between the observations is the switch from emission being molecular hydrogen dominated in 2013 to recombination dominated in late 2017. This implies in increase in accretion rate, although no corresponding outburst is seen in Figure 3.8 (2nd panel).

NEOWISE data has shown a $>$ 1mag outburst, that lasted for over a year, indicating a possible repeat of the originally detected outburst behaviour.

The final stars in this group are sources 144 & 476 which have spectra dominated by H I, with equivalent widths of-8.3Å & -23Å respectively (no other features are apparent). Both objects have an IR excess and are associated with local SFRs (Serpens OB2 and Cygnus-X respectively) so they are likely YSOs. For Source 476 specifically the extreme Bracket γ EW (< -23Å) would imply an eruptive event, however there is no indication of any such event within the MIR light curve. Such a problem forces us to question our ability to reliably detect shorter eruptive events, such as those seen in work by Guo et al. (in prep.). Those authors work will display the extent of short term spectral variation for EXor-like YSOs. For example it will be impossible to distinguish the multiple timescale variables (MTVs) found by Guo et al. (2020, 2021) (with numerous eruptive events on timescales shorter than the $\sim$6 month spacings of NEOWISE observations), that are likely to be prevalent within this sample. Given that these objects formed 52.6% of the latter of those authors samples, the two epoch sampling is a significant drawback in this regard.

3.3.2 Candidate FUors

The two following sources were initially included in the thesis of Contreras Peña (2015), wherein the combination of spectral features, NIR colours, and *K*-band amplitude led to their presumptive classification as embedded FUors. Here I add both the spectra, and 2MASS forced photometry to confirm this nature more explicitly.

Sources 236 and 500 both spectrally resemble FU Orionis-type eruptive YSOs, with relatively featureless (albeit noisy) spectra, and prominent absorption of 12CO. The equivalent width of the first bandhead is 11.1 ± 1.20*Å* for source 236 and 24.2 ± 0.93*Å* for source 500. Classically, confirming a FUor requires that the original outburst be observed, and in these cases it seems as if the UKIDSS photometry does not display enough of an increase to do this, with peak amplitudes in *Ks* of 1.7 (from 2007 to 2009) and 1.5 (between 2006 and 2009) for sources 236 and 500 respectively. This however does not show the complete picture for two reasons: first, more recent work has found two low amplitude FUors, such as VVVv16 and VVVv237 in Guo et al. (2021). Secondly because both stars show non detections in the earlier 2MASS survey (both 1998). The environments of the two stars are very different: source 500 is in a relatively uncrowded field in the Cygnus-X complex, whereas source 236 lies within a region of high extinction (The W48 complex), from nebulosity associated with local star formation. Thus the

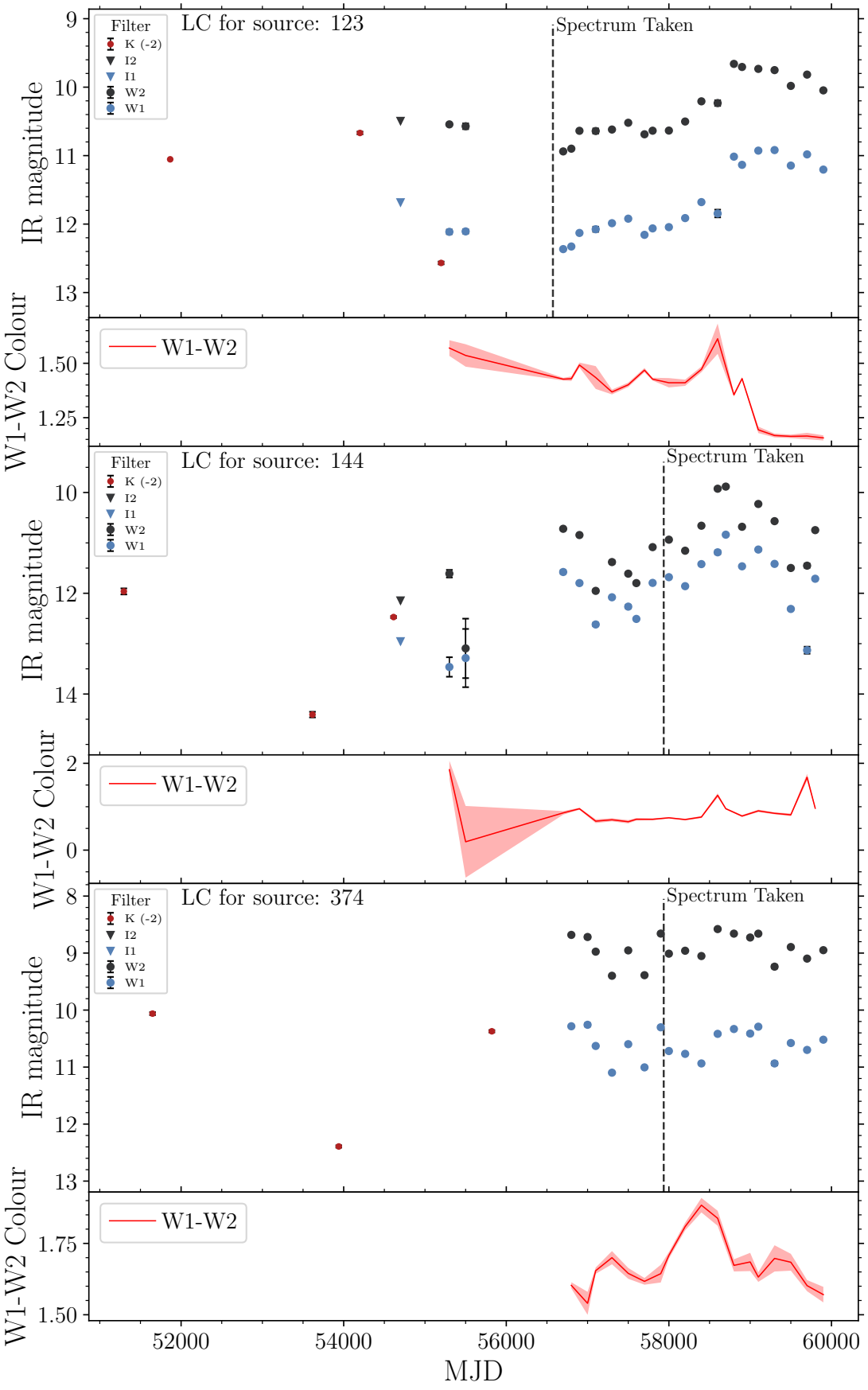

FIGURE 3.7: NEOWISE MIR light curves for three of the quiescent EXor candidates discussed in section 3.3.1.2. In addition to the NEOWISE $W1$ and $W2$, also plotted are the Spitzer $I1$ and $I2$ measurements, as well as UGPS and 2MASS K observations. The dashed lines indicate the MJD of any spectroscopic observations. The red line measures the W1-W2 colour at each epoch.

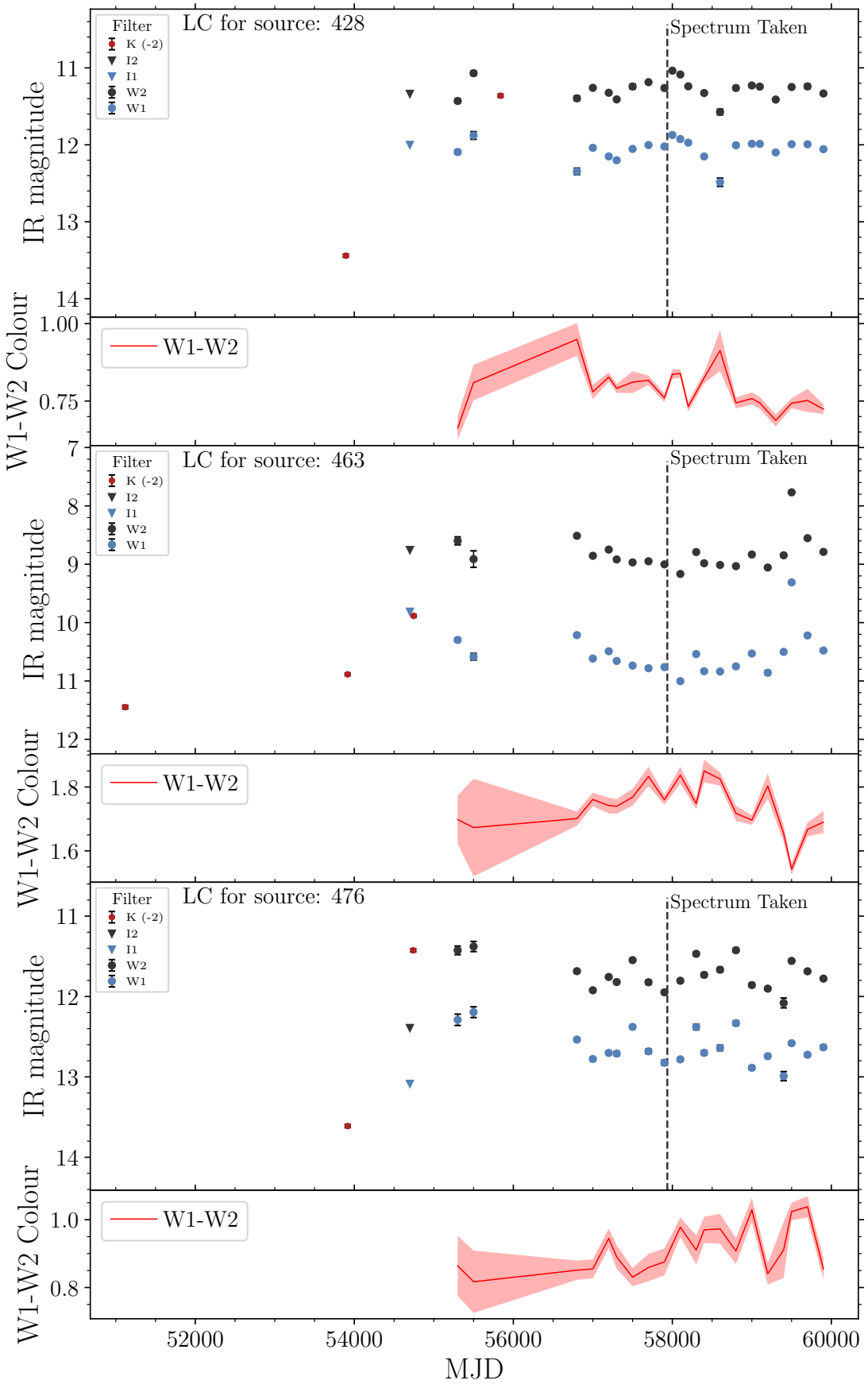

FIGURE 3.8: MIR light curves for the remaining three quiescent EXor candidates discussed in section 3.3.1.2.

lower limits for the 2MASS data are not the same for both stars, with the calculated 3σ lower limit (via a `photutils` routine [1]) for source 500's field at 16.0 mag, & source 236's at 14.5 mag. For source 500 the lower limit of amplitude can now be set at ≥ 4.02 mag, over ≈ 4000 days, which is similar in scale to VVVv721 (Guo et al., 2021), and thus confirmed as a FUor (as suggested in Contreras Peña et al. (2014a)). It is more challenging to offer the same confirmation for source 236 however, because even a 1σ lower limit (14.8 mag) is brighter than the fainter of the two UGPS measurements. A visual inspection of the image confirmed that the source is undetectable above the background (which is high as a result of the aforementioned nebulosity), and thus it can be reasonably assumed that the detected outburst is real, but the amplitude is still unknown.

In both cases the rise times for the sources are unknown, but could be up to the order of years. While not like the prototypical FU Ori, this fact is no longer of significant note, with similar behaviour seen in stars such as Gaia17bpi (Hillenbrand et al., 2018). NEOWISE and unTimely (see chapter 2) light curves for sources 500 and 236 respectively help to reinforce the assumption of a FUor classification:

- Source 236 is detected in the stacked unTimely catalogue in about half of the available epochs, with the nebulosity clearly affecting photometry. Epochs with good quality data do show a reasonably consistent trend however, with the star slowly fading by ≈ 0.2 mag in $W2$ and a little more in $W1$. One small 'dip' can be seen in late 2016, which are not uncommon in post-outburst FUors, and are normally more prevalent in the NIR, such as in VVVv237.

- Source 500 is gradually fading, displaying a reduction in brightness of approximately 0.5 mag in both *W1* & *W2* across the 5.5 years of available NEOWISE observations. This trend has continued from ALLWISE, and more noticeably from earlier Spitzer observations. The return to a quiescent state does seem faster than classical FUors, although more systems such as this are being found.

[1] This makes use of the `ImageDepth` method, within the `utils` package. The method takes the zero-point for the instrument, and a selection of magnitudes of stars in the image, and computes the lowest detectable flux for a given precision in sigma (quoted here are 3σ values) for a large number of randomly placed apertures.

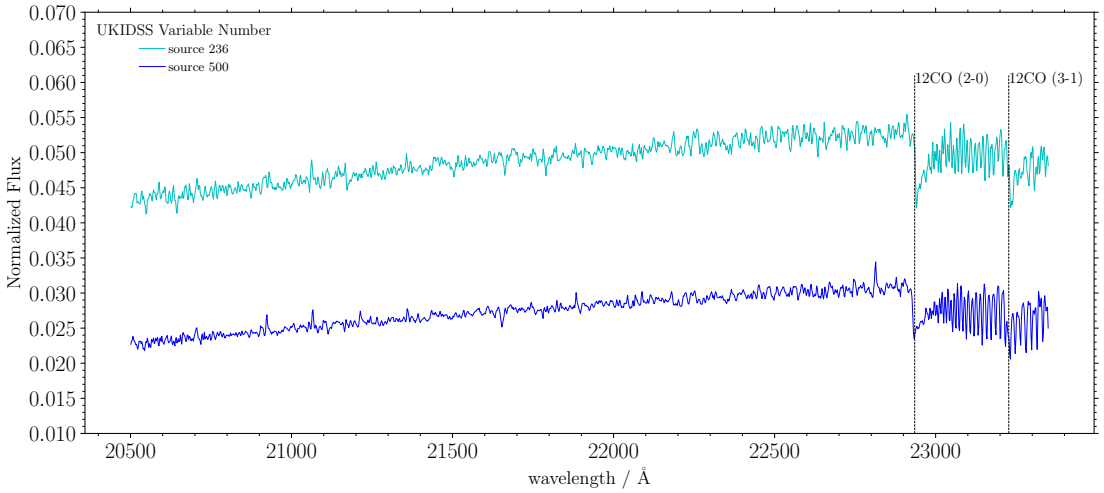

FIGURE 3.9: Gemini NIFS spectra for two FUor-like sources, first seen in the thesis of Contreras Peña (2015). Both are typical of FUors, with mostly featureless spectra, with notably strong absorption of 12CO.

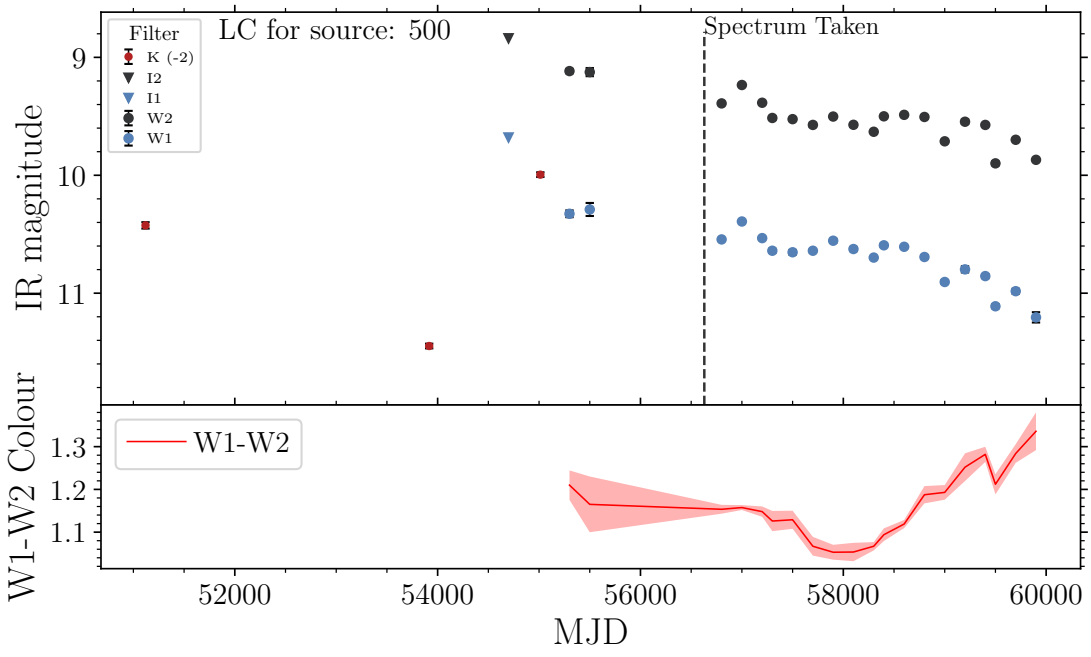

FIGURE 3.10: NEOWISE light curves for the FUor-like Source 500, it shows the fading trend of FUors post-outburst, with minor variation seen. In this cases the UKIDSS outburst was recorded before the original WISE observations, hence the lack of its signature within the light curve.

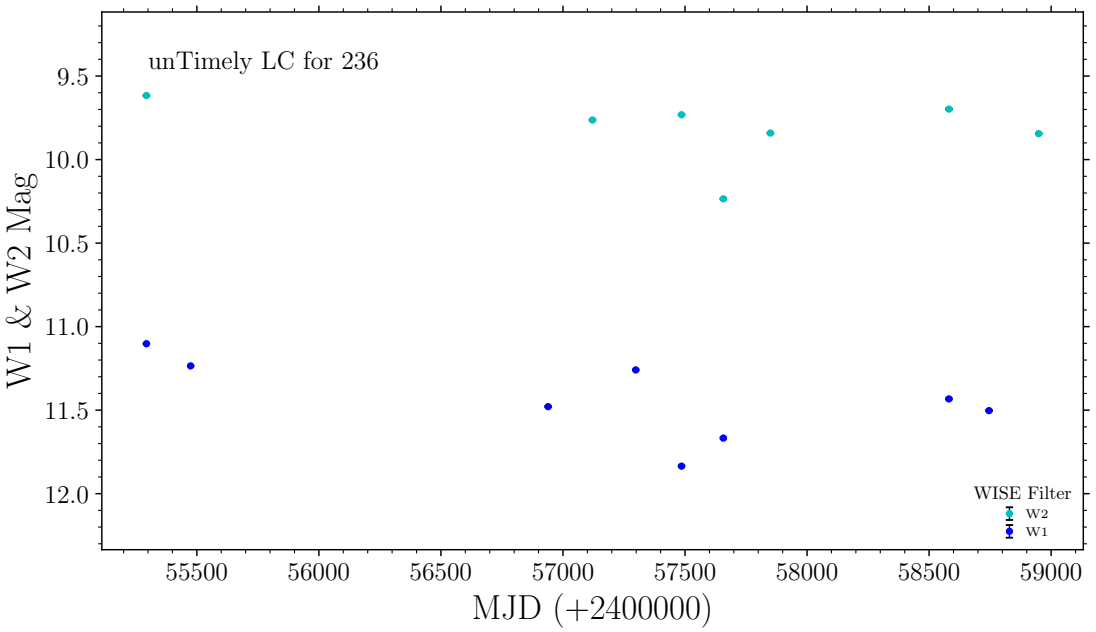

FIGURE 3.11: UnTimely light curves for the FUor-like Source 236. The overall trend is similar to other post-outburst FUors, fading by approximately half a magnitude, with some additional short timescale variability. The missing epochs are likely a result of the highly nebulous environment surrounding the star.

3.3.3 Non-Outbursting YSOs

16 of the thirty YSO candidates showed no obvious tracers of recent outburst-like behaviour, with weak or no emission features, no confirmed outflows, and minimal variation seen in time-domain MIR photometry. This group is spread throughout the colour-colour diagram in figure 3.1, with all stars following the standard CTTS tracks.

3.3.3.1 YSOs with Absorption Spectra

This loose grouping includes two sources with absorption spectra (see Figure 3.12), but lacking the CO absorption line strength and otherwise reasonably featureless spectrum of FUors. Source 441 has multiple additional absorption lines, notably sodium and calcium, with faint molecular hydrogen emission as well. Source 502 lacks these lines in absorption, although it does have faint H_2 emission lines, with 2.22μm being the most prominent. The spectral lines indicate that the CO gas is cooler than sources 236 and 500 in all three stars, indicating a lower accretion rate for the central object than seen in FUor-type systems, leading to less heating of the disk mid-plane.

The Light curves for Source 441 (see figure 3.13), shows possible quasi-periodic variation, likely driven by extinction via obscuration of the central star, possibly from a warped disk, in a similar vain to AA Tau. This appears to be on a timescale of ∼1800 days, but there is significant secondary aperiodic variation in concert with the longer duration trend.

Source 502 by comparison shows minimal variation aside from that which is expected in all YSOs. There is a weak dimming trend over the length of observation, in a similar manner to source 500 (and other FUor systems besides), with the reduction totalling 0.25mag. Whilst it is impossible to determine whether or not source 502 has previously undergone an FUor-type outburst with the available data, it is a possibility that cannot be ruled out.

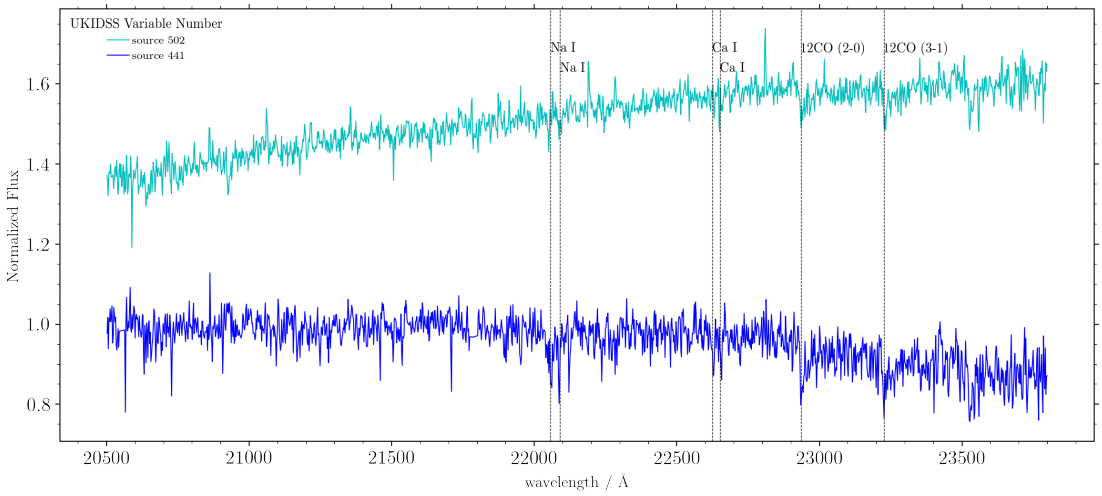

FIGURE 3.12: Spectra for the two YSOs described in section 3.3.3.1. All are absorption dominated spectra, with prominent 12CO lines. Source 502 has a redder continuum, and a faint H_2 emission line at 2.22μm.

3.3.3.2 YSOs with Fading/Dipping Behaviour

Two of the more noteworthy light curves belong to sources 465 and 474, which show drops in brightness of approximately 1 and 3 magnitudes (in both $W1\&W2$) respectively. The most recent NEOWISE (March 2022) data shows possibly repeating behaviour for source 465, similar to the 'dippers' discussed earlier. Missing data between the original WISE epochs and the later reactivation prevents two cycles being clearly seen however. For Source 465 the amplitude is 1.09 mag and 1.17 mag in *W1 & W2* respectively, with similar $W1-W2$ colours throughout. Source 474 has similar characteristics to 465, albeit at a much larger amplitude. In this instance recording a 3.33 mag drop in brightness since January 2017 in *W1*. In *W2* the change is 2.39

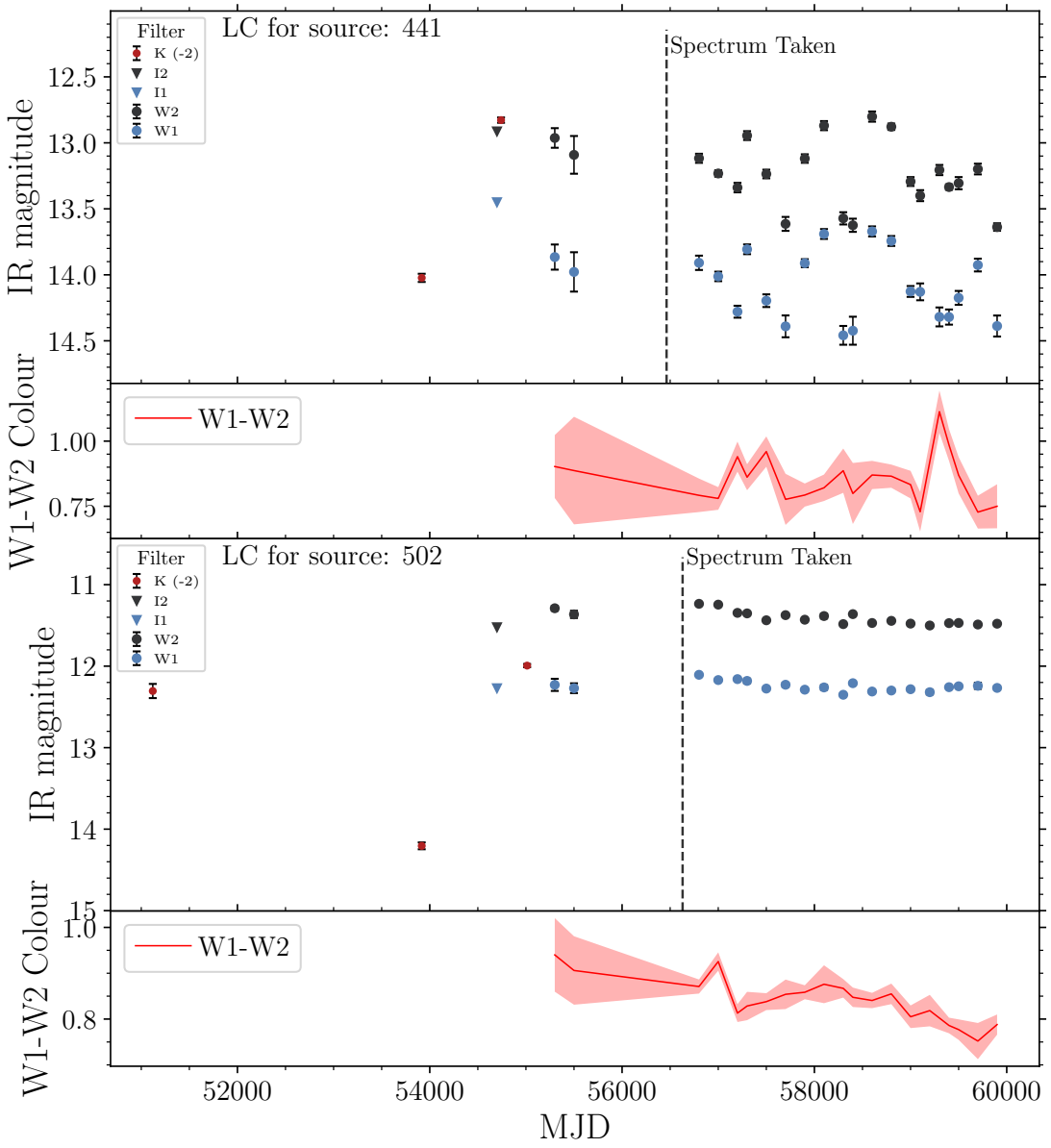

FIGURE 3.13: MIR (NEOWISE) light curves for the sources with absorption spectra. Source 441 has quasi-periodic dimming events, likely caused by extinction, given the time-frame. By comparison source 502 lacks any of the features seen in the other two stars, with the star fading by 0.25mag and 0.27mag in *W1* & *W2* respectively. It more closely resembles the light curves of sources 236 and 500, both FUor-like sources.

mag, with the $W1-W2$ colour getting redder as the system gets fainter, from 1.69 to 2.66, implying that the event is extinction driven. Both have spectra from NIFS, with source 474 having CO and Brackett γ clearly visible in emission. Molecular hydrogen is also present in emission, but the spectrum was partially damaged in the 2.12μm region by a cosmic ray so is hard to draw conclusions from. Combining the spectrum and the light curve for Source 474, similarities to V2492 Cyg (Kóspál et al., 2013b) can be seen, noting the faint emission spectra, low MIR colours and a deep fading event - although it should be noted that the MIR amplitude of the aforementioned YSO is not known for certain, the dimming event occurred in the time between ALLWISE and NEOWISE. The reddening between the bright and faint states (mjds - 58000 to 59000) is on the order of 0.5 mag, which is in line with the roughly 50% extinction relation predicted by Wang and Chen (2019) for the WISE passbands (i.e the difference in $\frac{A_\lambda}{A_V}$ is 0.039 mag - 0.026 mag for W2 and W1). This provides an indication that the observed variability is caused by extinction, rather than a drop in accretion rate.

Source 465's spectrum has a very low S/N ratio, but some absorption behaviour can be seen in the first two CO bandheads. This is contemporaneous with a dimming event, and is in broad agreement with other non-outbursting YSOs, as seen in the large samples of Greene and Lada (1996). Given the repetitive nature of the light curve it can be assumed the star is a 'dipper', although with some differences to sources 441 (as discussed in section 3.3.3.1). Notably the fading events are colour independent and of longer duration.

Source 446 is spectrally similar to Source 441 mentioned earlier, but with clear repeating (and quasi periodic at $\sim$1000 days) dipping behaviour, its $W1-W2$ colours peak at 1.16, recorded in the second dimming event. It remains to be seen if a similar event was the cause of the originally observed *Ks* variation, but it seems likely. Four dips are recorded (Five if the Spitzer non-detection can be trusted), the quasi-periodicity and long duration indicate that the variability is likely coming from a warped disk as opposed to extinction from an accretion column (observed in dippers seen in optical light). That hypothesis is supported by the slightly red slope of the spectrum and the associated absorption spectrum, normally indicators of emission from a warm disk. Given that the spectrum was obtained at a time likely to have coincided with another dip, we could assume that the same is true for the similar spectrum of source 441. Source 441 has more stochastic variation, but it lacks the pronounced colour change of source 446, as well as having lower amplitudes in both WISE bands. These two stars are likely the only two verifiable dippers in the sample.

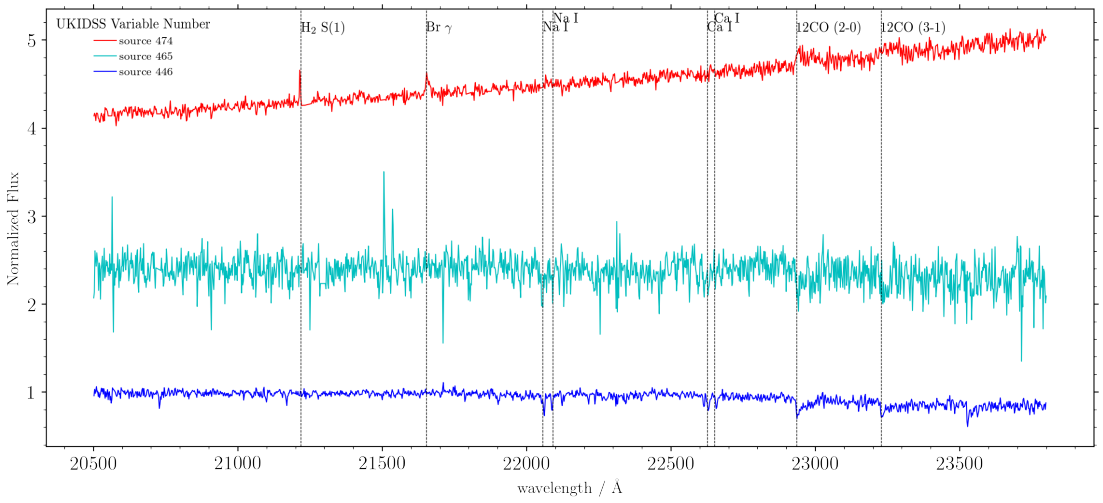

FIGURE 3.14: *Ks*-band spectra for sources 446, 465 and 474. Source 474 shows clear hydrogen emission features, both molecular and recombination. There is also faint CO emission (EW = -4.08±1.27). 465 on the other hand has 12CO in absorption, but given the low S/N of the spectrum, the EW isn't well constrained at 29.96±8.81*Å*. Both 465 and 446 have photospheric absorption features from sodium and calcium, common in class II YSOs.

3.3.3.3 Other YSOs

For the twelve other 'likely' YSOs, five have both usable spectra and full NEOWISE light curves (the other seven lack LCs), which can be viewed in figures 3.17, 3.18 & 3.19. Of particular note are the two class II sources, 510 and 542, with broad Brackett γ emission lines, but differing light curves. Source 542 has a light curve that can be likened to that of Source 502, featuring a three year $>$1.5 mag outburst in K, with the post-outburst flux being maintained thereafter. A key difference between those two light curves relates to Source 542's stochastic variations that occured after the brightening event, which are not seen in the two FUor candidates. Source 510 has an unusual light curve feature, wherein the NIR K & Ks flux is falling over a 13 period, whereas the MIR flux is slightly increasing. A final discussion point is the recent outburst of Source 152, which is circa 2 magnitudes in amplitude for the $W1$ band, and approximately 1 magnitude in $W2$. This significant blue colour change could indicate an accretion dominated outburst event, possibly repeating the burst seen in the UGPS data, which was of a lower amplitude, but similar duration.

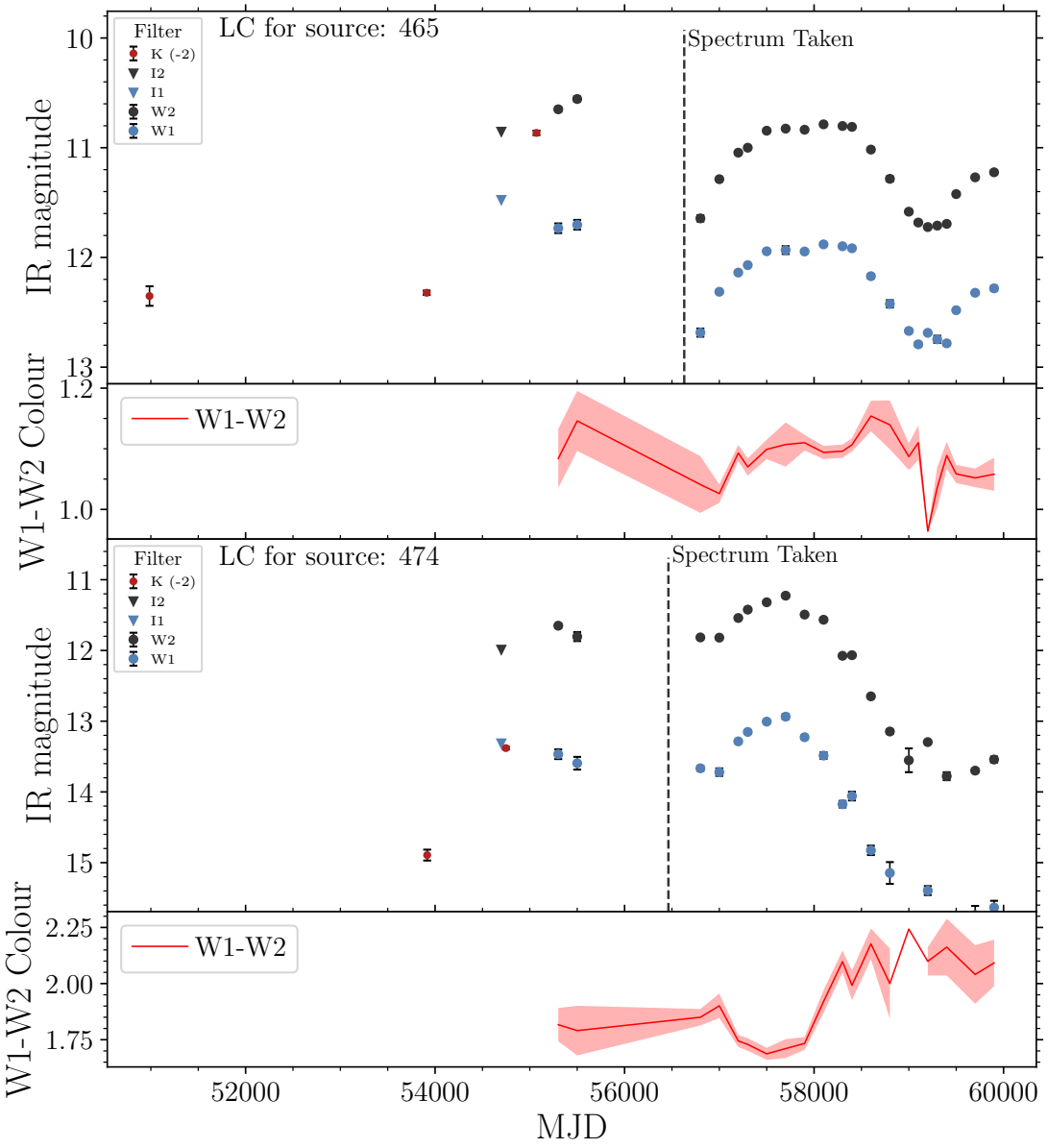

FIGURE 3.15: MIR light curves for the sources with prolonged fading behaviour. The mechanism driving the variation is likely different in each case: source 465 has minimal variation in $W1-W2$ of 0.21, so is possibly accretion driven. Source 474 has overall redder colours, and a colour difference of 0.56 (although this is trending higher as of 2023), which makes the variation clearly caused by extinction.

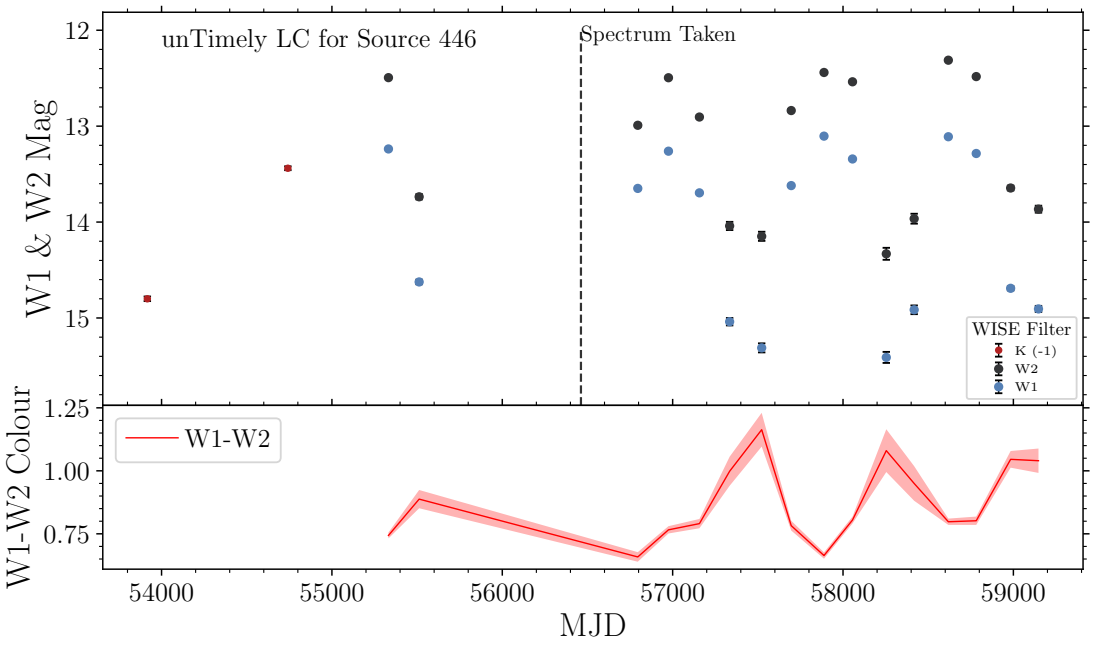

FIGURE 3.16: The unTimely light curve for Source 446 which shows AA Tau-like dips. Peak amplitudes are 2.31 and 2.02 in $W1$ & $W2$ respectively, with a maximum $W1-W2$ colour of 1.16, seen during the second dip. The dips, while repetitive, are not truly periodic, but seem to occur roughly every $\approx$ 2.5yr. This behaviour might also explain the Spitzer $I1$&$I2$ non-detection.

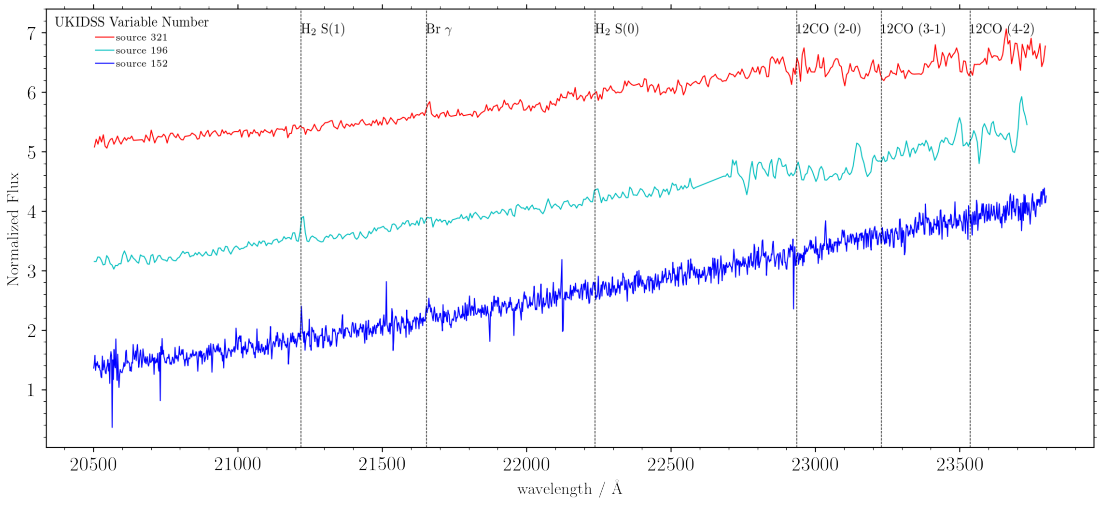

FIGURE 3.17: NIR spectra for 3 of the YSOs with less prominent spectral features.

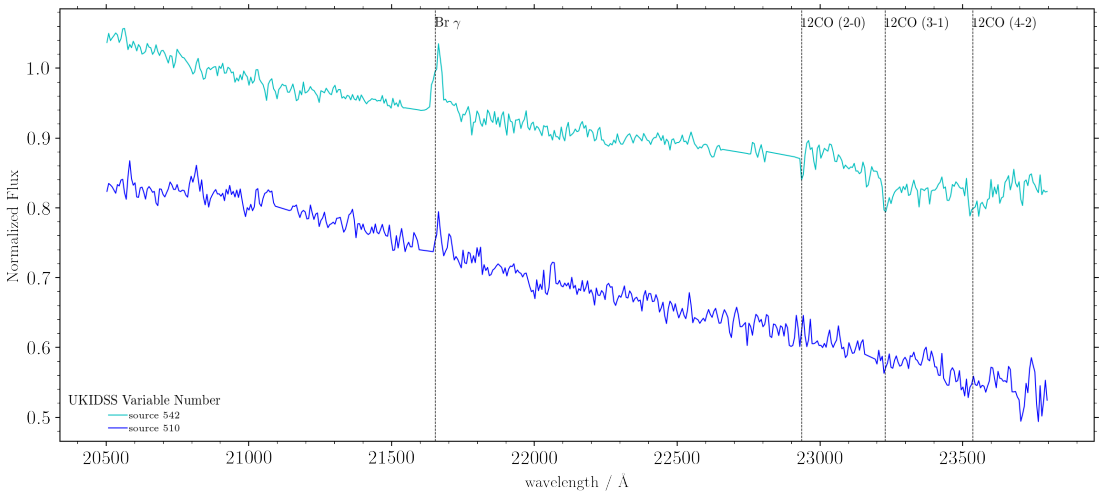

FIGURE 3.18: NIR spectra for two class II YSOs. The presence of Brγ emission is indicative of ongoing accretion, while 12CO can be faintly seen in absorption for source 542.

3.3.4 Sources with Unusual Spectra

The final four sources to be discussed show unusual spectral behaviour either in the near or mid-infrared: 136, 284, 443 & 519 all include Brackett γ emission, but with 12CO in absorption (see Figure 3.21). All of these lines are fairly weak, with low equivalent widths, and these spectra are otherwise featureless. In addition Source 136 has He I in emission, with a measured EW of $(-7.2 \pm 0.092\text{Å})$. Absorption by water vapour can be observed most clearly in source 519, but it is still observable in 136; almost none is seen in the other two systems. A final feature of note is of 13CO, where the 2-0 and 3-1 transitions can be identified, albeit at varying strengths within the group; sources 519 and 284 show it prominently in absorption, 136 has only the second bandhead, and source 443 is lacking any 13CO lines. These features are most associated with D-type symbiotic stars, and it is worth considering this classification for the sources discussed above, owing to the precedent set by Guo et al. (2021) for VVVv319 and VVVv370. These stars' spectra contain similar features, notably the combination of Brackett γ in emission and 12/13CO in absorption.

D-type symbiotic stars are a subgroup of white dwarf & M-type AGB close binaries, wherein the WD accretes from its companion via Roche-lobe overflow causing variability on short periods, whilst long period variability can be exhibited from Mira-type behaviour from the AGB companion. D-types are separated from similar S-type systems by the presence of warm dust (see Munari (2019) for a further review), leading to the observed NIR excess. This interpretation of

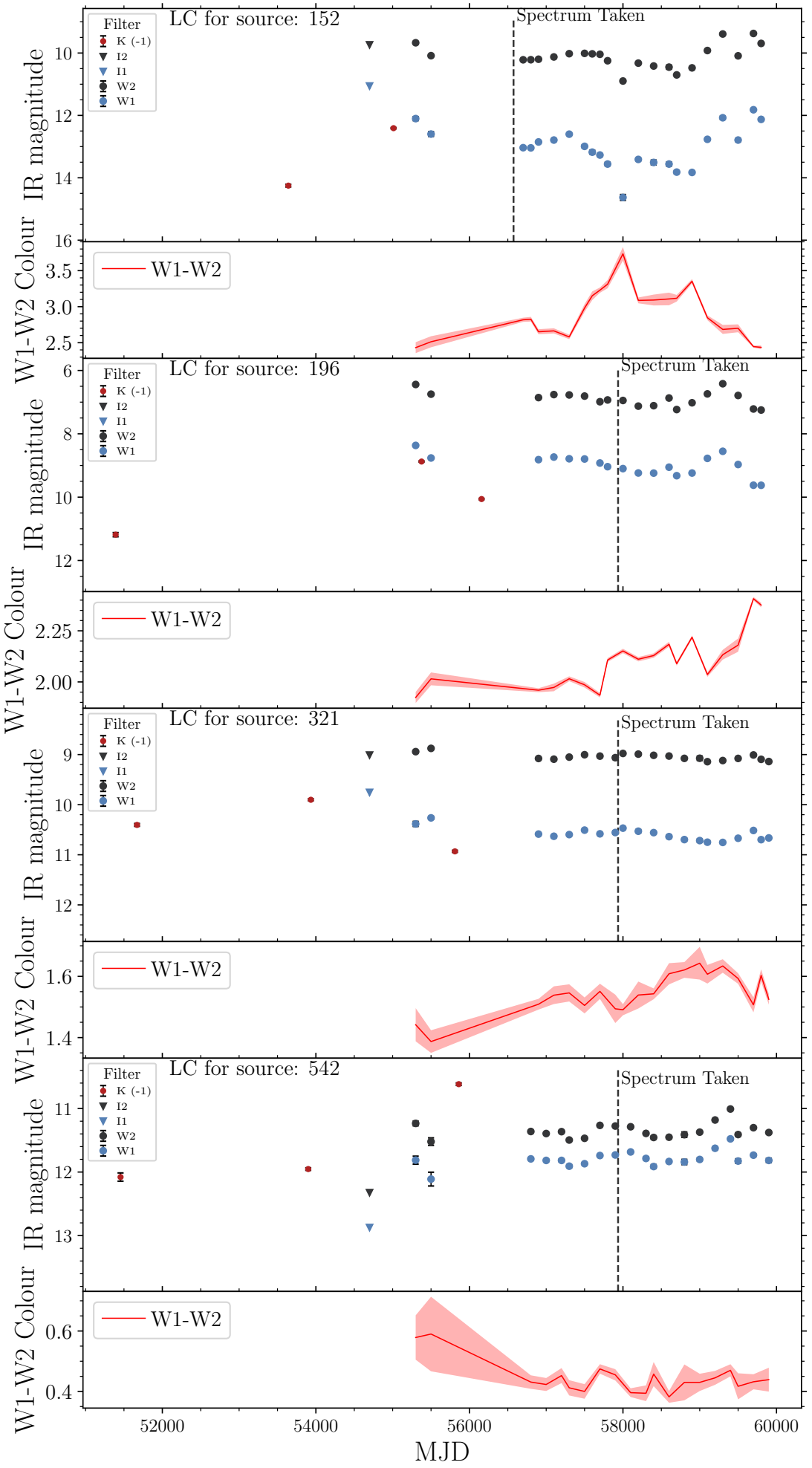
LC for source: 152
Spectrum Taken
Filter
K (-1)
I2
I1
W2
W1
IR magnitude
W1-W2
W1-W2 Colour
LC for source: 196
Spectrum Taken
LC for source: 321
Spectrum Taken
LC for source: 542
Spectrum Taken
MJD

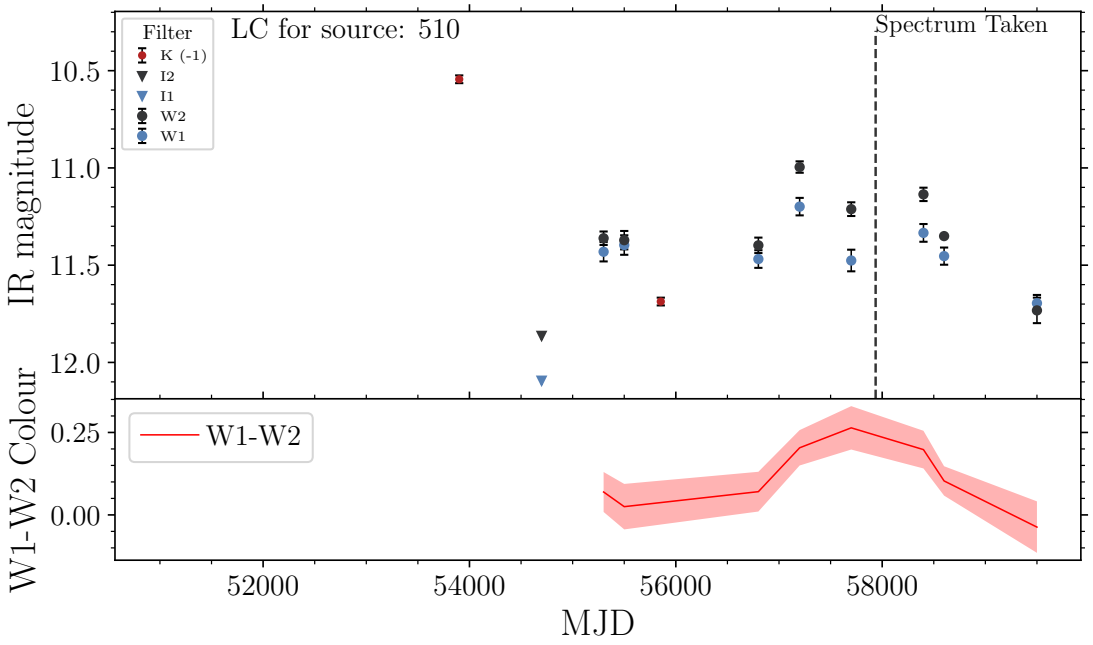

FIGURE 3.20: MIR light curve for Source 510, the only class II YSO in the group of non-outbursting YSOs.

these sources provides explanation for the observed spectral features, with the hydrogen recombination tracing accretion by the WD, with the CO and water features originating in the pulsating photosphere of the AGB companion. NEOWISE light curves are available for source 136 and 284 only (Figure 3.22), but they show minimal variation and no obvious periodicity. Given the unreliability of measuring short period variation within WISE, it's not unsurprising that the rotational variation of the WD is not seen. The absence of long period variation does cast the D-type variable explanation into doubt, because a 400-700 day pulsation period is normally required, attributed to Mira-like variations (slightly longer than field Miras, see Whitelock (2003)). The aforementioned v319 and v370 both have long period variable-like (LPV) light curves, combined with MIR colours that are bluer than than traditional AGB stars ($W1-W2<1.5$), hence the authors presumptive classifications. Of the sources with WISE data covered here, Source 136 has blue YSO-like colours in both $W1-W2$ & $W2-W3$ (0.49 and 2.23 respectively), and Source 284 features an average $W1-W2$ of ≈ 0.65. The remaining stars have results from unTimely (only $W1$ & $W2$), with colours between 1 and 2, although both of these are lightly blended with nearby objects.

It is worth noting however that D-type classification does only require the presence of warm dust. Other explanations for the spectral features could be low temperature shock excitation of

disk material around a YSO, where the absorption features are of a photospheric nature. This does not explain the strength of the He I line in source 136 however, hence this system could still contain an evolved companion and a disk. One caveat exists for sources 284 and 443, as these have statistical distances from Gaia eDR3 (Bailer-Jones et al., 2021), at 1.1kpc and 2.5kpc respectively (the geometric distances place them at 0.8kpc and 1.4kpc). Whilst this would make a WD binary classification unlikely, if the systems are binaries then the distances would likely not be accurate. Overall the position of these stars in an area of the NIR CC diagram that can contain symbiotes, in addition to a collection of evolved star tracers in their spectra make a YSO classification less likely than thought previously. Hence for the purposes of the upcoming discussion we will count these four sources as 'non-YSOs'.

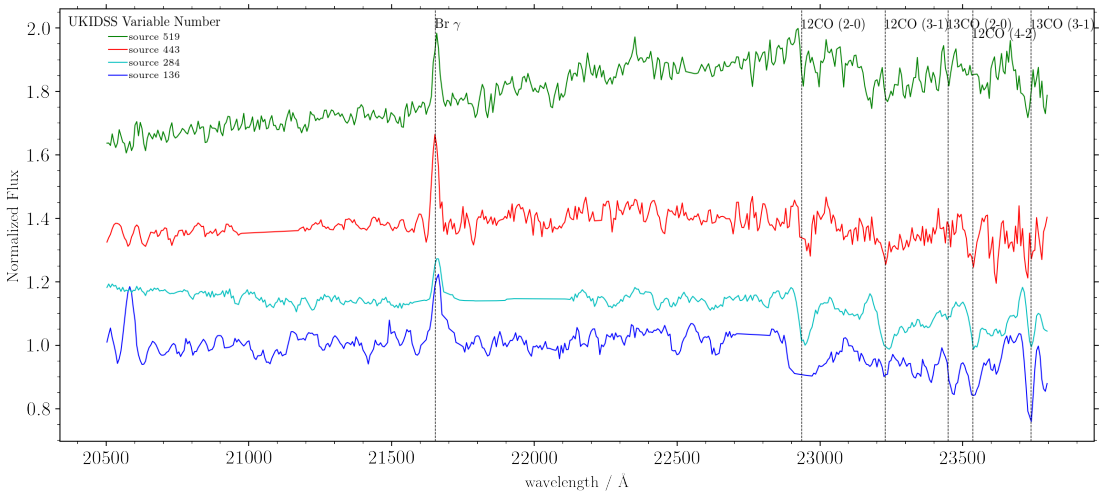

FIGURE 3.21: *Ks*-band spectra for 4 stars with the unusual combination of hydrogen emission and 12CO absorption. For all sources the hydrogen emission is recombination (Brγ), and is broader than seen in the wider sample. All the lines are faint, with EWs ranging between -4.24 to -8.02 for Brγ and 3.55 to 19.61 for 12CO. 13CO can be seen in sources 284 & 519 clearly, and potentially in source 136.

3.4 Discussions

3.4.1 Eruptive Variable Star Confirmations

For the data in this work, we can estimate what fraction of high amplitude variables are genuinely eruptive sources, as confirmed by either spectroscopy or MIR monitoring.

Assuming a uniform prior (to be further discussed in due course), and a simple binomial distribution; a star in the sample is either a true eruptive variable YSO or it isn't, we can thus find the

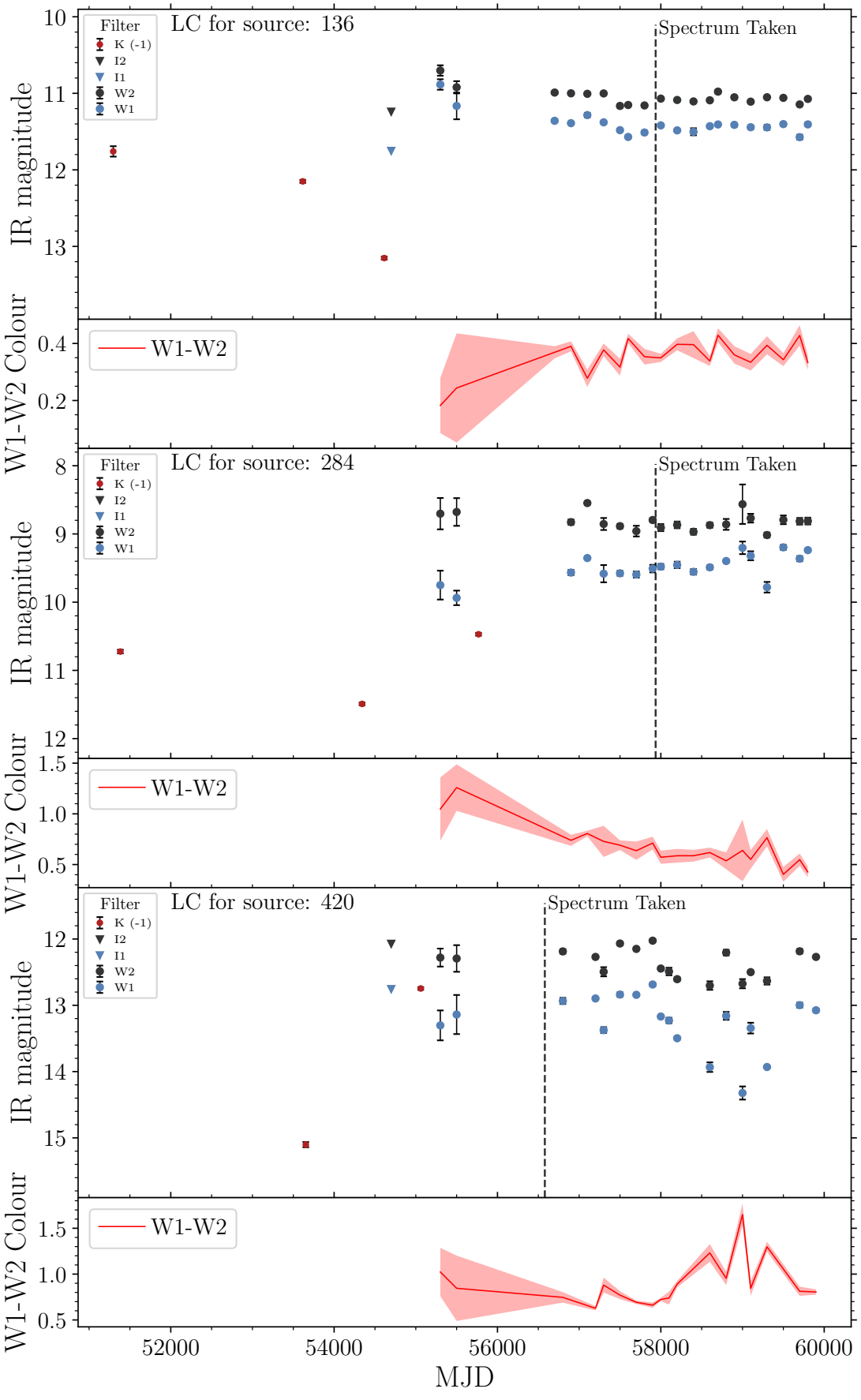

FIGURE 3.22: NEOWISE light curves for three of the four unusual sources (source 443 is only visible with unWISE/unTimely). Of note is source 420, which shows continuous aperiodic variation, of both colour and amplitude. The peak change in W1 is 1.64 with a colour change of 1.02, and all variations within the light curve follow the 'redder when fainter' trend.

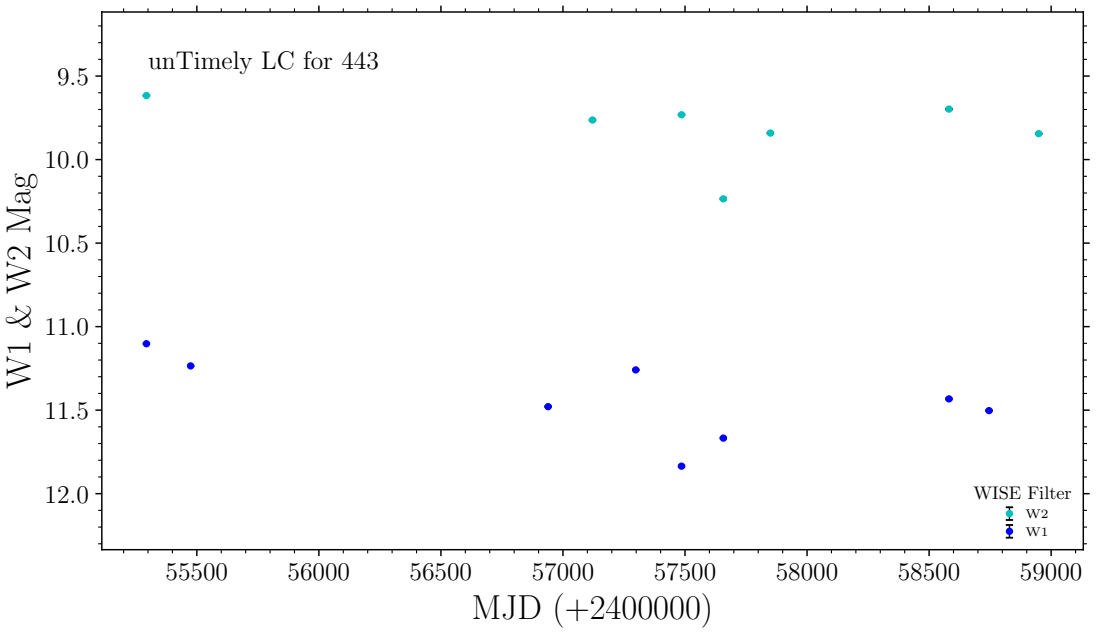

FIGURE 3.23: UnTimely light curve for source 443, for both W1 and W2 bands. There is no periodic behaviour present, and minimal variation. Epochs with no data are as a result of blending rather than genuine high amplitude variability.

difference between our observed and expected prevalence for EVs. There are several different values for the number of observed eruptives, depending on our confidence:

- **Case 1**: The two FUors are the most likely to be accurate classifications, and as such is the minimum observed eruptive value (2/25). All ratios will be given out of 25, thus removing the small number of possibly evolved objects.
- **Case 2**: The addition of source 533 as an EXor candidate is slightly less certain, owing to the slight difficulty of distinguishing it from a dipper with an emission spectrum (although the H_2 outflow still makes a good case for a previous eruption). A strong case does exist however that the star could be a long-duration EXor, like those found by Guo et al. (2021), and in this instance the eruptive fraction would become 3/25. The aforementioned work did find a roughly equal number of long duration emission-line sources as compared to FUor-like systems, hence it is likely that this sample would contain at least 1.
- **Case 3**: The least certain ratio of 9/25 includes the six stars of section 3.3.1.2, which have higher amplitudes than seen in the non-eruptive short-term variables (STVs) and colour behaviour more suited to an EXor classification than as dippers. Although the UX

Case	Observed Percentage	Expectation Percentage	σ
1	8.00%	11.11%	$\pm$0.20%
2	12.00%	12.10%	$\pm$0.18%
3	36.00%	30.24%	+$\pm$0.14%

TABLE 3.4: Table showing the range of observed and expectation eruptive variable ratios, separated into 3 groups of varying confidence, as discussed in the text.

Ori type dippers have similar colour behaviour their amplitudes are usually lower than 1 magnitude.

An expectation value for the percentage of YSOs (found within the Lucas et al. (2017) sample) to be eruptive is calculated in a bayesian fashion (i.e using a prior and observed value to predict a likelihood), using a binomial distribution (see equation 3.2). A binomial distribution is a reasonable choice as a star either is or isn't an eruptive YSO. The expected number of eruptive variables is taken as the mean of the probability density function (PDF), with the stated errors being the 1σ standard deviation of the probability distribution.

$$P(EV_{frac}) = \frac{T!}{(T-r)! \times T!}(EV_{frac})^r(1-EV_{frac})^{T-r} \tag{3.2}$$

Where EV_{frac} is the range of possible fractions of eruptive variables in the sample (from $\frac{0}{390}$ to $\frac{390}{390}$), r is the observed number of eruptives, and T is the number of trials (the size of the spectral sample). For this work, we take r to be either 2, 3 or 9 (for case I, II & III respectively), and T to be 25 (the sample of YSOs we had spectra for).

The expectation values for the incidence of true eruptive variables in the Lucas et al. (2017) sample of 'likely' YSOs can be found in Table 3.4, which show some agreement with the observed values, except in case 1. Additionally, for the 29 'likely-YSOs' observed, we find 25 of these to have YSO-like spectra, with 4 potential D-type symbiotes (albeit where 2 are more confident than the others). The values in the table are quoted out of 25 rather than 29 or 30 to better understand the rates of eruptive variability amongst YSOs, rather than purely NIR selected variables. and thus we discount the 4 potential D-type symbiotic stars, as well as the AGB star.

Comparing these findings to the results of the similar sample of Guo et al. (2021), our sample is likely to be dominated by STVs, which were deliberately not selected in the Guo et al. sample. This can be inferred because 10 of the 25 YSOs show minimal variation in post UGPS

measurements, and combine this with standard YSO spectral features, indicating that the originally observed variability is low amplitude and on timescales shorter than can be observed with NEOWISE.

Guo et al. (2021) had their spectral sample dominated (90%) by emission line sources, whereas the value in this work is only 56.7% (15/25), possibly indicating that STV's have higher probability of having absorption dominated or featureless spectra. The emission-line versus absorption-line ratio seen by those authors for the long duration sources was roughly even, with a possible preference towards emission sources, although with low number of long term objects in this work, it is challenging to corroborate. Another key difference between the two samples is in the prevalence of quasi-periodicity, with 26% of the 2021 sample having some form of repetitive behaviour (although not all of these are truly periodic), whereas this work has 15% with quasi-periodic behaviour. There exists a caveat for this however, because the time sampling of NEOWISE (6 months per epoch) prevents confirming variability on short timescales, although not confirming of any $\sim$1000 day periodic variables (like DR4_v55) is unexpected. Sources 446 and 465 do show repeating variability on this timescale, but are not provably periodic.

To generate a more complete picture of the prevalence of eruptive events within star formation generally, there must first be a measure of the completeness of the two-epoch selection method. Building on the work of Contreras Peña et al. (2014a, 2017); Lucas et al. (2017) I adopt a UGPS completeness fraction for eruptive variable candidates of 20%. Those authors reach this value via randomly selecting 2 observation dates (set at the same duration apart as used in UKIDSS) and placing these on a well sampled VVV light curve. An eruptive variable was considered 'recovered' if the Δmag was $>$ 1 mag, thus replicating the selection method of Lucas et al. (2017). The above method recovered 25% of the eruptive light-curves, which gives a final value of 20% when taking into account the fact that VVV itself has an estimated completeness of 80%, for long duration outbursts, following simulations in Contreras Peña et al. (2017). This implies that there should be $\sim$1950 YSOs with $>$1 mag NIR variability (assuming the 390 recovered by Lucas et al. (2017) was 20% of the true value), and thus there should be between 216^{+17}_{-6} (for case 1) and 590^{+73}_{-106} (for case 3) eruptive variable stars amongst them.

In order to test our expectation value, we can use MIR light-curves to search for eruptive variables from a known selection within an SFR that was also covered by UGPS. Going forward we will consider the Cygnus-X region (because of it's excellent MIR coverage with a long time baseline), and it will be examined in Chapter 4.

3.5 Conclusions

This work demonstrates some of the benefits of applying a multi-wavelength approach to the study of eruptive behaviour in YSOs, and additionally illustrates the large variety of behaviours seen in these objects across an approximate 10 year time-span. The following points summarise the key findings:

- Spectroscopy provides the clearest indication of the type of any eruptive behaviour identified, but is most effective when the observations are undertaken nearer to the start of any outburst.
- NIR colours combined with spectra can play a role in disentangling post-outburst EXors from traditional accreting YSOs (see figure 3.1), although this also requires lower limits of the amplitude of an observed outburst.
- Selecting targets for spectroscopy based upon observed (past) high-amplitude NIR variability and positions & colours associated with star formation, leads to a varied sample, with no particular biases. The selection features two probable FUors, three dippers (possibly four), and up to seven objects with high accretion rates and possibly EXor-like behaviour (including a candidate long-duration EXor). It should be noted that post-MS contamination is still non-zero however, with at least 1 AGB star and up to 4 possible D-type (or similar) symbiotic systems within the final collection. For eruptive variable YSOs in the UKIDSS two-epoch sample of high amplitude variables more generally, we find an expectation value of $11.1^{+0.9}_{-0.3}\%$ for the long duration outbursts, and $30.2^{+3.8}_{-5.4}\%$ for all candidate eruptive sources. A final point to make is that while our method did recover a number of new eruptive sources, the larger numbers and variety found by selections from VVV indicates that better time sampling does provide significant improvement.
- Time-domain MIR data is a useful tool to provide an indication of post-outburst behaviour, able to reliably identify possible long-period systems, and those with clear long term trends. For stars with repeated burst-like behaviour (such as sources 144 & 463) the increasing number of epochs provided by NEOWISE can also be used to ascertain when additional bursts are in progress, and can thus be used to guide spectroscopic follow-up.

Chapter 4

Investigation into Cygnus-X Selected Variable YSOs in the Mid-Infrared

4.1 Introduction

Having previously made estimates of the incidence of eruptive variability from a sample of variable 'likely' YSOs with spectroscopy (see chapter 3), one of the principal issues was the $\approx$20% completeness of the original search. Improving the return of candidate eruptive variables from the original sample of $\Delta K \geq 1$ mag is therefore of importance if one wants to make more accurate claims on the incidence of eruptive (and other high-amplitude) variability in YSOs. Given that the UGPS survey (Lucas et al., 2008) covered a large number of known star forming regions, existing YSO samples from these regions can be leveraged to provide a sample of pre-selected YSOs. These can then be further examined for signs of eruptions, both during and either side of the UGPS photometric measurements.

The long duration time coverage of existing MIR all sky surveys, with Spitzer, WISE and the current NEOWISE (Hora et al., 2007; Wright et al., 2010; Mainzer et al., 2014), provides the ability to find all but the more short-term variable events (such as STVs), and the event's that last for a century or more (such as the post-outburst behaviour of some FUors). Provided YSOs selected from studies in the MIR have a UGPS counterpart, then any displayed variability could trace eruptions missed in the sample of Lucas et al. (2017), providing an increase to completeness for that work. The nearby region of Cygnus-X (at roughly 1.4kpc) makes an excellent test site for this method of increasing completeness, because of the large sample of Kryukova et al.

(2014), which identifies over 2000 candidate YSOs, in a region also covered by NEOWISE, UGPS and 2MASS (Skrutskie et al., 2006a).

The incidence rate of eruptive variability in YSOs is important when considering the 'proto-stellar luminosity spread problem' (the observed spread in luminosities across a star forming region), but the variance in amplitude (with respect to the photometric bandpasses being used for observations) hasn't been probed in detail previously. Using an sample of nearby YSOs (without a bias imposed by amplitude cuts) we can use the NEOWISE data discussed above to examine the range of eruptive behaviours seen in MIR selected YSOs. This should provide insight into how common the usual FUor and EXor (and the more recently uncovered variants thereof) variables are among a MIR selected population, or if other eruptive stars will dominate this feature space.

In this chapter I will discuss the combined sample of candidate eruptive YSOs seen in both catalogues (Krykova+ and Lucas+ 2008), highlighting individual stars of note, and the wider trends seen with regard to variability in the MIR. A special note will be made to examine the rates of eruptive variability in this region, building on the work in chapter 3.

4.2 Data Selection

Cross-matching the 2007 MIR colour selected YSO candidates of Kryukova et al. (2014), with the UKIDSS Consortium (2012) UGPS DR6 yields 1476 (73.5%) sources. However, recovery of NIR selected Cygnus-X members from the sample of (Lucas et al., 2017) in the wider selection of Kryukova et al. (2014) is only 22.7% (i.e. 77.3% of the Cygnus sources from UGPS are not selected in the MIR). This could be due to source confusion, with the $2''$-$3''$resolution of Spitzer being less precise than that of UKIRT WFCAM ($0.75''$). The UGPS sample does have a wider survey area (to be labeled as 'Cygnus X' in the 2017 catalogue) than the Spitzer equivalent, but was not a major contributing factor to the number of dropouts (5 of the 91 UGPS targets were not in the region of Spitzer coverage). The depths of both surveys are roughly comparable, Spitzer $I1$ and $I2$ are available to 17mag and 15mag respectively in the Spitzer data, while UGPS K is complete to $\approx$ 17 mag. While the overall depths of the surveys are comparable the selection methods do differ, with the Spitzer selection method (as detailed in Kryukova et al. (2012)) setting a lower limit on the gradient of the SED slope (at $\alpha = -0.3$), in order to remove class II YSOs (this is the most likely explanation for the missing sources).

The catalogue of Kryukova et al. (2014) lists 2MASS *Ks* magnitudes for sources where available (down to $\approx$ 15 mag), but deeper UGPS measurements are available for many more of the YSOs.

Using the aforementioned Kryukova et al. (2014) sample, it's possible to make an improvement to the completeness of Lucas et al. (2017), through the location of sources that have undergone events that take the star from below the detection limit to above it (and vice versa). To limit this selection to YSOs only (and those that are not already part of Lucas et al. (2017)), a sample can be drawn from the 1476 targets in both catalogues, then adjusted to contain sources visible at: only one epoch of UGPS photometry, and with a minimum brightness of 16 mag in *K*. The threshold was set to make sure all detected variability events were still of the same $\Delta Ks > 1$ mag as the original sample, thus covering the UKIDSS-UGPS *K* lower limit of 18 mag. This was later relaxed to any sources with only one detection and genuine variability, in order to increase the sample size. For a visual interpretation of this process, please see figure 4.1

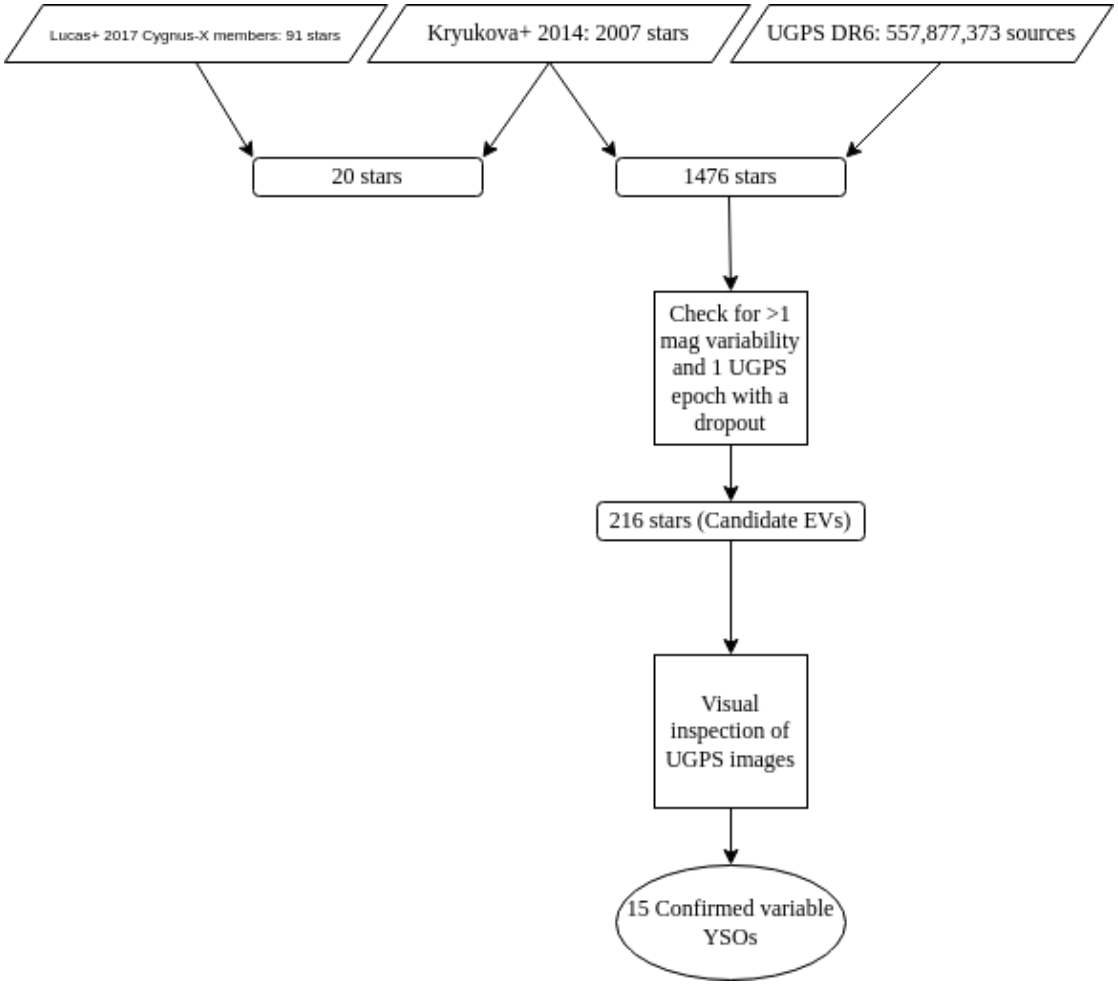

FIGURE 4.1: Flow diagram covering the selection and cross-matching process for the YSOs in this chapter.

4.3 Results from the Combined Sample

The expanded selection method defined earlier yielded 216 sources, which were visually inspected for genuine variability. This involves discounting UGPS tiles that contain over-saturated stars, fields that contain 'ghost' artifacts, and tiles that were subject to photometric processing issues. After removal of false variables, 'real' sources were labeled as such based upon the following criteria: there is a clear single-epoch detection, and a second non-detection as a result of either low flux or features associated with nebulosity (such as cometary nebulae or visible outflows). Both of these factors can imply significant changes to the accretion rate of a YSO, and thus make good candidates to examine for further indications of eruptive variability.

Real variables account for 6.94% (15) of the selection of which 93.3% (14) have true variation of over 1 mag in K, these can be seen in Table 4.1. Of these 33.3% (5) display nebulosity characteristics in the NIR that have been known to be attributed to FU Orionis-type outbursts. NEOWISE light curves for the 12 sources with complete coverage (detections in all NEOWISE epochs) are displayed below in Figures 4.2, 4.3, 4.4, 4.5 & 4.6, with each figure grouping targets with similar trends in both WISE filters.

RA	Dec	Ks 1	Ks 2	Kryukova et al. 2014 No.
306.4641	39.3761	non-detection	15.04	obj362
306.5152	39.8826	16.47	non-detection	obj378
306.6478	39.2476	15.85	non-detection	obj446
306.8452	40.1089	non-detection	17.40	obj519
307.5208	40.2659	16.65	non-detection	obj820
308.0105	40.3108	non-detection	17.93	obj1017
308.0878	41.1318	17.28	non-detection	obj1048
308.357	39.9459	non-detection	15.87	obj1169
308.5565	38.3443	non-detection	16.92	obj1242
308.7622	38.6997	non-detection	15.50	obj1312
309.1605	42.4853	non-detection	17.23	obj1508
309.4808	42.6797	11.85	non-detection	obj1615
309.9553	42.1135	16.96	non-detection	obj1762
310.0635	41.9026	17.68	non-detection	obj1799
310.8884	42.112	non-detection	12.06	obj1964

TABLE 4.1: Table containing the co-ordinates and *Ks* magnitudes (at both UGPS epochs) for the 15 real variables found within the expanded sample of prospective eruptive variable YSOs. Owing to the selection method, one *Ks*-epoch is always a non-detection.

Of particular note are the three stars (as seen in Figure 4.2) that brightened significantly in the NIR, whose post UGPS outburst light curves are all fading, albeit at different rates. Object 1964 would make a good candidate for spectroscopic observations, owing to its higher luminosity and smaller $W1-W2$ colour. The bright K-band magnitude ($\sim$12 mag) should be high enough to

achieve a good S/N at a facility such as IRTF. The nebulosity seen in the UGPS images is a practical indicator for possible FUor-like behaviour, either from ejected winds or as a cometary nebula created in a flyby event (which have been known to produce FUor events, possibly including the progenitor of the group FU Orionis, in addition to the well studied star Z CMa (Pérez et al., 2020; Borchert et al., 2022; Dong et al., 2022; Cuello et al., 2023)). Object 1017 is also relevant to this discussion (see Fig. 4.3) as its outburst can be clearly seen in the MIR light curves. Peak amplitudes of 2.30 and 2.51 in $W1$ & $W2$ respectively are potentially lower limits, given that the star is brightening considerably from the start of the NEOWISE reactivation epoch, and would've most likely been fainter than seen pre-outburst. The change in MIR colour should be noted because it varies by 1.61 mag across the outburst, possibly indicating line-of-sight extinction, with the highest colours associated with the dips post-outburst.

Two further sources are shown in Figure 4.3, for which smaller bursts are visible within the NEOWISE light curves. The burst for Object 1017 is clearer, increasing in brightness by 2.30 mag & 2.51 mag in $W1$&$W2$ respectively. The shape of the light curve bears resemblance to those of VVVv16, VVVv181 & DR4_v10 from Guo et al. (2021), labeled as long-term eruptive candidates, showing similar burst amplitudes and duration to Object 1017. A follow up spectrum for this source in particular would be useful in determining if this star is FUor-like with a lower than average amplitude, or more akin to an MNor-type, containing emission features. The light curve for Object 820 does not contain the proposed initial rise of the outburst directly, with that likely falling in between the ALLWISE observations and the reactivation for NEOWISE, although the peak amplitude change is still sizeable with $W1 = 1.71$ mag & $W2 = 1.47$ mag. Given that the star had continued to fade between the first and second UKIDSS epoch (falling in the region not covered by WISE), It is reasonable to assume the actual outburst amplitude may have been higher than has been measured.

An additional eruptive star (Object 1048, see Figure 4.4) has a light-curve unique amongst this selection, containing an eruption of 4.05 mag in $W1$, which is sustained over 11 years of MIR observation. The light curve in this instance is not directly acquired from NEOWISE, but via the unTimely catalogue (Meisner et al., 2023). Despite the considerable (circa 1.3 mag) decrease in $W1 - W2$ colour, the star is not yet optically visible, lacking a detection in PanSTARRS, or a more recent Gaia alert. The behaviour of the source bears strong similarity to the star Stim1 from Guo et al. (2021), which had an emission spectra (see Figure H2 in that paper), implying magnetospheric accretion, hence Object 1048 would make an excellent candidate for follow-up spectroscopy.

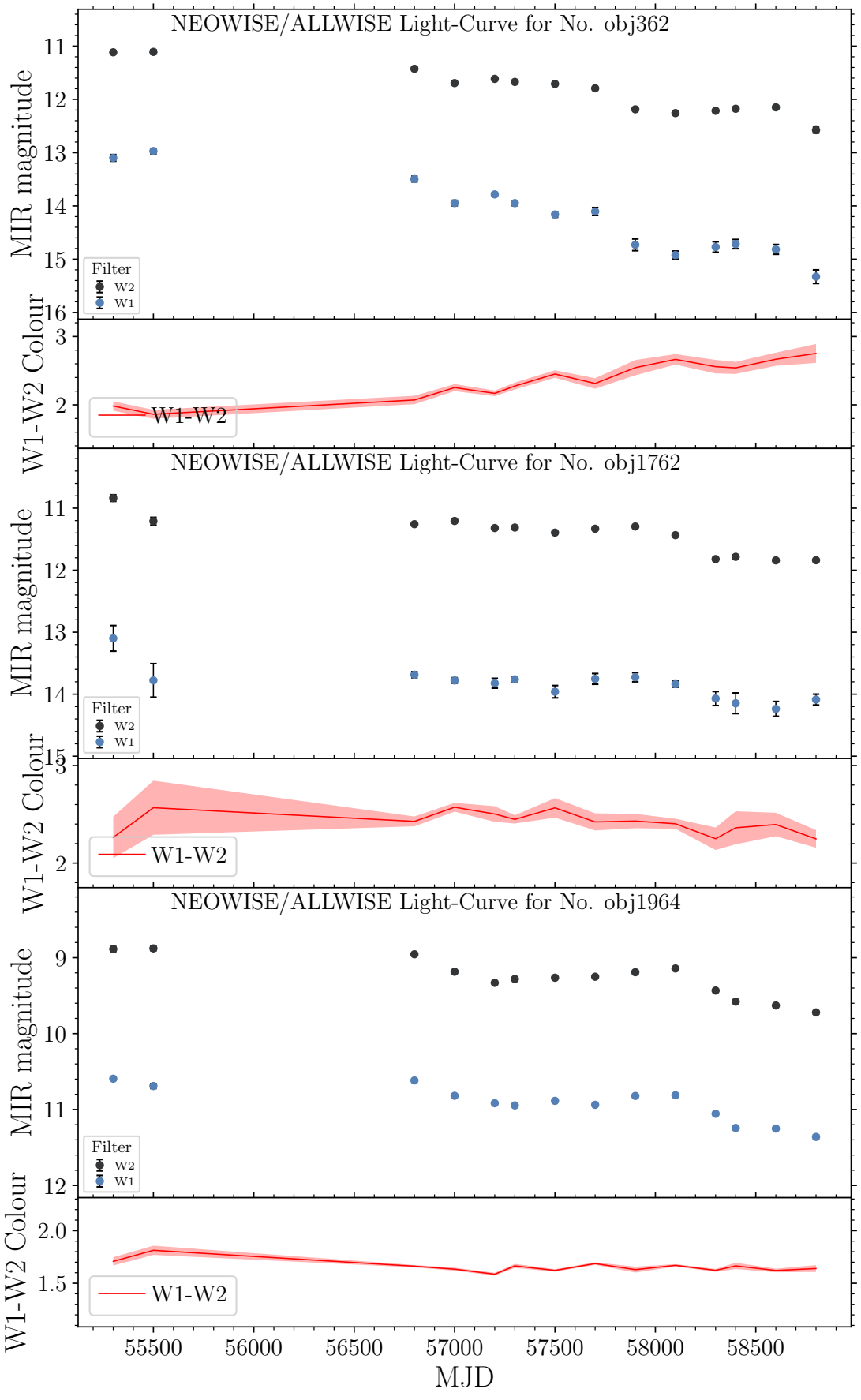

FIGURE 4.2: NEOWISE light curves for the three Cygnus X targets with significant long-term fading behaviour, with amplitudes in $W1$ between 2.36 mag and 0.767 mag, and $W2$ between 1.47 mag and 0.84 mag. Objects 362 and 1964 both represent non-detections at the first UKIDSS epoch, and also show likely associated nebulosity in the images from the second epoch, making them good candidates for spectroscopic follow-up as possible FU Ori-like stars.

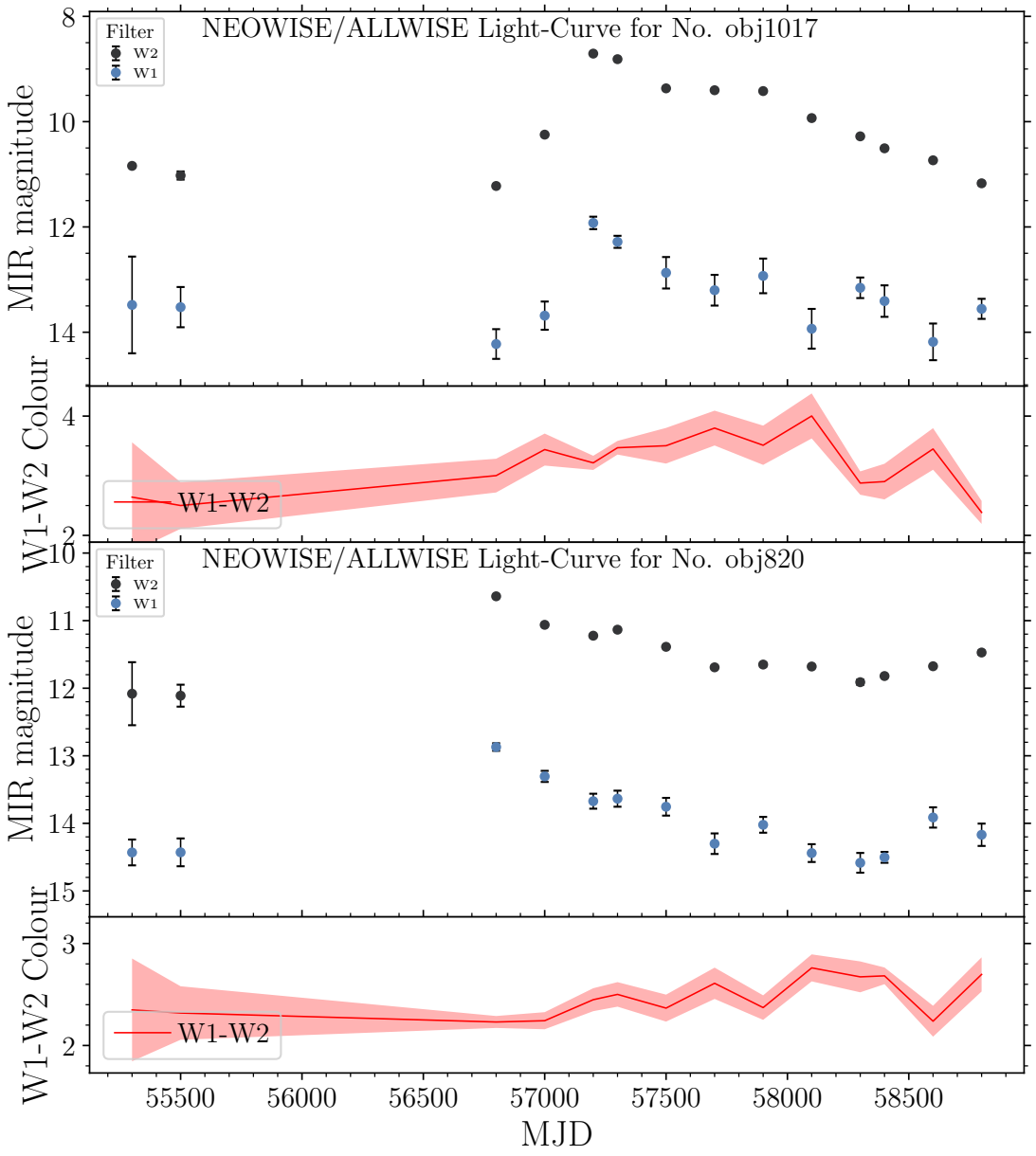

FIGURE 4.3: NEOWISE light curves for the two sources that showed a significant brightness increase within the $\approx$ 10 year observing window.

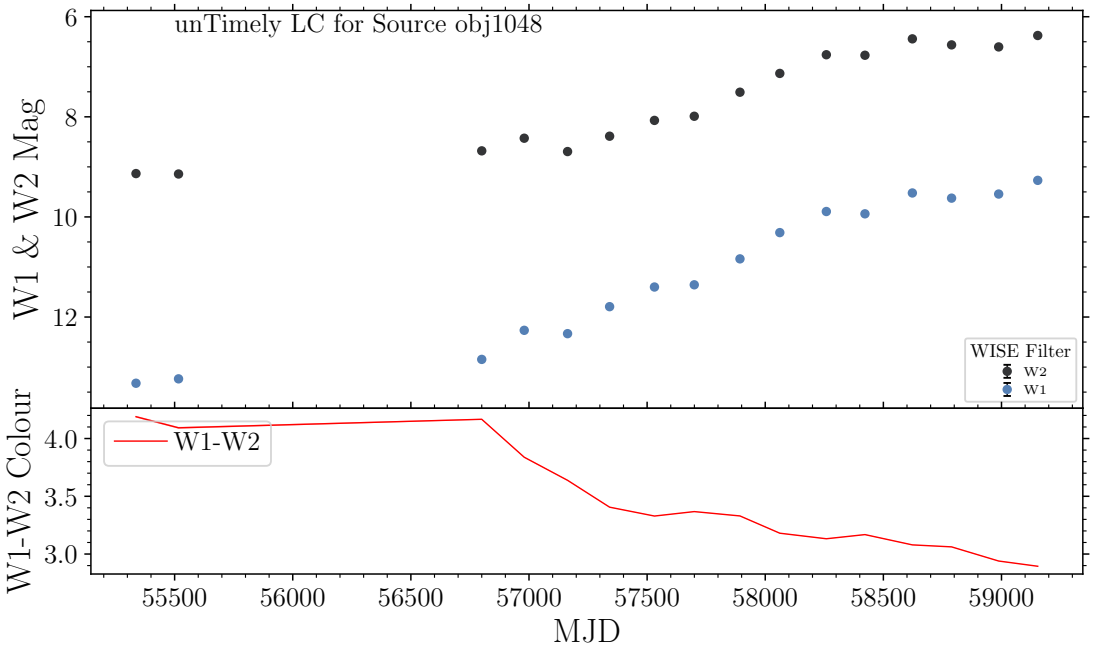

FIGURE 4.4: MIR light curve for object 1048, the data points are from the unTimely (Meisner et al., 2023) catalogue of stacked NEOWISE images. This stacking allows for greater depth and source accuracy than can be obtained in the traditional NEOWISE Catalogues, where this star is not detected, likely due to source confusion. The star has brightened by over 4 magnitudes in $W1$ and over 3 magnitudes in $W2$ at a consistent rate, this is far slower than seen in a traditional FUor-type eruptive variable, and could indicate that this eruption is not accretion-dominated. The star is becoming bluer over time with $W1 - W2$ falling from 4.89 to 2.89.

Three of stars in this sample lack any large scale changes in the MIR data, seen in Figure 4.5. Numbers 378 and 1615 have some small variation over what is an otherwise stable light curve, comparable to many other YSOs, Source 446 has variation with a peak amplitude of 1.22 mag in $W1$, and 0.970 in $W2$, with peak reddening occurring at minima of the light curve. The implication being that the variation is driven by extinction, likely occultation by the mid-plane of the circumstellar disk, either from an asymmetry or from misalignment. This tracks with the nebulosity seen in the NIR images, wherein the star appears asymmetrical.

Sources 519, 1242 & 1312 (Figure 4.6) are grouped as a result of brightening trends, either short or long-term. The corresponding NIR images all have non-detections at the first UGPS epoch, but with varying amplitudes for the second: Source 1312 increases in brightness by at least 3 magnitudes, contrasting to the $\approx$ 1 magnitude of Source 519. It's worth noting the lower $W1 - W2$ colours for 519 and 1312 (as compared to the other targets), which average at 1.26 and 0.83 respectively, with alpha values at 0.56 and 0.48 (these taken from the Spitzer $I1$ to [24] filters). These indicate that the targets are still class I YSOs, but do have flatter MIR SEDs

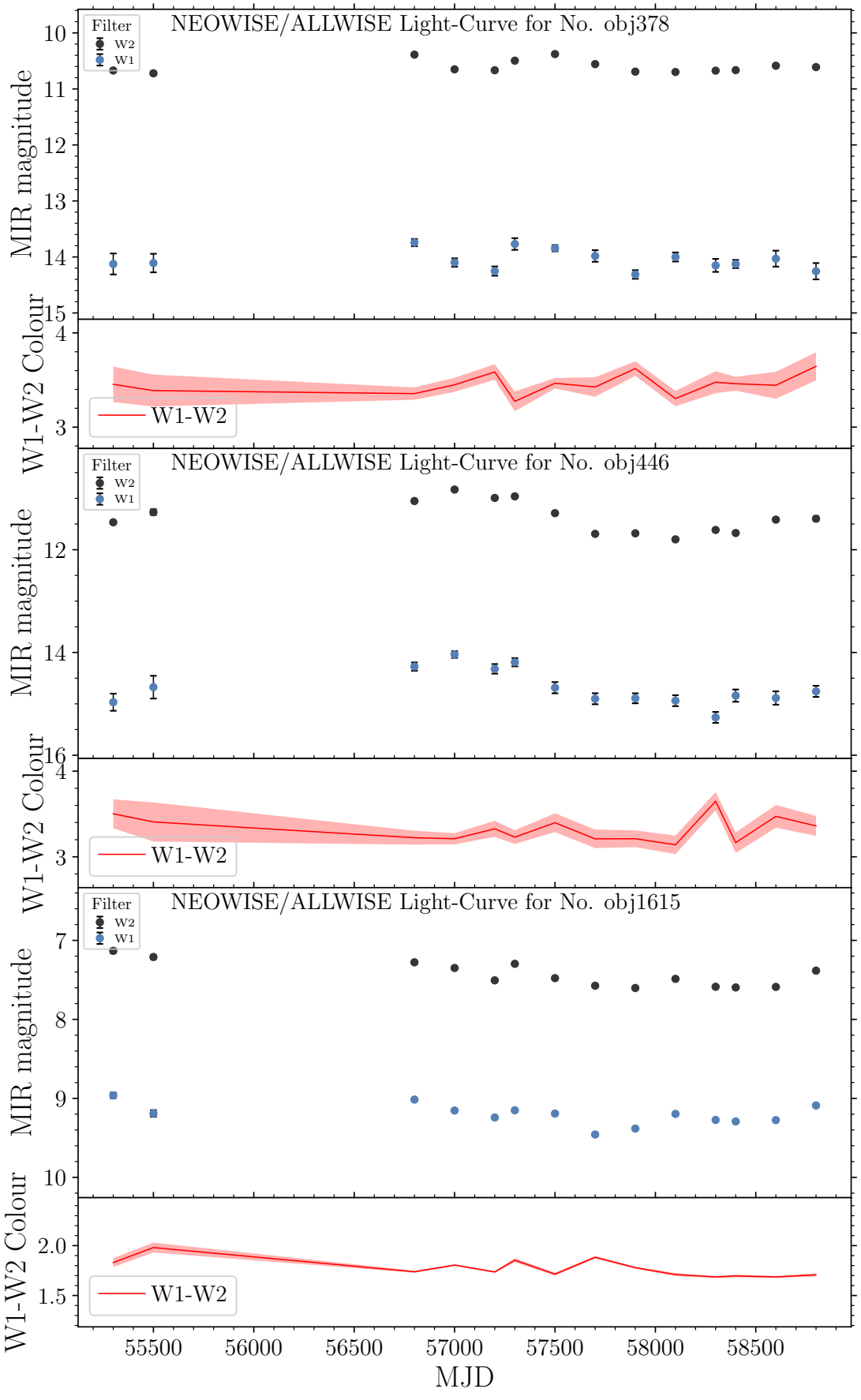

FIGURE 4.5: NEOWISE light curves for sources with variability of ≤ 1 mag. All three of these stars had variation on the order of 1.0 mag in UKIDSS, and thus were the least variable in the NIR in this sample. Object 1615's NIR variability was contemporaneous with spatially extended emission from the source

than others in this group. Checking the Green et al. (2019) extinction maps does show enhanced extinction in the line-of-sight (i.e: foreground absorption) towards both stars (on the order of 5 mag in *Ks*), which may be the reason for the higher alpha value than the WISE colours would suggest. These colours should be larger than observed if the stars are true Class I objects owing to reprocessing from the thicker envelope, although in this case we cannot also rule out disk geometry playing a role in affecting the SED.

4.4 Wider Investigation of MIR Variability in Cygnus-X

When considering the incidence of eruptive variability for YSOs more generally, we can refer to the wider 216 sources of the original UGPS & Cygnus-X combined sample. These provide a selection that contains comparable YSOs to those found in Lucas et al. (2017) (although lacking class II sources), but without the pretext of any previously observed variability.

From the above sample, 156 stars had available NEOWISE light-curves, and was further cut to 123, by removing stars (20) where the data quality during potential outbursts fell significantly; having a PSF with a $\chi^2 \geq 5\sigma$ from the median average for the epoch, for either W1 or W2, were removed. Finally, a small number of stars (3) were removed by manual inspection, all those with a large error on high-amplitude points in the light-curve, or those with single burst like events, visible in only one filter and epoch. These are usually associated with a large fault in a single scan, that then affects the binned average photometric measurement for the epoch.

In the final sample variability of more than one magnitude has an incidence rate of 28.5% in W1 and 20.3% in W2, see the histogram in Figure 4.7. The disparity between the WISE bands is not unsurprising given that YSO variability amplitude more often peak in the optical/NIR regime, with some notable exceptions (these could be driven through expansion of the emitting disk region as can be seen in Be stars). The distribution falls sharply past 1.5 mag, falling to just 2% of the sample with amplitudes greater than 3 magnitudes. A selection of the high amplitude variables have their light curves presented below (figs: 4.8, 4.9 & 4.10), with 4 stars similar to those in Figure 4.4, and another that is fairly unique within this work.

The four targets of Figure 4.8 have amplitudes of between 2 and 2.8 mag, but all follow the same trend of long-period consistent brightening. Given the $W1 - W2$ colours of between 2 and 4, it can be assumed that these disks are likely all class I systems, but are undergoing sustained periods of high accretion. The three upper-most panels in the figure show stars' whose outburst

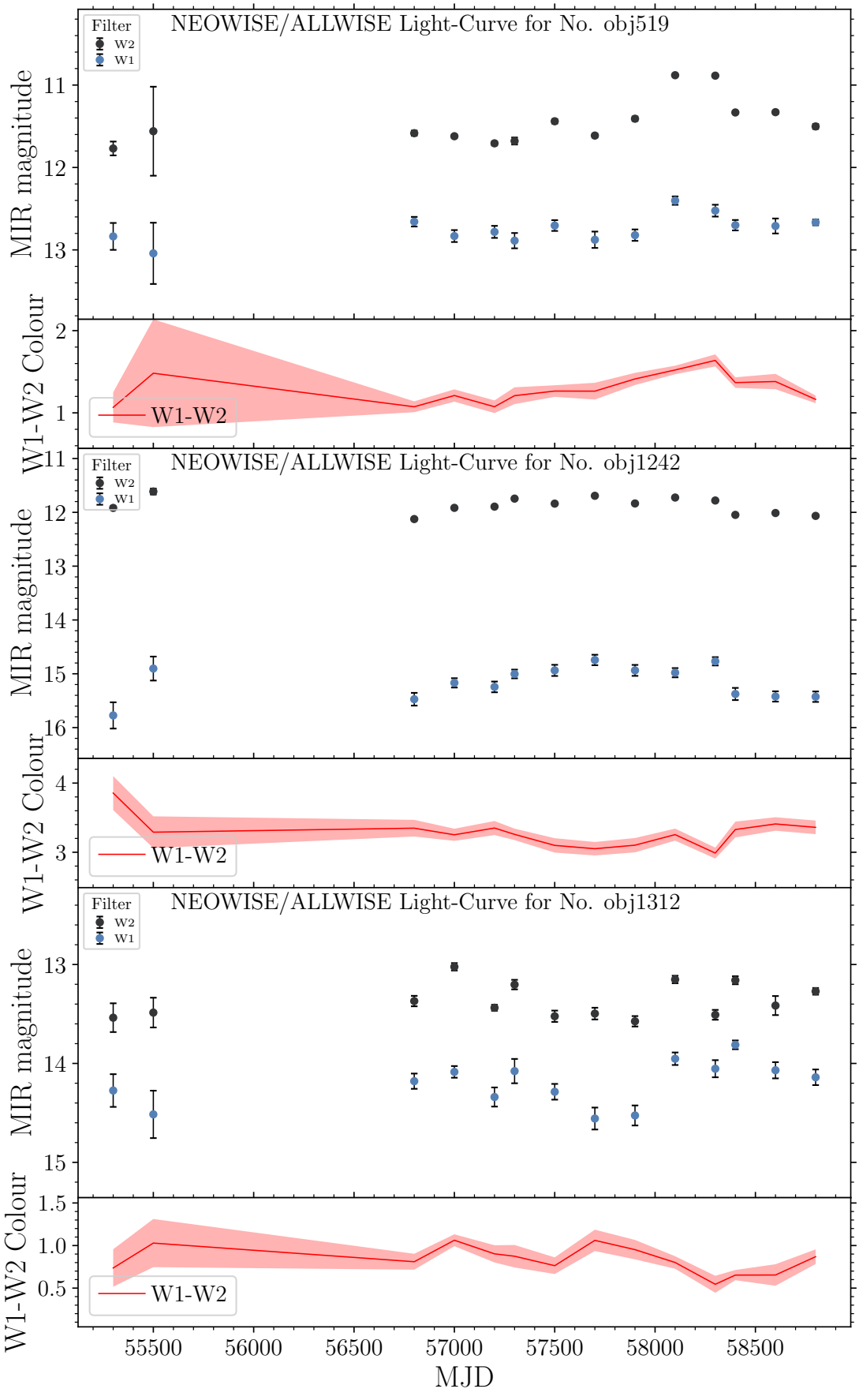

FIGURE 4.6: NEOWISE light curves for additional targets with minimal variation. All three stars have amplitudes of < 1 mag in both WISE filters, but share no other obvious trends. Object 1312 has repeated instances of variability, and is bluer when brighter, indicating possible variation in the accretion rate.

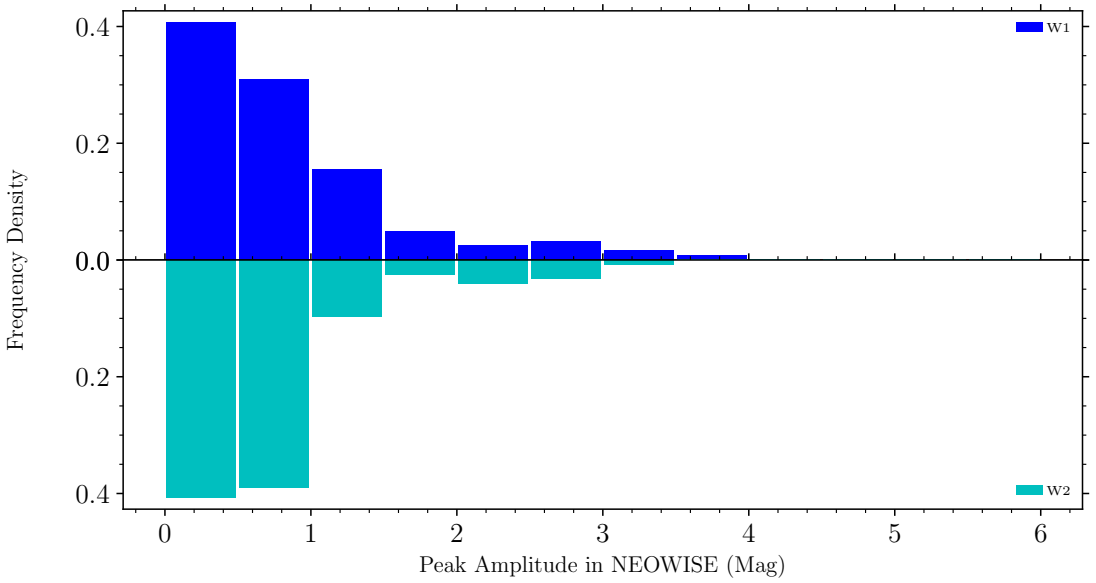

FIGURE 4.7: Peak MIR amplitude frequency distributions for the combined UKIDSS/Kryukova et al. (2014) sample, totalling 123 YSOs with at least 8 epochs of NEOWISE observations. While the most frequent maximum amplitude is below one magnitude, 8% of stars have variability ≥ 2 mag, reducing to 2% & 0.8%, at ≥ 3 mag, for $W1$ & $W2$ respectively.

appears to be ending, putting a circa ten-year duration on each event. The variability shown is more likely to be of the V1647 Ori-type (i.e. an eruption of mixed characteristics), with similar NEOWISE light curves to VVV-v721 (A likely FUor) (Contreras Peña et al., 2017; Guo et al., 2021). The four stars shown here have lower peak variation than other long-duration eruptive YSOs (as discussed above), which could imply slightly different accretion methods to both FUors or MNors. Without additional multi-wavelength observations it is hard to determine the cause of the variability, although given the colour and shape similarities to the aforementioned higher amplitude variables, a hypothesis can be generated. Given that the $W1-W2$ colours are stable during the eruption, it can be assumed that variability is not driven by extinction, and thus an increase in accretion rate provides the best solution. Refining the scale of this increase (and whether or not the amplitude is due to the rate or level of embedding of the source) would be best accomplished through NIR spectroscopy, although owing to the red SED -the pre-outburst K-band magnitudes for these 4 stars range from 17.2 to 16.3- an 8m-class telescope would be preferred, although they could be substantially brighter, making a facility like IRTF a reasonable choice.

Figure 4.9 shows the MIR light curve for the known YSO [KMH2014]J202214.41+372827.35 (Kryukova+ No. 121), which is novel within this work, for having multiple ≥ 1 mag outbursts

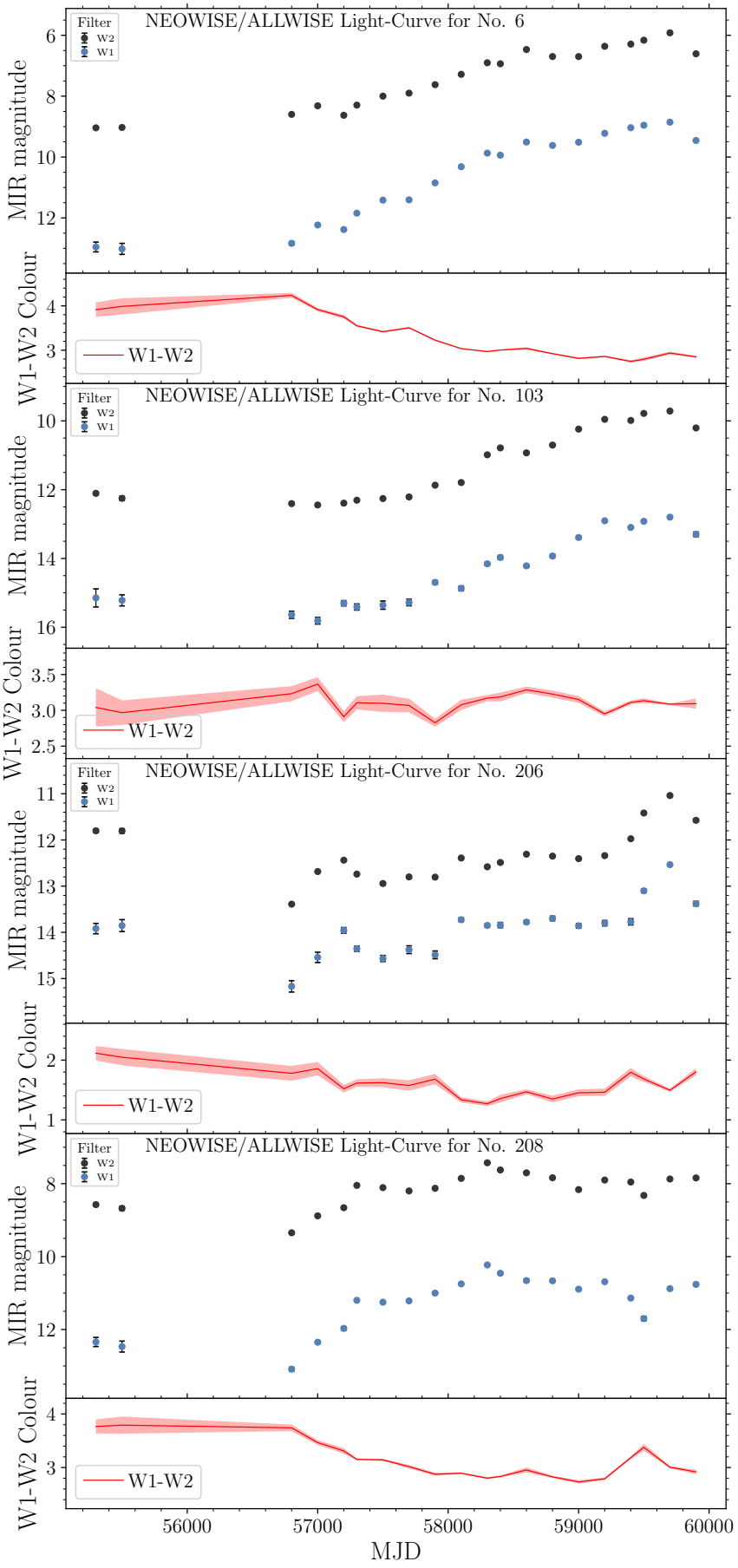

FIGURE 4.8: Light curves for four of the YSOs that showed variability or greater than two magnitudes. These are grouped together owing to the long-period brightening combined with reducing $W1-W2$.

within the observation window (three are observed with a fourth possibly ongoing). Peak amplitude is 1.88 mag in $W1$ and 2.18 mag in $W2$, although there is no clear period between bursts, so the driver of the variability is unlikely to be from the shape of the disk, and is thus probably caused via changes in the accretion rate. The source lacks any optical data, with non-detections with both Gaia and ZTF, there is also only one UGPS detection, and no 2MASS detection either. Using the unTimely catalogue tool (via WISEView) to investigate the stacked NEOWISE images at each epoch, it can be confirmed that the variability is real, with the changes in flux unrelated to the behaviour of a nearby over-saturated star. A similar star can be seen in Figure 4.10, a 'flat-spectrum' SED class star found in the lower amplitude sample (22 stars). Repeating bursts of circa 1 mag can be identified, with a significantly bluer $W1-W2$ colour seen in the outbursting state.

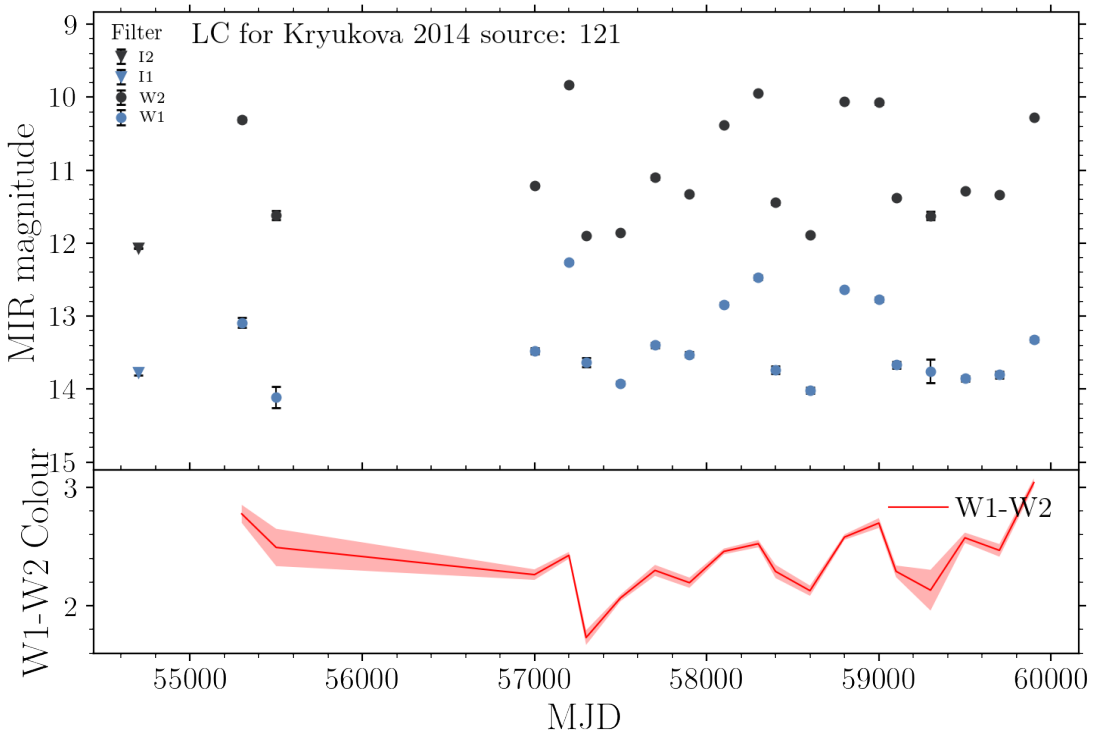

FIGURE 4.9: NEOWISE light curve for one of the high amplitude MIR variables. This is the only star in the group with multiple outburst-like events, none of which have previously been published. The outbursts are brighter in $W2$ than $W1$, with variability not detected in UKIDSS owing to an artifact in of the images.

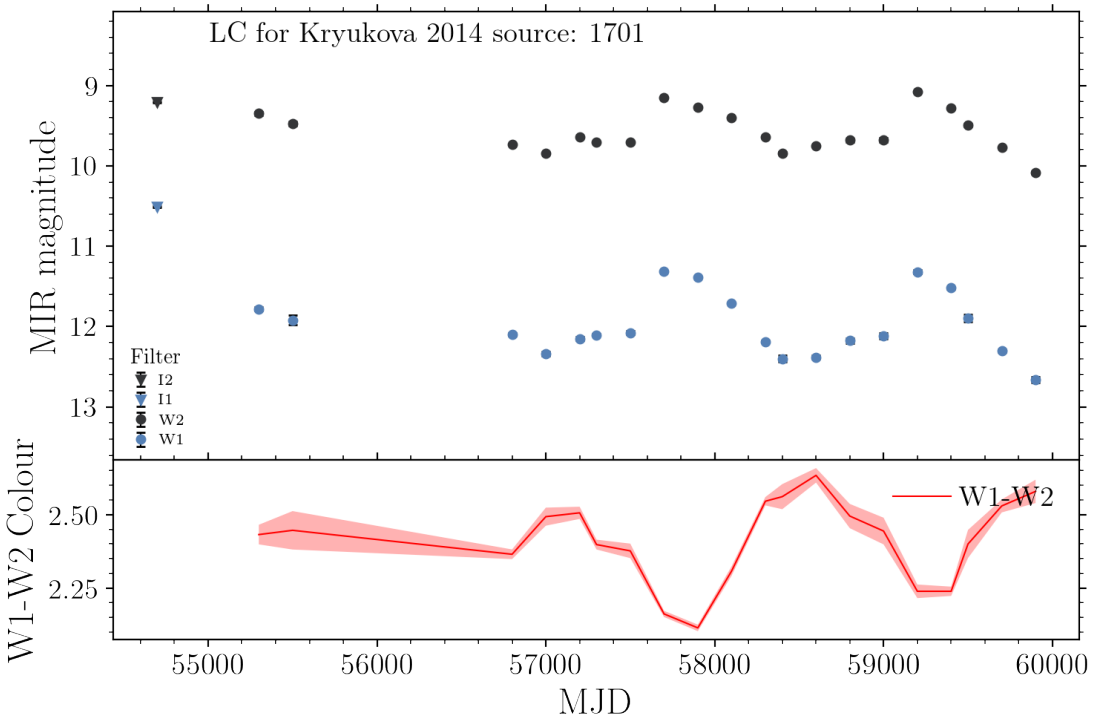

FIGURE 4.10: NEOWISE light curve for one of the lower amplitude MIR variables. Two outburst-like events can be seen, albeit with lower amplitudes than seen in Figure 4.9. The outbursts are brighter in $W1$ than $W2$, and feature a increase in $W1-W2$ of 0.55 mag between the first outburst and the following quiescent period

4.5 Discussions

Collating these findings, it can be inferred that the identification of significant drop-outs in a two epoch dataset (in the context of a time-domain survey) is a good tool for the identification of high amplitude variability from within a pre-selected sample of likely YSOs.

To test the effectiveness of this search we perform a similar Bayesian approach to that used in section 3.4.1, but using an updated prior informed by the previous search. The findings can be broken down into three categories: EV detection among NIR drop-outs, eruptive sources in the broader sample, and the identification of 'dippers', discussed below:

- The attempt to increase the completeness of the original Lucas et al. (2017) sample to eruptive sources through the inspection of non-detected sources, has been successful. The search in chapter 2 yielded 3 likely eruptive candidates, with an expectation of $14.8^{+0.4}_{-5.4}\%$[1] (from among the 25 'likely' YSOs). This compares with the retrieval of between 3 and

[1] All errors on expectation values are the 90% confidence limits

6 eruptive candidates[2] from the 15 'real' variables described in Table 4.1. We calculated expectation value for the number of EVs as $23.9^{+1.8}_{-4.6}$% (This value is calculated in the same manner as done in section 3.4.1). Comparing to the observed value, which indicates it could be up to 40%, it can be suggested that we have improved the completeness (20%) of EVs by $\approx 170\%$ (14.8% expected from section 3.4.1, but 40% recovered).

- Through the examination of the NEOWISE and unTimely light curves of 123 YSOs with a UGPS detection, the incidence of eruptive variability among a large sample (123) of well constrained (with regard to age & distance) local YSOs can be estimated. Here an additional 6 candidate eruptive sources are found[3], making a total of 11/123 after including the 6 other discussed above.

  By running the same statistical methods as used previously in this work, we produce an expectation value of $9.6^{+0.6}_{-1.8}$%, which is reasonably consistent with the values obtained in the previous chapter. Given that both a targeted and more unbiased sample returned a similar expectation value for the proportion of eruptive variables from among YSOs (circa 10%), we can extrapolate this to the entire YSO sample of Kryukova et al. (2014), which would return 192^{+12}_{-36} candidate eruptive variable YSOs. Some caveats are worth noting at this juncture, most notably is that the time domain behaviour of the EVs in both samples is different, with the Cygnus-X sample favouring gradually brightening high amplitude sources, whereas the spectral sample from chapter 3 was able to identify FUor like sources more efficiently. The reason for the latter is relatively obvious; without a confirmed NIR outburst, the gradually fading or flat post-outburst light curves of a FUor are almost impossible to distinguish from a 'normal' YSO. Likewise the novel high-amplitude sources found in this chapter would not be selected from UGPS, as their NIR increase would likely be <1 magnitude. An additional caveat exists that only 56.9% of the UKIDSS selection had NEOWISE or unTimely light-curves, leading to a selection bias towards brighter or more isolated sources, owing to the reduced resolution of the WISE camera's as compared to UKIRT's WFCAM. The UGPS method employed earlier is far more effective at identifying sources with repeating, short-timescale (on the order of months) bursts, and those with very high amplitudes, than those targets with gradual increases in luminosity, i.e. $\approx 0.2\text{magyr}^{-1}$ in $W1\&W2$ (like those in Fig 4.8)

[2]The candidates in question are objects: 362, 820, 1017, 1048, 1762 & 1964, of which the sources from figure 4.2 are FUor-like, but have an eruptive classification from the UGPS data primarily

[3]These sources being those displayed in Figures 4.8, 4.9 & 4.10.

- An unusual result from both of the samples in this chapter has been the complete lack of any stars that could be classified as 'dippers'. This stands in contrast to the three, or possibly four identified in chapter 3, with the expectation value falling from $18.5^{+1.1}_{-5.7}\%$ to $3.3^{+0.3}_{-1.3}\%$. The reasoning for this unexpected result is unclear, however given that the selected YSOs were of earlier type, and that the 'dippers' found in chapter 2 have smaller MIR colours (compared to this sample), they may simply be harder to select from MIR surveys. This is born out when considering the class II SED slope of 2 of the four dippers found in chapter 3, as these stars are removed from the sample of Kryukova et al. (2014). Additionally, if the amplitude of any 'dippers' in the original 216 star sample was sufficiently high, they would likely have numerous non-detections in NEOWISE, and thus would have been cut from my final 123 star selection. Following this up with a investigation into the unTimely light curves for the removed 93 stars might provide an insight into any MIR selected 'dippers'.

This work does demonstrate the efficacy of using MIR time-domain data to aid in the classification and identification of eruptive YSOs, with the provision that the initial targets are suspected young stars, in order to alleviate contamination from post-MS stars. There are drawbacks to using MIR data in this regard, because the amplitudes for YSO variability (especially that which is accretion driven) are lower in this wavelength regime, and can thus lead to biases against the selection of the lower amplitude EX Lup type events. Hence it is still worthwhile to combine MIR with NIR data where available as to place a lower limit on observed changes in luminosity.

4.6 Conclusions

- Using additional publicly accessible YSO surveys to search for eruptive variable candidates at or below the UGPS/UKIDSS detection limit provided a 27.8% increase in the number of candidate eruptive stars within the Cygnus X region, preferentially identifying higher amplitude sources than were found by the original sample.

- The above method also allows the investigation into the rates of eruptive variability more generally, finding up to 28% of NIR detected YSOs in Cygnus X displayed variability of greater than one magnitude in the MIR, as identified in NEOWISE light curves. Noting that YSOs often have lower amplitudes in the MIR, the rates of near-infrared variability of similar strength are likely higher than this. Given the wide coverage in wavelength and

time-domain environments for Cygnus-X, it is plausible to employ the methodology used in this chapter to an expanded sample of YSOs, from the SPICY catalogue. Although outside of the direct scope of this work, this is likely the next step in identifying more stars similar to those in Figure 4.8, as variability in this feature space is unstudied at the current time.

- With regard to eruptive variability, an extrapolation was made into the wider Kryukova et al. (2014) sample, predicting that between 173 and 233 eruptive YSOs could be identified through MIR light curves alone. This coincides with an overall expectation value of $10.67^{+1.0}_{-1.83}\%$ for the proportion of EVs within nearby SFRs (combining the work in this and the previous chapter).

- A large array of unstudied behaviour exists within the mid-infrared, which will shine a light on the differences in variability for younger or more heavily embedded systems.

Chapter 5

Unusual Objects in the Near Infrared: Using Multi-wavelength Observations for Classification of a New CV

5.1 Introduction

The object UGPS J194310.32+183851.8 (hereafter referred to as Source 363, Lucas et al. 2017) was imaged twice as part of the UKIDSS Galactic-Plane Survey (UGPS), displaying 1.97 mag infrared variability in K over the 4 year interval and Hα emission in the IPHAS survey photometry (Drew et al., 2005). One of the infrared colours was exceptionally blue: $J-H=-0.6$, but $H-K=+0.7$. Lucas et al. suggested that this might be due to variability on the 7 minute timescale of UKIDSS filter changes, supported by marginal detections in the 2MASS images that suggested unremarkable colours. Additionally, the Gaia satellite has determined a fairly nearby location (see Section 2.1). Consequently, from the lack of any previous detection of X-rays, gamma rays or radio waves by facilities such as Fermi-LAT, ROSAT and the Very Large Array Sky Survey (VLASS), (Atwood et al., 2009; Voges et al., 1999a; Lacy et al., 2020), I infer that the system does not contain a neutron star or black hole. Thus I must be looking at a white dwarf (WD) binary system most likely of the cataclysmic variable (CV) type.

Cataclysmic variables (CVs) are binary systems containing a WD and a close companion (of comparatively low mass), wherein the WD primary accretes mass via Roche-lobe overflow from the secondary star (see Knigge et al. 2011 and Schreiber et al. 2021 for comprehensive reviews).

These systems are subdivided into magnetized and unmagnetized systems (based largely on the presence or absence of pulsations caused by the accretion flow proceeding along the magnetic field lines), and further subdivided based upon the method of WD accretion. The magnetic CVs consist of polars and intermediate polars (IPs). Polars accrete matter following the magnetic field lines directly to the surface of the primary due to their high magnetic field strengths of 7-230MG (Oliveira et al., 2017). This high field strength also causes the orbit and the spin of the WD's magnetosphere to become synchronous. In contrast, in IPs the Alfven radius is smaller than the circularization radius of the accretion disc, but larger than the white dwarf's radius, allowing an outer disc to exist. This disc is truncated, and then leads to the flow following magnetic field lines at free-fall velocity in the inner region. These systems are also notable for the spin and orbital periods ($P_{\rm spin}$ & $P_{\rm orb}$) being different from one another. It should be noted that a small subgroup of IPs can transfer mass via both disc-fed and stream-fed methods; for example FO Aqr, TX Col (Littlefield et al. 2020, Littlefield et al. 2021) and others still are known to be solely stream-fed and are referred to as discless IPs, such as EX Hya and DW Cnc (Andronov and Breus, 2013; Rodríguez-Gil et al., 2004). They are differentiated from Polars as a result of the WD spin & orbital periods not being synchronous.

Their hard spectrum arises because the gas is in free-fall on to a white dwarf, so if the accretion column is optically thin, the emission will come out as bremsstrahlung radiation with energies $E \approx kT \sim 10-30$ keV. The innermost region will usually be optically thick, and then can give emission in soft X-rays or EUV, depending on the luminosity and the size scale of the polar region spot at the base of the accretion column. It's reasonable that some of these are missed because of absorption effects, but that's still unsettled. X-ray spectra frequently show ionized iron in emission, caused by shock excitation from the free-falling disk material.

In the optical regime, the systems are highly variable and multi-periodic, with periodicities associated with the WD spin, the binary orbit and beat interactions between these two periods. Spectrally, IPs are characterised by broad emission of hydrogen recombination lines, as well as emission of helium (both neutral and ionized), carbon and nitrogen. Absorption features can be used to understand the composition of the companion (providing they are of high signal to noise), as well as the disc inclination. By comparison, polars have stronger but narrower emission features (often having Zeeman splitting due to the high magnetic field strength), including a prominent doubly ionized nitrogen line at 4650Å produced in the accretion column.

In this paper I present the discovery of Source 363's nature as a new magnetic CV. I report on

optical spectroscopic observations showing unusually broad emission lines (Section 3.1). I then detail numerous photometric monitoring observations which illustrate the system's behaviour on short timescales (Section 3.2), revealing periodicity at $\approx$ 2760s. Finally I report on new X-ray observations by the *Neil Gehrels Swift Observatory* (hereinafter *Swift*) which have provided the first detections of X-ray emission from the source, consistent with our classification of the source as an accreting WD system (Section 3.3). I then conclude with a discussion on the nature and novel properties of the source, given the various dichotomies our combined approach has uncovered (Section 4).

5.2 Source Information and Observations

Previous optical and infrared observations of the source have been carried out as part of UGPS, 2MASS, UVEX, IPHAS, Gaia and Pan-STARRS (Lucas et al. 2008; Skrutskie et al. 2006a; Groot et al. 2009; Drew et al. 2005; Gaia Collaboration et al. 2018a, 2021; Flewelling 2017). They reveal the source to be an optically faint but comparatively infrared-bright variable star (Table 5.1[1]) , with a prominent Hα excess. Rapid variability is clearly seen in the sparsely sampled Pan-STARRS 1 optical light curve: it varies by a factor of 4 in 15 minutes or less in *r*, confirming the fast nature of the source's variability. This indicates that the system includes a compact object of some type. The latest distance from Bailer-Jones et al. (2021) using Gaia EDR3 put the star at $900.7^{+288.3}_{-245.6}$ pc, which leads to an absolute magnitude in *G* of 10.61, although some care should be taken with this due to the variability of the source, as the prior used by Bailer-Jones et al. (2021) is more suited to non-variable stars. All these features together were indicative of Source 363 possibly being a compact object, although there was no associated X-ray emission recorded in previous all-sky surveys, so the flux must be less than 5×10^{-13}erg cm^{-2} s^{-1}, the limit for ROSAT (Voges et al., 1999a). The absence of X-rays of the required intensity can safely rule out a neutron star system, but a CV system would still be plausible for a faint X-ray source. The combination of the strong, rapid variability and the lack of X-ray emission in all-sky surveys led to the acquisition of targeted X-ray observations, several high cadence light curves, and an optical spectrum.

[1][1]:Contreras Peña et al. (2014b); Lucas et al. (2008),[2]:Monguió et al. (2020),[3]:Gaia Collaboration et al. (2021, 2018a, 2016a),[4]:Flewelling (2017)

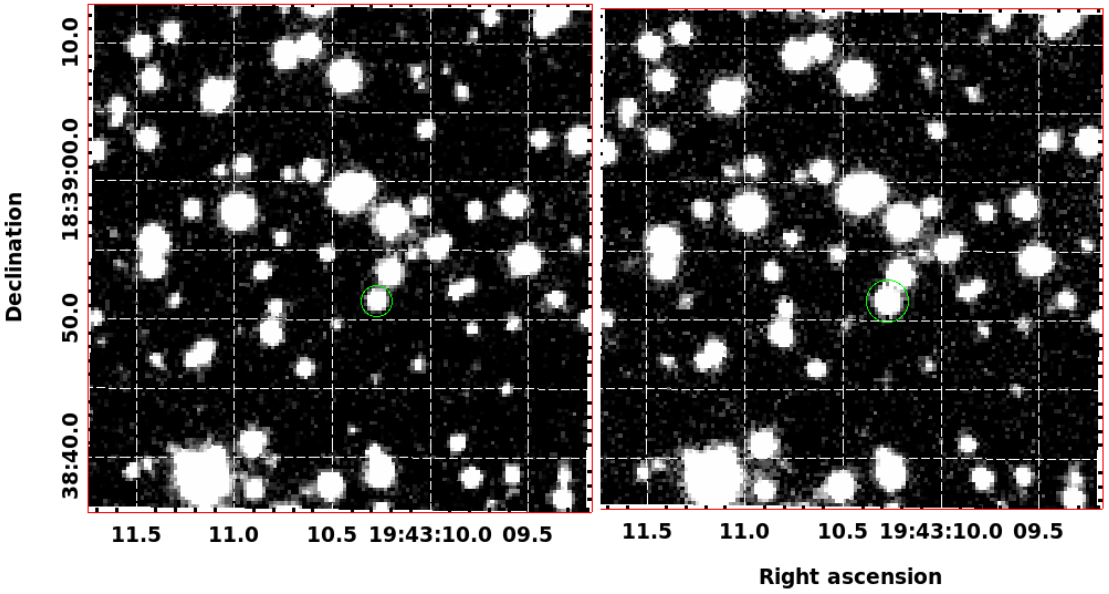

FIGURE 5.1: WHT PF-QHY r'-band images of Source 363 (within the green annulus), showing the short timescale variation, with the 1.1 magnitude change across 16 minutes. The left panel has an MJD of 59386.153 and the right panel of 59386.164.

TABLE 5.1: Table of selected archival measurements for Source 363. N.B., an asterisk in No. of Epochs implies that more epochs were available but they are not included because of poor data quality.

Survey	Filter	Mean Magnitude & Error	No. of Epochs	Maximum Variation (mag)
UKIDSS[1]	*Ks*	16.70±0.08	2	1.97
UKIDSS[1]	*H*	18.36±0.11	1	N/A
UKIDSS[1]	*J*	17.76±0.03	1	N/A
IGAPS[2]	*r*	20.54±0.06	4	1.94
IGAPS[2]	*Hα*	19.42±0.06	2	N/A
IGAPS[2]	*i*	19.27±0.07	2	N/A
IGAPS[2]	RGO *U*	19.68±0.03	2	0.37
Gaia[3]	*G*	20.02±0.10	3	0.72
Pan-STARRS[4]	*g*	20.35±0.04	8*	1.46
Pan-STARRS[4]	*r*	20.83±0.07	8	1.82
Pan-STARRS[4]	*z*	19.64±0.07	4*	0.55

5.2.1 SOAR Observations

5.2.1.1 Spectroscopy

I obtained a single low-resolution spectrum of the source on 2021 May 12 with the Red Camera of the Goodman Spectrograph (Clemens et al., 2004) on the SOAR telescope. The exposure time was 1800 s, and the observation used a 400 l mm^{-1} grating and a 0.95″slit together with a GG395 long-pass filter, yielding a full-width at half-maximum resolution of 5.4Å (about 250 km s^{-1}) over a usable wavelength range $\sim$ 4000–7820 Å.

The spectrum was reduced and optimally extracted in the usual manner using IRAF (Tody, 1986). The resulting spectrum has an average signal to noise ratio of ~ 14 per resolution element (~ 8 per pixel) in the continuum.

5.2.1.2 Imaging

Follow up imaging was obtained on 2021 June 9, using the Red Camera of SOAR/Goodman in imaging mode. I obtained 29 exposures, each of 180 s duration, using the SDSS i' filter. These totalled 87 min on source over a time span of 98 min. The average airmass was 1.62 and typical seeing was $1.5''$.

The raw images were corrected for bias and then flat-fielded with sky flats using standard routines in IRAF (Tody, 1986). I performed differential photometry of Source 363 with respect to 17 nearby, non-variable stars and calibrated these magnitudes using their Pan-STARRS DR2 (Chambers et al., 2016) i' mags, the final results can be seen in Figure 5.4.

5.2.2 WHT Observations

I made use of recently offered service time on the William Herschel Telescope for testing the new PF-QHY camera[2] to obtain two high cadence light curves. These were using Sloan u' and r' filters, with 62 & 61 epochs of data covering 90 and 89 minutes respectively and individual exposures of 80 seconds in each band. PF-QHY is a wide-field camera with a CMOS detector, its field of view being 10.7' by 7.1' and a pixel scale of 0.267" using 4x4 binning. Data reduction and calibration were carried out using the `photutils` (Bradley et al., 2021) and `astropy` (Astropy Collaboration et al., 2013, 2018) libraries for `python`, with profile-fitting photometry being used in the crowded r' images. Aperture photometry was used in the u' images as the field is comparatively less populated with sources. Calibration was done via a standard star SP 1942+261, with corrections to individual epochs being averaged across non-variable stars in each frame.

[2]See the instrument page for details: 'www.ing.iac.es/astronomy/instruments/pf-qhy/'

5.2.3 Swift XRT/UVOT Observations

I obtained X-ray and UV data from Swift via a successful target of opportunity (ToO) program on the 2nd of July 2021, using both the XRT and UVOT instruments in parallel, with 4 ks of observation in the photon-counting mode. These data produced the standard X-ray images, light curve and spectrum, as well as additional images and a light curve in the UVOT U filter. The data were provided pre-reduced via the Swift ToO server (Evans et al. 2020, 2009) with the spectrum being fitted with a power law, and adjusted for galactic absorption along the line of sight. Calibration for the UVOT data was done in `python` using the same packages described previously. All other XRT reduction was carried out using `XSPEC` (Arnaud, 1996), using the specific setup for Swift-XRT.

5.3 Results and Analysis

5.3.1 Optical Spectrum

The SOAR spectrum (Figure 5.2) displays a number of features consistent with CVs in general, most notably Hα and Hβ in emission, with additional emission features from both neutral and singly-ionized helium (see Table 5.2 for details of individual lines). All emission lines are broad and single-peaked, with a wavelength resolution of 100.5 kms^{-1} at 5910Å (the mid-point of the spectrum). The wide range of velocities suggests the presence of a disc, or possibly a symmetric wind, although this cannot be further identified due to the blending of any C III / N III lines into the wings of the He II line at 4686Å. Fitting of line profiles (using a Voigt profile to account for both Doppler and Stark broadening) provides an average radial velocity (RV) of -280.2 ± 12.9kms^{-1}, see Figure 5.3. This value, while high, is not unexpected when only one spectrum is available, and the system's mean radial velocity is likely less than this. Some absorption features could be present in the spectrum, however the modest S/N ($\approx$14 per resolution element) precludes any reliable identification of these, and thus I have to determine the characteristics of the companion star through another method.

From the equivalent width (EW) ratio of He II/H$\beta = 0.18 \pm 0.10$ I cannot be certain whether the system's accretion is primarily magnetic (see Silber 1992), due to the noise in the detection of the He II line: a ratio above 0.4 is indicative of magnetically controlled accretion. It should be noted that those authors also suggest that the EW of Hβ should be $\geq$ 20Å in magnetic systems:

TABLE 5.2: Table of equivalent line widths for notable features in the I-band spectrum. While faint absorption features from a companion star can possibly be seen, they are not prominent enough for us to provide analysis. It's worth noting the approximate 9/3/1 ratio between the Balmer lines, while the helium ground state transitions indicate a higher population at higher energy levels, with the 3-2 line being most prominent. The helium lines were affected by noise and some blending, and thus have not been fitted for RVs and widths.

Emission Line	Equivalent & Width Å	Width kms^{-1}
H I 4340Å (5-2)	-21.7±5.7	1746.6
H I4861Å (4-2)	-49.3±2.6	2302.9
H I6562Å (3-2)	-161.6±2.2	2747.5
He I5875Å (3-2)	-31.3±4.2	N/A
He I6678Å (2-1)	-19.4±5.2	N/A
He I7065Å (1-0)	-16.2±4.9	N/A
He II4685.7Å	-9.0±5.1	N/A

here I have EW=49.3±2.6Å. I reason that the observed hydrogen line ratios may be as a result of a more complete than usual disk (for an IP), bearing resemblance to those observed around dwarf-novae. In those cases the slower rotating outer disk regions limit the excitation of the more energetic recombination lines, leading to lower fluxes from Hβ and Hγ than normal IPs.

I cannot be sure if Source 363 was in a brighter than average state at the time of observation; pre-spectroscopic imaging places the star at an intermediate brightness level (compared to its maxima and minima). However I cannot interpret whether the star was pre- or post-outburst, which given the length of the subsequent observation could place the star at either state. This is especially true given the low S/N of the He II line, meaning that the true ratio might be higher than the 0.4 value that is assumed to indicate magnetized accretion.

In comparison to objects from the literature, I note the absence of emission from N III and C III, which is commonly seen in fully magnetic polars (Warner, 1995). In addition the fringes of the H_β line do not contain the characteristic absorption features that are associated with a high disc inclination angle. Given that a broad range of velocities is observed the disc inclination angle cannot be very low so I can reason that the inclination angle is intermediate. The same line can also show the hallmarks of cyclotron radiation, as an overall increase in the localised continuum, which I note that Source 363 does not display, so cyclotron radiation is unlikely to be the cause of the observed near infrared excess.

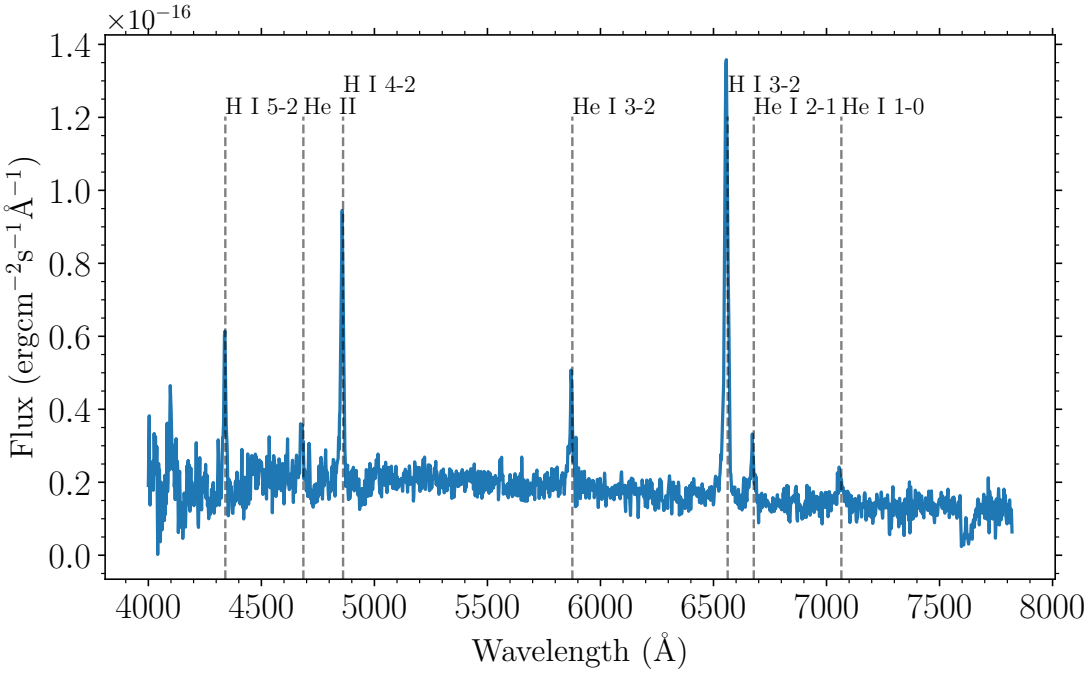

FIGURE 5.2: Optical spectrum of Source 363, using the Goodman Spectrograph at SOAR. Hydrogen recombination lines are prominent, and broader than those seen in more typical CVs. Other common CV lines such as He I and He II are also present, although the 4606Å Na III line often associated with IPs is not seen above the noise.

5.3.2 Light Curves

The three light curves (Figures 5.4, 5.5 and 5.6 for u', r' and i' respectively) each display amplitudes between 0.9 and 1.2 mag, but each wavelength shows differing behaviour: The u' curve shows symmetric behaviour with minimal time spent at either bright or faint states, whereas the r' curve is at a faint level for approximately two thirds of the observation, with the rise taking ≈ 7 min, followed by a 20 min decline to a state of quiescence, resembling behaviour reminiscent of stream-fed accretion on to the WD. This is similar to that seen in polar-type magnetic CVs (mCVs). The longer duration observations in i' show two peaks, with a separation and shape consistent with the u' data, including the scatter about the curves' minima. The peaks are separated by 51 ± 2.2 minutes and 65 ± 2.1 minutes for *i'* and *u'* respectively, with the *r'* curve having a less clear cycle, although the curves' minima are separated by $\approx 64 \pm 2.1$ minutes. These estimates provide a rough baseline for the most visible timescales of variability.

The u' and i' light curves show small amplitude variation at low brightness states not seen at the maxima, although at this time it cannot be wholly rejected that these are indicators of short period variability (not unlikely given the magnetohydrodynamic processes present in the disc). I

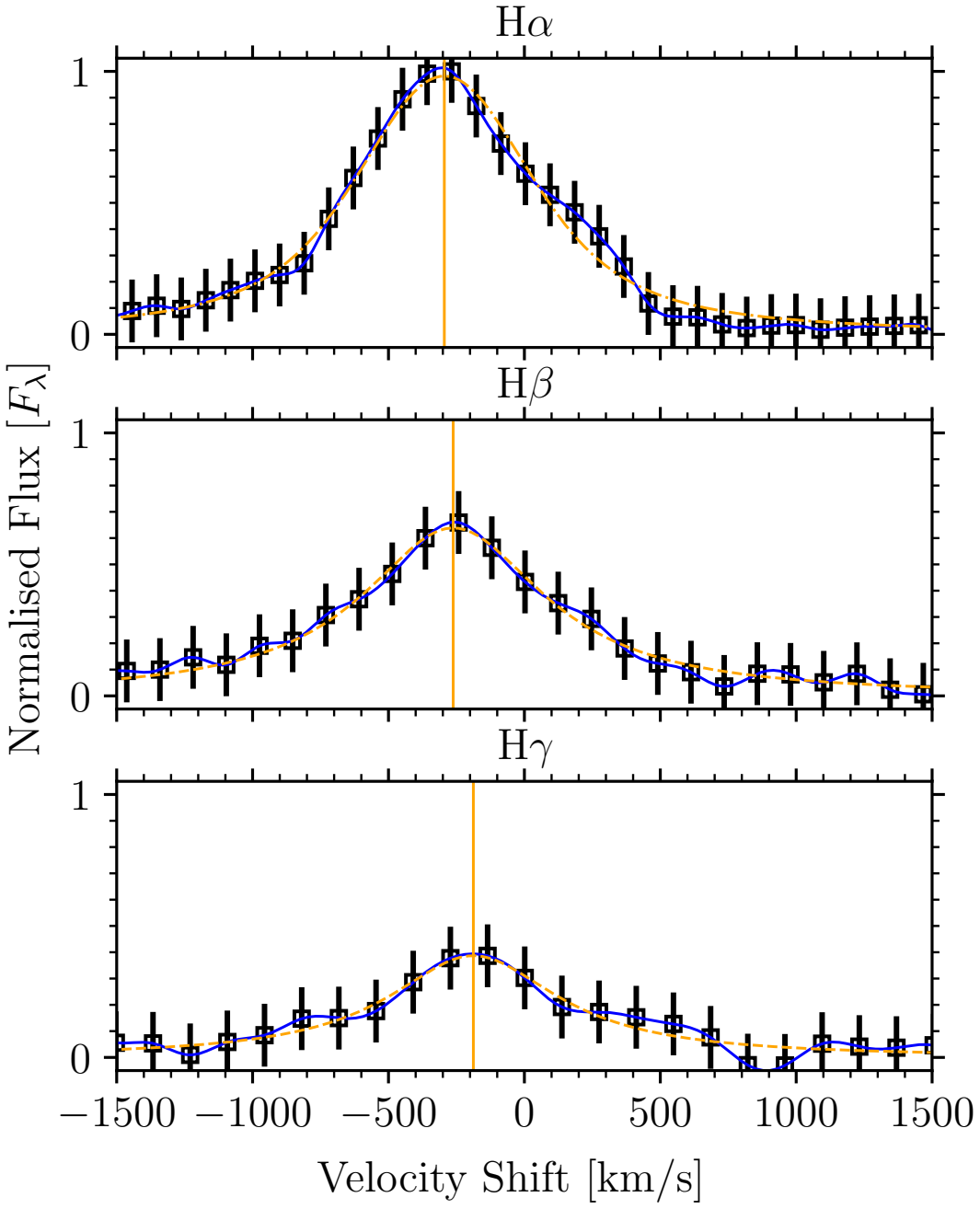

FIGURE 5.3: Fitted line profiles and radial velocities for the hydrogen recombination lines. Points and blue lines are the data, yellow dashed lines are the fits, using a Voigt profile, and converted into velocity space. The median radial velocity of the star was -283.9 ± 9.3 kms^{-1}, relative to the Local Standard of Rest. The individual radial velocities fitted to each line are marked with solid yellow lines. Fluxes are normalised with respect to the HI $3 \rightarrow 2$ line.

investigated this by fitting a third order spline to light-curve, phase-folded on the 66 minute best fit period (using `scipy`, Virtanen et al. 2020) and checking the residuals to this fit. This revealed no obvious periodicity. It would seem therefore that the variations during the system's minima are more likely the result of increased Poisson noise from the lower count rate. In addition a 19 hour LC (with approximately 1 hour on-source) in UVOT U-band was produced, consisting of 6 epochs of varying exposure time. Whilst not much can be gleaned from the shape (given the known rate of variability), the maximum variability amplitude was ≈0.8 mag, in keeping with data from other bands.

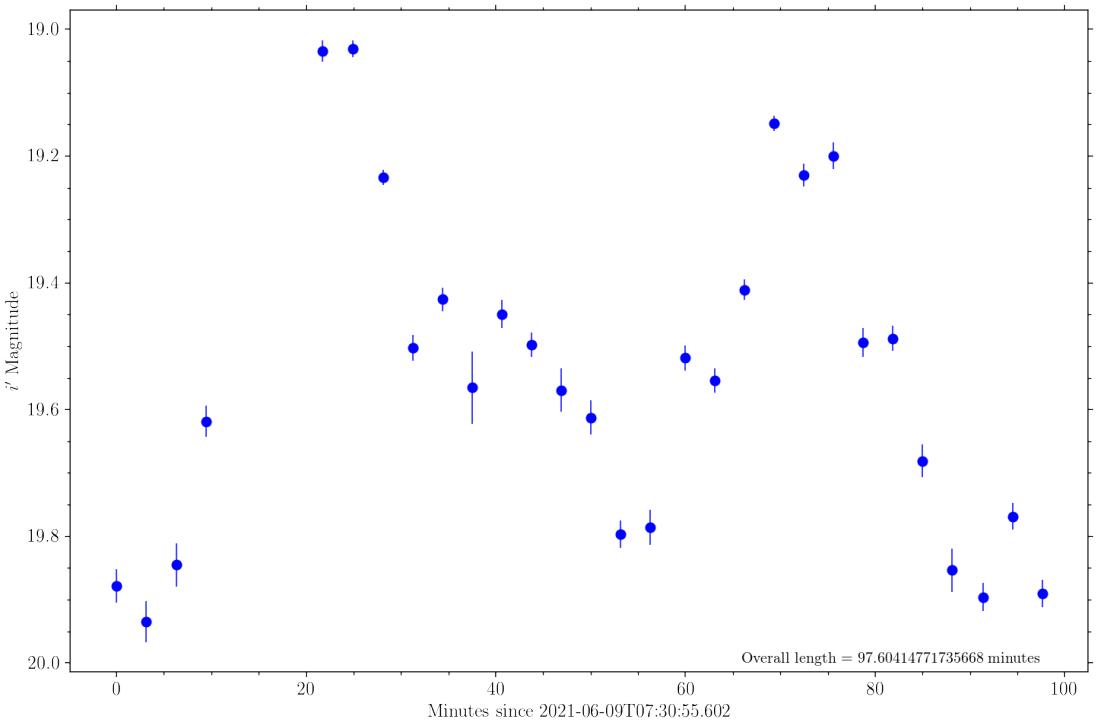

FIGURE 5.4: i'-Band light curve for Source 363, using SOAR's Goodman spectrograph in imaging mode. Fainter exposures were averaged with sequential epochs to recover signal. The peaks are separated by ≈51±2.2 minutes and the amplitudes are ≈0.9 mag.

Interpreting the nature of the observed variability is a challenge due to the limited time span of the observations, although a few causes can be inferred. A common cause of variability in CVs is flickering, a phenomenon that is thought to relate to modulation of the accretion rate and flares associated therein (see Bruch 2021 for a comprehensive review). A second driver of variability could be the spin of the WD primary star, seen via the accretion columns or polar hot-spots (depending on observed wavelength). A complication can arise from the orbital side-band: a side-band represents the reprocessing of the WD primary's emission by its disc, which causes an interaction between the spin period and the orbital period of the secondary, observed as a distinct

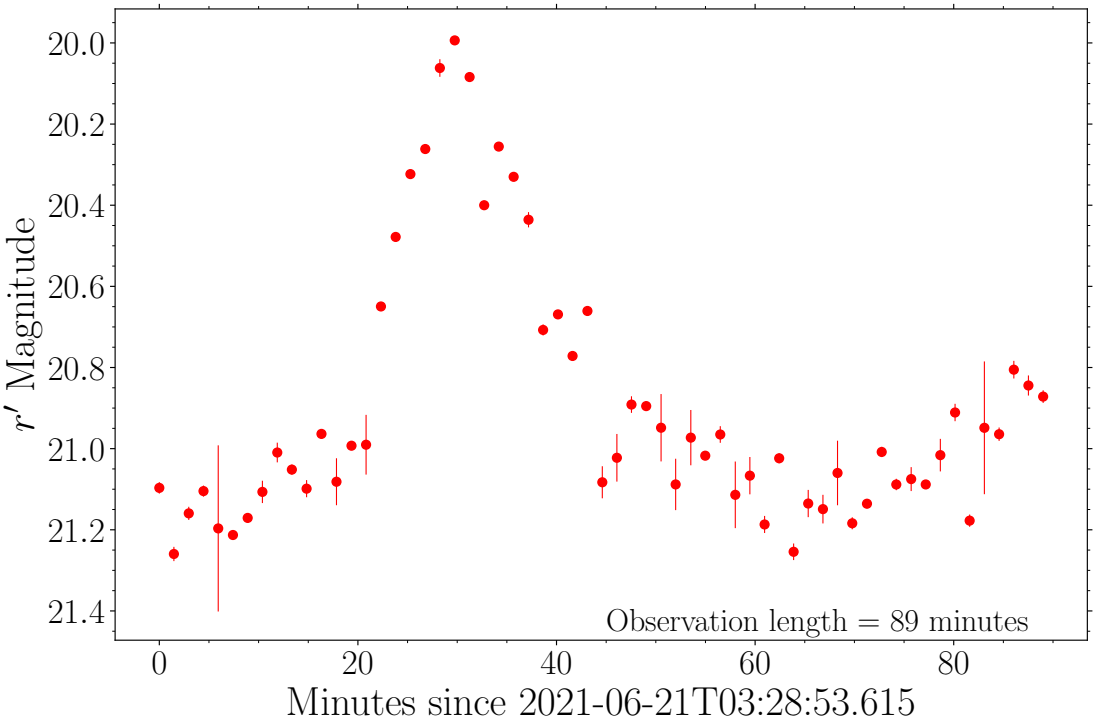

FIGURE 5.5: r'-band light curve, obtained with the PF-QHY instrument on the WHT. The peak shows an amplitude of ≈1.2 mag and resembles flare-like behaviour, with a comparatively fast rise followed by extended cooling time. If I assume this behaviour repeats based upon data from other filters, the timescale is of the order of approximately 66 minutes, from the start of the event to the next rise.

frequency, $\omega_{spin} \pm \omega_{orb}$, with a positive sign in most in cases, e.g. AO Psc (Bonnardeau, 2015) and a negative sign if the orbit is retrograde. While there are currently not enough individual cycles to confirm any periods, I note that the lack of observed periodicities at short timescales (≈20 min) in any of the curves is interesting. This could imply that the WD does not spin at the common period of approximately 10-15 min.

5.3.3 X-ray Photometry

The Swift-XRT observations detect a single source at RA = 295.7935°, and Dec = 18.6475° with an astrometric uncertainty of 3.0″ (see Figure 5.7) given by the Swift-XRT data products generator' software (Evans et al., 2014). These coordinates are offset from the optical/IR coordinates by 1.9″, which is consistent with zero offset within the uncertainties. I note that the rather scattered distribution of X-ray photons shown in Figure 5.7 is typical of Swift/XRT observations of a single faint source, see `https://www.swift.ac.uk/analysis/xrt/xrtcentroid.php` for an example of how real sources are distinguished from noise.

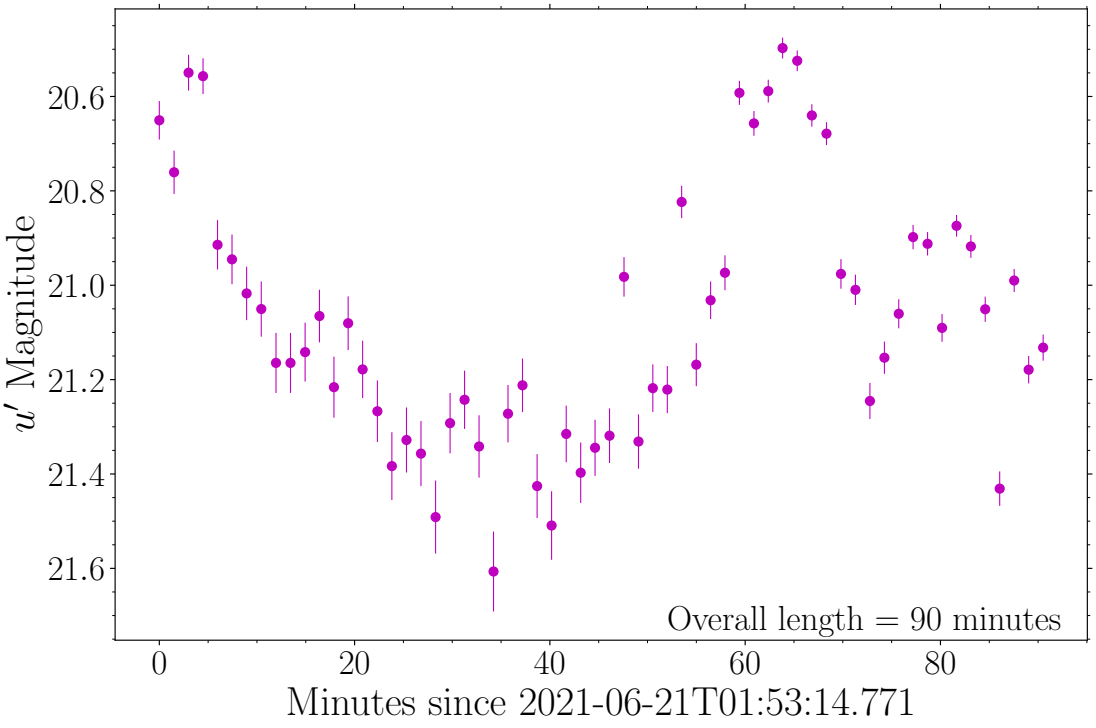

FIGURE 5.6: u'-band light curve, obtained with the PF-QHY instrument on the WHT. There is significant scatter in this curve, likely because of the u' bands increased sensitivity to changes in seeing. However the the same high amplitude, short timescale behaviour can be seen as in other filters. The two apparent peaks are separated by between 64 and 67 minutes, which is analogous to the timescales seen in the *r'* curve.

Given the lower resolution of Swift's instruments than the optical ones discussed thus far, the possibility of chance association should be considered. Therefore I consider X-ray source density of 0.27 objects per square degree in the Galactic plane, as determined from the ROSAT catalogue Voges et al. (1999b)) at Galactic coordinates $30^\circ < l < 90^\circ$, $-3^\circ < b < 3^\circ$. With this figure the probability of a chance alignment within $3.0''$ is 3.78×10^{-6}. Given that the fitted XRT spectrum is brightest at the lower energy regime, the low sensitivity of ROSAT to higher energies is not detrimental to this estimation. Further to this, whilst there are two optical/IR sources within the XRT astrometric uncertainty radius, the associated UVOT light curve displayed high amplitude variability consistent with that observed in Source 363 and the second star is not optically variable. Therefore it is clear that the XRT X-ray source is Source 363. The measured X-ray flux is brighter than the ROSAT sensitivity limit, generally taken to be on the order of $1.5x10^{-13}$ergs^{-1}cm^{-2}. The XRT bandpass is broader than that of ROSAT (0.2-10 KeV compared to 0.5-2 KeV), but the observed flux is still a factor of two greater than the sensitivity limit ($3.43x10^{-13}$ergs^{-1}cm^{-2}) when reprocessed into the ROSAT bandpass with WebPIMMS.

The average count rate over the length of observations was 0.01375 counts s^{-1}; this was then converted into a flux via fitting an absorption adjusted power law to the XRT spectrum (see section 5.2.3), with a photon index of 1.9. The previous lack of detections implied that the overall flux would be low, but our measured fluxes (adjusted for absorption) of $1.3^{+0.4}_{-0.3} \times 10^{-12}$ erg s^{-1}cm^{-2} are above the lower limits for surveys such as ROSAT. Luminosities corresponding to these fluxes have a range that's higher than average for IPs ($\sim 10^{30}$ erg s^{-1}). Depending on the distance used, luminosity ranges from $6.9 \pm 1.8 \times 10^{31}$ erg s^{-1} to $2.3 \pm 0.6 \times 10^{32}$ erg s^{-1}, at the closest and furthest distance estimates respectively (as discussed in Section 5.2). The associated X-ray light curve shows only an intermittent signal, however with only 27 photons in total, no time-domain analysis is possible.

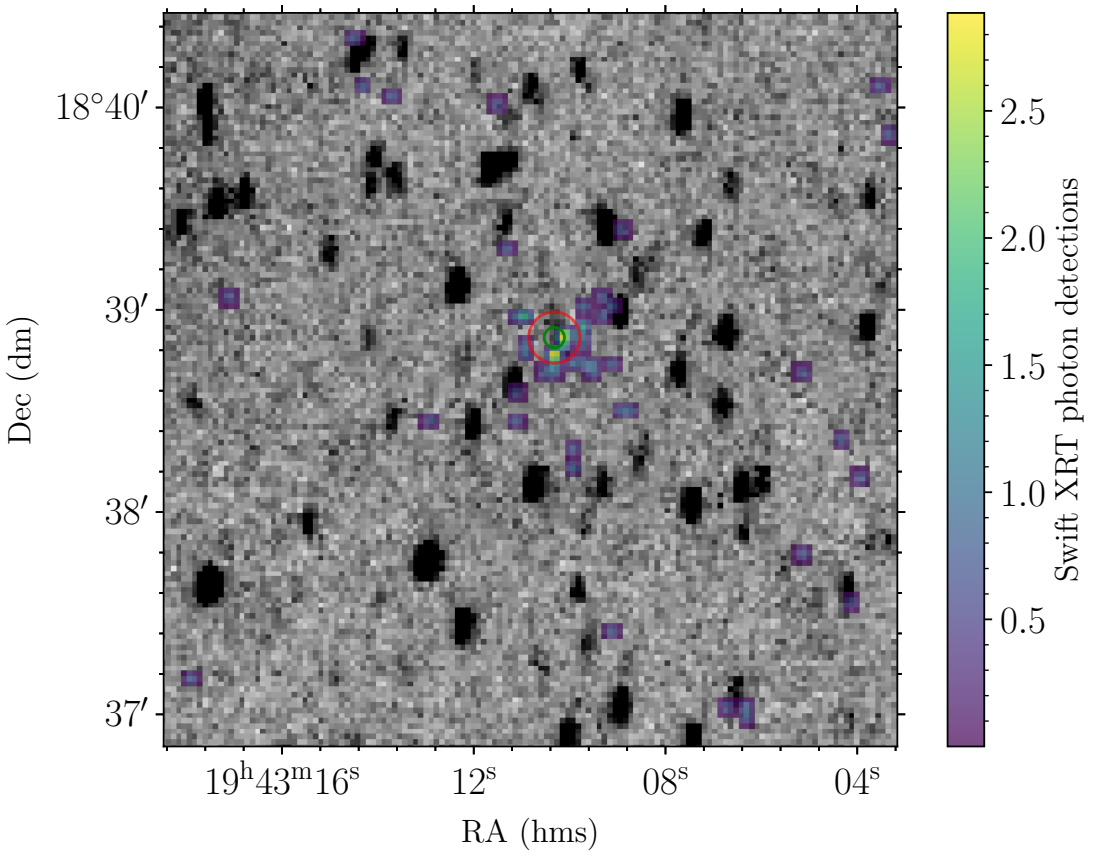

FIGURE 5.7: XRT photon-count mode image (blue/green/yellow) overlaid on a stacked UVOT-U band image (grayscale), Source 363 is located within the red (7.6″) and green (3.0″) annuli. These represent the source detection confidence radii (without and with UVOT astrometry respectively), as calculated by 'The Swift-XRT data products generator' (Evans et al., 2014). Our system is faint in the stacked UV image, but the XRT image provides the first indication that the star is an X-ray source.

5.4 Discussion

5.4.1 Comparison to sources in the literature

Existing IPs with some degree of similarity to Source 363 have often been detected either through their X-ray emission or optical narrow-band flux. Thus I must compare the overall behaviour of Source 363 to these systems, in order to understand the observed behaviour. Constructing some approximate optical to near infrared spectral energy distributions (SEDs) (see Figure 5.8) I note that Source 363 has both the lowest overall luminosity at the wavelengths measured and an unexpectedly faint optical SED. This SED has been formed by averaging all available measurements at each wavelength (including each individual measurement from this work, as well as all available archive data), with the full range of values also marked on the plot. It should be noted that the J (1.25 μm) and H (1.65 μm) data are single measurements that may not be representative: the J datum may be near a peak value, given the exceptionally blue $J-H$ colour (see §1). Having noted this caveat, the SED appears to have a redder slope than other systems, possibly a byproduct of the disk being optically thicker than other examples. The two most similar objects (EX Hya and DW Cnc) are both short-period systems that lack discs, and exist in a separate portion of the IP spin-orbit period diagram, where $P_{orb} \approx 2 \times P_{spin}$ (see Figure 5.9 [3]), as opposed to the more common ratio $P_{orb} \approx 10 \times P_{spin}$.

I propose that our source might also be a part of this small population, given the lack of a detectable short spin period in any of our observations, and the lower limit on the orbital period given by the low mass of the companion (see Section 5.4.2). Our u' light curve is also similar in shape to DW Cnc (Rodríguez-Gil et al., 2004), although it is a factor 2 higher in amplitude, with both sources having periods of under an hour. The corresponding r' light curve from the same night of observations shares little in common with any typical IP system in the literature.

A more comparable object is the short-period IP V598 Peg (SDSS J233325.92+152222.1, Southworth et al. 2007 & Szkody et al. 2005), which has a spin period of 43 minutes, and a confirmed (via Pointed XMM-Newton observations by Hilton et al. 2009) orbital period of 86 minutes. The shape of the optical light curve when phase folded (Figure 4 in Hilton et al.) is almost identical

[3] References for Figure 5.9: Hilton et al. (2009), Rodríguez-Gil et al. (2004), Andronov and Breus (2013), Buckley et al. (1998); Buckley and Tuohy (1989), Hellier (1993), Kemp et al. (2002), Norton et al. (2002), Staude et al. (2003), Woudt and Warner (2003); Woudt et al. (2012),Kim et al. (2005), Joshi et al. (2011), Masetti et al. (2012), Mateo et al. (1991), Kaluzny and Semeniuk (1988), Burwitz et al. (1996), Hellier (1997); Evans et al. (2006), Norton et al. (2002), Pretorius (2009), Sazonov et al. (2008) - The URL of the Mukai's 'The Intermediate Polars' (where this data is collated) is as follows: '`https://asd.gsfc.nasa.gov/Koji.Mukai/iphome/iphome.html`'

to the r' band curve (see Figure5.5). In addition, the Hα to Hβ ratio of 1.87 is of a similar order to Source 363's.

For comparison purposes (in Figure 5.8) I have included two of the aforementioned short-period IPs (DW Cnc and EX Hya), as well as the traditional IPs DQ Her and EI Uma, both of which have well sampled SEDs publicly accessible. V795 Her is also included because it has only one confirmed period (thought to be the orbital), at 2.5 hours, and no detected X-ray periodicity in much the same way as Source 363.

To compare our spectrum to the literature, I find Oliveira et al. (2017) to be a good source of similar candidates due to their survey also using SOAR's Goodman spectrograph. Source 363's slightly blue continuum (by comparison to polar-like sources) and broad lines bear the closest resemblance to MLS2054-19, MLS0720+17, CSS1012-18 and SSS1359-39 (see Figure 1 in the aforementioned paper). Interestingly, three of these are classified by those authors as discless IPs (MLS0720+17 was suggested to be a polar). Some small differences to these sources are worth noting, in particular the relative strength of the Hβ line compared to Hα, with all of these sources having the 4-2 transition as strong or stronger than the 3-2 line, the inverse of our finding.

5.4.2 Nature of the System?

As it stands, I can say with some confidence that if the apparent $\sim$45-70 minute variation timescales are related to the WD spin period (e.g. with the spread of values caused by stochastic flickering) then the system cannot be a polar CV. All hydrogen-rich stars will over-fill, rather than fill, their Roche lobes for such short periods (leading to a rapid cut off of the mass transfer via magnetic braking), and the optical spectrum of the source clearly shows strong hydrogen emission lines, indicating that accretion is taking place. The argument could be made that there are two accretion streams, from both poles of the WD being magnetized (synchronising the system) much like the system V2400 Oph (Hellier and Beardmore, 2002), and thus the spin period would then be on the order of 90 minutes. However given that the spectrum suggests a disc, it is more likely the orbital period is longer than the spin period and just below 'period gap', making the system some form of IP.

With the IP explanation preferred based on the optical spectrum, it then becomes important to investigate the evolutionary state of the system, in order to explain the unusual behaviour

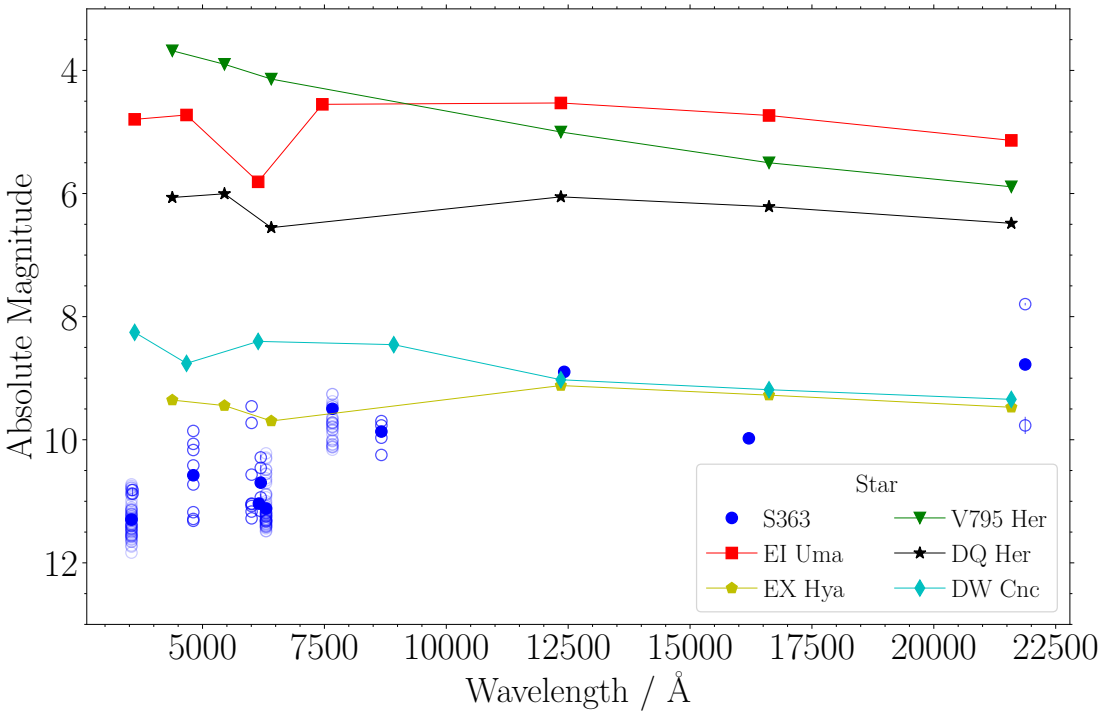

FIGURE 5.8: Optical and near infrared SEDs (AB system) for Source 363 (blue) and a selection of existing IPs from the literature. The solid blue points represent the median optical values from the new light curves in this work (u', r', i'), the 3 Panstarrs passbands and two IGAPS passbands with multiple epochs: (g,r,z) and (u, r), respectively. The single-epoch J and H UKIDSS data and the mean of the two UKIDSS K values are also shown as solid blue points. Open circles are the individual measurements from which the medians were computed. (For readability the Panstarrs r, WHT r' and IGAPS r data in slightly different filters have been offset by 250 Åbut u and u' are almost identical so they are combined into one average). Note the high red optical and IR luminosity compared to shorter wavelengths. This is not present in previously classified IPs. The selected IPs are those with long spin periods and orbital periods ($P_{\rm spin} \sim 0.3 P_{\rm orb}$), with distances coming from (Bailer-Jones et al., 2021), using Gaia EDR3.

(high variability amplitude, red SED and low overall luminosity). I can add constraints to the orbital period of the system by considering its near-infrared brightness and the amplitude of the associated variability; using the Bailer-Jones Gaia EDR3 distance of $900.7^{+288.3}_{-245.6}$ pc, I find Source 363 has $M_K \approx 6$, and in order to explain the observed variability the companion object must be be at least one magnitude fainter than that. This is because the variability is intrinsic to the WD, and thus the companion must not be providing the majority of the flux. These two factors combined lead us to place constraints on the classification of the companion, finding that it should be no more massive than an M3V star at 0.36 $M_\odot$ (Pecaut and Mamajek, 2013). This proposed limit on the companion mass would put the orbital period at roughly 2.5 hours or less, where a 2.5 hr period sits in the IP 'period gap'. Equally using Figure 13 in Knigge et al. (2011) for our two *Ks* observations leads to orbital period limits of between 2.1 and 1.4 hours.

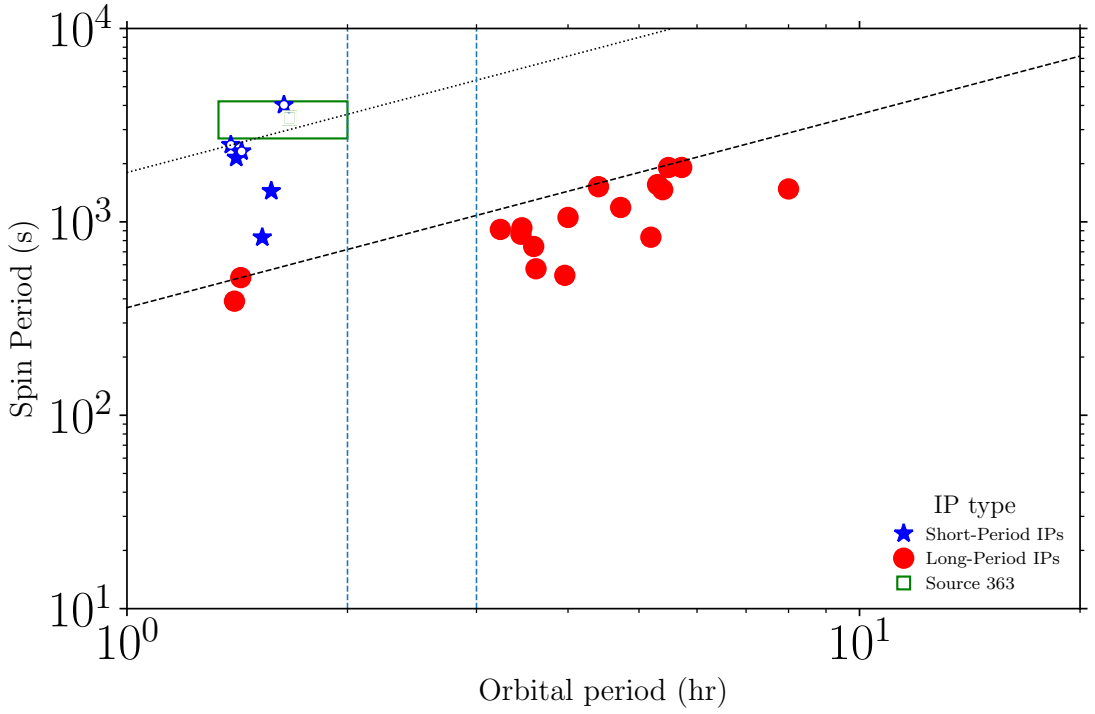

FIGURE 5.9: Orbital period versus spin period for a selection of known IPs (data from Mukai's 'The Intermediate Polars' - see footnote). The blue stars represent short period systems (those with white dots being mentioned in the text), red circles typical IPs. The green rectangle represents the likely range of orbital and spin periods of Source 363, these being constrained by the minimum orbital period of ≈80 mins (Knigge et al., 2011) and the lower limit of the period-gap. The two dashed vertical lines at $P_{orb} = 2\ hr$ & $3\ hr$ represent the 'period gap' where magnetic braking due to angular momentum transfer will cut-off mass-transfer between the WD and its companion. The diagonal dashed line is where $P_{orb} = 10 \times P_{spin}$, below which long-period IPs are found. The additional dotted line demarcates the region where the orbital period is twice the spin period, which is a common feature of short-period IPs.

While this is a wide spread of values it does place the system below the period gap, in the region between that and the minimum IP orbital period of 80 minutes.

Thus I can reasonably then assume the orbital period is less than the 2.1 hour lower limit (Rappaport et al., 1982), especially given the higher than average X-ray luminosity (stars within the gap have very low accretion rates, and thus low X-ray luminosity). Additionally a companion star of the described nature would have a short orbital period if in an IP-like system, lending further credence for Source 363 to exist below the period-gap. There is an argument to be made that the orbital period is in fact less than 90 minutes, as can be seen in Figure 5.9, because a number of short-period IPs (including the aforementioned V598 Peg) have settled into orbital periods at twice that of the white dwarf spin, but with the same magnetic moment as more normal IPs, as predicted in Webbink and Wickramasinghe (2002). With an orbital period in this range I would expect a typical IP system to have a spin period on the order of 5-9 minutes, which is not seen in

our data, hence I posit that Source 363 may be a member of the short period sub-class mentioned above. This would roughly place the spin period of the white dwarf between 41 and 63 minutes, which mimics the timescales observed in our optical data.

Finally the observed strong IR excess (as described in Section 5.2) can then be assumed to be tracing the accretion flow, made more likely due to the lack of cyclotron emission features in the optical spectrum. Combining this with the short period, I can infer that our system has a reasonably high accretion rate for its short-period type. The method for this accretion is still uncertain, but it could be novel; Our light curves suggest direct accretion, whilst our SED and spectra suggest the presence of a disc, and thus disc-fed accretion. In order to make sense of this dichotomy, there is a possible explanation that Source 363 is currently undergoing an evolutionary transition between a typical (long-period) IP, and the short-period systems, such as has been described by Southworth et al. (2007) and Norton et al. (2008).

There is currently an open question as to what the number density of short-period IPs should be (Pretorius and Mukai, 2014). The small binary separations in short period systems should easily allow the WD magnetic fields to connect with the convective donor star, and thus quickly synchronise the orbits, with system thus becoming a polar CV - provided $\mu_{WD} \lesssim 5 \times 10^{33}$ Gcm^3 (Norton et al., 2004). This interpretation would render the subgroup short-lived, thus explaining their low observed numbers. On the other hand white dwarf magnetic fields can fall over time (Ohmic decay), and hence dramatically extend the time taken to become synchronous, in turn making such systems quite old, increasing the number density of this subgroup by extension. With a higher accretion rate than usual for short-period IPs, ram pressure would likely exceed magnetic pressure, which would then produce a disc, lending credence to this explanation for Source 363.

5.5 Conclusions

I report on the discovery of a new magnetic cataclysmic variable star system with an observed near-infrared excess, and have determined that our source is most likely a short-period IP system, with a higher than average accretion rate. This classification was based upon the following:

- Our optical spectrum shows emission of H I, He I and He II, all of which are indicators of magnetic CV systems. In addition the presence of disc-like features indicates that the

magnetic field is not solely responsible for the accretion, making the case that the star is a polar unlikely.

- The low optical luminosity of the system implies a low mass companion to the WD, which sets an upper limit on the orbital period of the binary.

- Combining this with the lack of an obvious spin period near the expected range of 5 to 9 minutes, I can infer that the system does not fit with the standard $1:10$ ratio between spin and orbital timescales. This deduction then places Source 363 within the loose group of short-period IPs, such as EX Hya.

- The confirmed detection of X-ray emission from the system in targeted observations is interesting given that the star is absent from previous wide field X-ray surveys that cover the region (it does not feature in Pretorius et al. 2013). The non-detection by ROSAT would normally suggest that the overall X-ray luminosity is lower than typical IPs, a phenomenon that has been observed in other short-period systems. However, the X-ray luminosity measured by more recent observations with the Swift/XRT of $1.31 \pm 0.34 \times 10^{32}$ erg s^{-1} (using the Gaia EDR3 Bailer-Jones estimated distance of 900 pc) is higher than that of most short period IPs (with these being between the orders of $\times 10^{28}$ erg s^{-1} & $\times 10^{31}$ erg s^{-1}).

- Additionally, I make a case that given the short orbital period and low optical brightness, that the system has a lower than average accretion rate (for an IP in general) and a companion star of a very faint type. This provides contrast with other short-period systems, making Source 363 seem fairly unique.

With such an unusual nature, implications from this work are twofold:

- It re-iterates that there is a population of under-luminous CVs that continue be missed in all wide area X-ray surveys completed thus far. But this work indicates a chance that the X-ray luminosity of these sources may not be as low as current literature suggests. Previously identified short-period systems have $L_X \approx 10^{31}$ erg s^{-1} whereas Source 363 ($L_X \approx 10^{32}$ erg s^{-1}) shows that these systems can exist above this cut but still below the more usual value of $\approx 10^{33}$ erg s^{-1} seen in typical IP systems. With the suggestions of a population of under-luminous IPs that may be responsible for some of the observed X-ray excess in the galactic bulge (Hailey et al., 2016), Source 363 might be a useful laboratory

to probe this idea further. The ongoing eROSITA (Predehl et al., 2021) survey should be deep enough to detect similar objects.

- It shows the usefulness of using near infrared variability to locate this kind of object, as well as the benefits of multi-wavelength astronomy to classify variable stars that are unexpected or unusual upon initial discovery.

The next steps in our investigation are to further constrain the system's parameters, specifically the WD and companion masses, as well as the spin and orbital periods. In addition, having these parameters will allow us to test our ideas for the system's unusual behaviour, as described in Section 4.2. In addition I aim to find additional candidates within the Vista Variables in the Via Lactea survey (VVV, Minniti et al. 2010), via collation of short period variable stars (Smith et al., 2018) with close distances and observed H_α excess from VPHAS+ (Drew et al., 2014b). This will allow us to build an idea of the scale of this population, and thus the expected X-ray flux that would be produced. In turn, this would provide a useful metric to determine whether they are the cause of the aforementioned flux excess.

5.6 Additional Work Post-Publication

After this work was originally published (Morris et al., 2022), further investigations were carried out, in order to reinforce the stated conclusions. This takes a two-pronged approach: by confirming the white dwarf spin period, and undertaking a search for similar systems within the survey area of VVV, via the VIRAC2B (Smith et al. (2018), Smith et al. In Prep.) catalogue.

5.6.1 Period Confirmation with the Liverpool Telescope

Following the original publication, I was awarded time on the Liverpool telescope via PATT, for further investigation of Source 363's periodicity. On the tenth of August 2022 source 363 was observed for 314 minutes, over 60 300 second epochs with the Liverpool Telescope. These data were made using the IO:O instrument with the *r'* filter, which has a field of view of 100 arcmin^2 and a pixel scale of 0.15" per pixel. Initial data reduction steps (flat fielding, bias subtraction) are carried out before the data is released, further reduction was carried out using a custom pipeline written in `python`. This uses tools contained in the `astropy` and `photutils` packages, with flux densities being measured with standard aperture photometry routines.

The five hour observation window provided almost five complete white dwarf spin cycles, a significant increase over previous observations, which featured no more than two. Figure 5.10 shows the completed light curve, calibrated with the LT's specified standard star for the night.

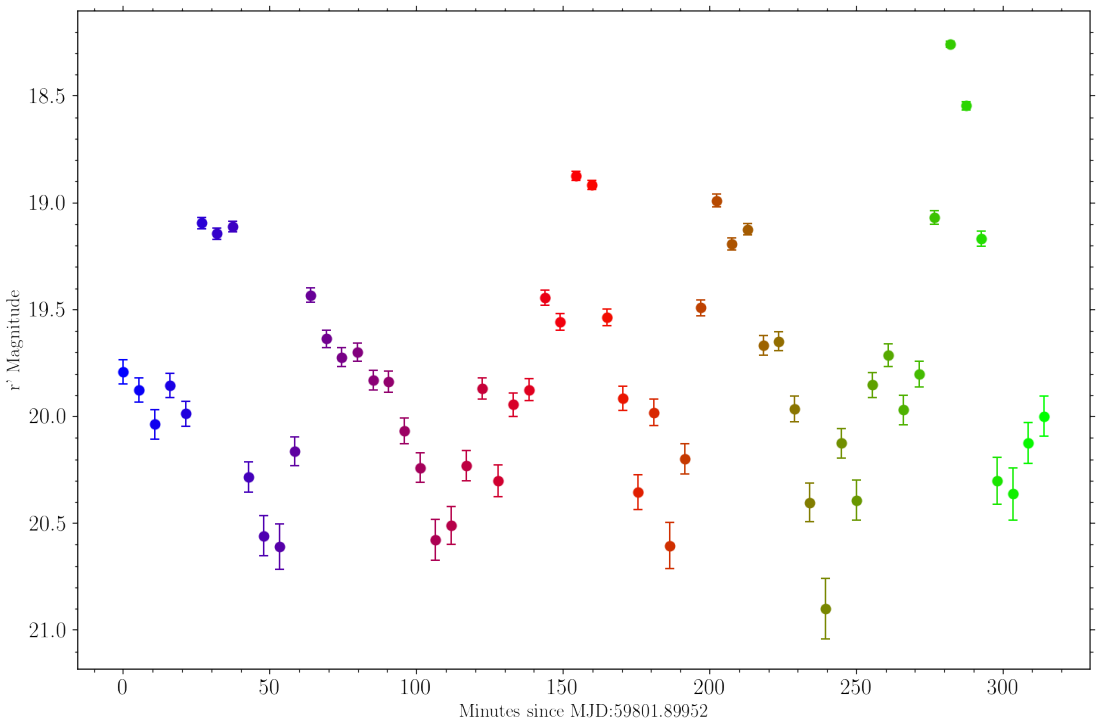

FIGURE 5.10: Light curve for source 363, showing four complete cycles, with five peaks. The peak amplitude is 2.64 mag, but this value only reflects the final observed cycle, and is otherwise higher than any other observation. The range between the ninetieth and tenth percentiles is 1.34 mag, and provides a better indication of the systems average amplitude. The colours are linked with MJD, to be used in a later plot (figure 5.11)

Five peaks in the curve allows for accurate fitting by the innovative neural network of Miller et al. (Submitted.), as well as the separate Time-Series Analysis Pipeline (Miller et al. In Prep). Given that the star had obvious short period variability, it makes an excellent laboratory to test all aspects of these upcoming codes. The time-series modules applies four period finding methods to a raw light-curve, but in the case of Source 363, methods using gaussian processes (GP) and Lomb-Scargle (LS) Lomb (1976); Scargle (1982) were not used; the star's variability is not sinusoidal, and thus LS is ineffective in the computation of a periodogram. By running LS on data such as this, there is a high risk of finding an alias of the star's true period (or other unrelated periodic phenomena associated with the observations) which would then be very difficult to disentangle from the actual result. The rest of the time-series analysis methods provided a clear picture of the system however, with a Phase Dispersion Minimisation (PDM)

(Stellingwerf, 1978) periodogram computed to give a second period estimation compared to that by eye. This was computed linearly in frequency space from $P = 0.0001$ days up to the temporal length of the light curve (300 minutes). The calculated period was 63 ± 1.6 minutes for the r' light curve. An additional check using a Conditional Entropy period finder (Graham et al., 2013) gave the same result.

Separate to the above method, a recurrent neural network (RNN) was used to provide both an estimated period and the associated False Alarm Probability (FAP), 2% in this instance. This technique involves training the RNN on over 10,000 real light curves of known periodic variable stars and over 100,000 synthetic light curves (both periodic and aperiodic) which were generated from real aperiodic light curves with periodic variability added. Synthetic light curves are generated via the application of a parametric shape (representing one of a random type known periodic variable star, such as a CV, EB, Mira or Cepheid) to a flat signal with induced noise. The aperiodic variables are taken from a combination of known aperiodic variables as well as randomly shuffled real periodic variables and randomly shuffled synthetic periodic variables. The random shuffling is exclusively performed on the photometric axis to leave any aliasing from the observing cadences present. i.e. a light curve is created of random photometric noise, but maintaining the correlated noise associated with the observing program. This trains the neural network to identify real variability by looking for structure within the phase folded light curve. This is analogous, but fundamentally different, to the PDM method. The network provided a best-fit period of 63 minutes, which is similar to that provided for the two WHT light curves, using the traditional period finding methods. Phase-folding about this period can be seen in figure 5.11, this also reveals the large scatter in amplitude, ranging from one to two magnitudes, which correlates with previous observations. The figure does illustrate the slight spread in period, as a result of the flickering intrinsic to the system, although the start point for the outbursts seems to be well constrained by the 63 minute period fit. Depending on the point in the cycle that any flickering occurs, the observed peak of the light curve, may move slightly before or after the actual peak, hence the slight spread in the LT light curve. Additionally inclination effects or disc asymmetries may play a role in the changes to peak brightness and the timing thereof. The optical spectrum's H I line ratios suggest a thicker, more complete disc than other IPs, thus the typical aperiodic changes associated with other systems with discs should be considered. A simple sawtooth waveform was best-fit to the phase-folded light curve, using `scipy.optimize.curvefit` with 4 free parameters: amplitude, base brightness, period, and width (which represents the angle of the between the base and peak of the triangle). This fit is

just a visual aid, as there would be a bias associated by choosing the type of waveform to fit by eye.

Our measured period fits well within the limits that were established previously (see section 5.3.2), and therefore strongly supports the interpretation that the star is a member of the short-period IP subclass.

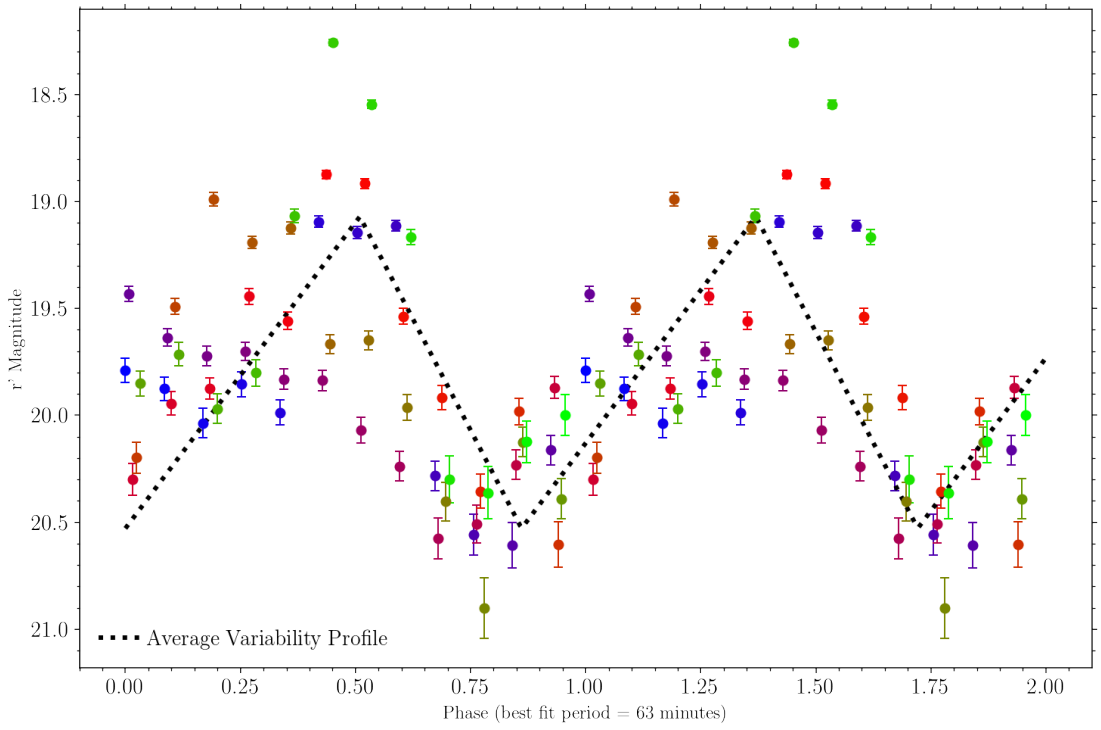

FIGURE 5.11: Two-cycle phase curve for the LT observations, folded at the best-fit period of 63 minutes. The colour scale represents the observation time, and is identical to that used in Figure 5.10. It can be seen that the amplitude varies strongly for each cycle, but the period fits well. This plot is showing two iterations of the cycle (i.e each point is repeated twice), to enhance readability. The dotted line is the best-fit variability profile, using a sawtooth waveform with 4 free parameters.

5.6.2 Identification of New Candidates with VVV

With a single source it is a challenge to make predictions on the number density of these IP systems, especially with regard to the infrared. These kinds of CV are considered to be rare objects, and worthy of further study on this basis alone, but when the novel discovery method (and optically faint SED) are taken into account, a search for more candidates becomes pertinent. Previously these sources have been predominantly detected in all-sky x-ray surveys, which imparts a selection bias towards the brightest members of the class, owing to the shallow depth

of these surveys. As discussed previously, this is carried out by cross-matching sources with desired characteristics from multiple catalogues:

- VVV & VVV/X targets were selected via the VIRAC2B database, with the following parameters observed: the star has a peak amplitude ($Ks_{max} - Ks_{min}$) greater than one magnitude in *Ks*, the star is detected in at least 60% of all epochs, the inter-quartile range in variability is at least half of one magnitude (removing variables with only a few, possibly spurious, variable data points), and that the photometric error is less than one tenth of a magnitude. These cuts selected over one million potential candidates, that were reduced further through the inclusion of limits to the Stetson I (Stetson, 1996) and Von Neumann η (von Neumann, 1941) indices. These provide a numerical measure of a stars variability and correlation between successive data points, wherein I can select stars that are highly variable, but with a greater allowance for short timescale variation. The Stetson I cut was set at values ≥ 100, to ensure the high amplitude variability is correlated. For this sample the η index has been chosen as ≤ 1, as to find uncorrelated variability at shorter time sampling, which should be the case for CVs, owing to variation on timescales shorter than the Nyquist limit for VVV.

- The NIR selection were then limited to nearby targets via Gaia eDR3 astrometry, with a 2kpc limiting range. This limit is applied because at longer distances the prospective systems would be too faint in the optical regime to be reliably detected.

- VPHAS+ photometry provides the final cross-match to the selection, CVs are Hα emitters, hence only stars with an excess in the NB_659 Hα filter are retained.

The final sample can be seen in Figure 5.12, includes approximately 75 stars with an observed $r - H\alpha$ above that predicted by the main sequence (those sources above the orange line). The number of stars with a true Hα excess is lower, as these must be significantly above the main sequence line, however a number of factors require an increase to the range of colours that are permitted in the sample:

- CVs are highly variable sources, both photometrically and for individual spectral lines. Hence the level of excess seen in Hα is not so constant as to provide a meaningful selection criteria by itself.

- The transmission through the NB_659 is effected by the radial velocity of the Hα line. This reduces the observed flux for increasingly negative velocity offsets. In the case of Source 363, the offset of $\approx -280\text{kms}^{-1}$ would be enough to reduce any observed excess by between 0.05 mag & 0.3 mag, see Figure 12 & 13 in Drew et al. (2014a).

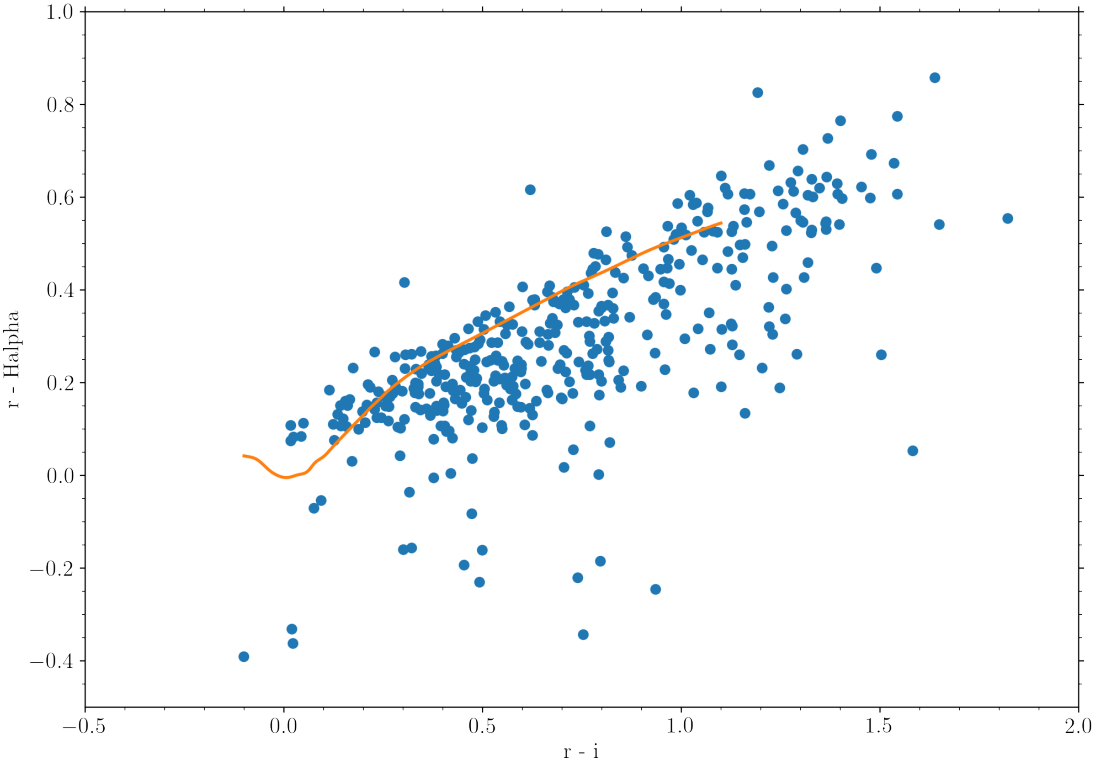

FIGURE 5.12: VPHAS $r-i$ against $r-H\alpha$ colour-colour diagram for the 2kpc NIR variable star sample. The colours are de-reddened using data from Wang and Chen (2019). The orange line denotes the de-reddened main sequence, and is identical to the line in Figure 20 of Drew et al. (2014a). Stars above this line were selected for manual inspection of their VVV light-curves and associated images.

Manual inspection of these stars' light curves found no evidence of CV-like behaviour, with almost all of the observed variability being as a result of the over-saturation of nearby sources, or a failure of the astrometry to pinpoint the correct star within a crowded field. Further work to produce a sample is ongoing, but using differing methods. First by cross matching the combined Gaia & VPHAS+ DR4 sample to known periodic variable stars from VVV. Second using a novel machine learning based approach, which involves using a feature based classification tool (in this case HDBSCAN by Campello et al. (2013)) to group a catalogue of phase folded periodic light curves. Within this set is a model of Source 363, which can then be used to identify possible groups that contain other NIR selected CVs, with the output being visualised with the dimensionality reducing tool UMAP (McInnes et al., 2018). Both of these methods rely on a

pre-made sample of periodic variable stars from VVV and VVV/X, one of which is already available as part of Molnar et al. (2022), although I am using the in prep. work of Miller et al.

Chapter 6

Multi-Wavelength Approach to Variable Star Classification

6.1 Introduction

The wide selection criteria of Lucas et al. (2017) and Contreras Peña et al. (2017) lead to a number of non-YSOs being present in the final catalogue of 618 high amplitude variables from UKIDSS. 37% of the stars in the catalogue belong to other stellar classes, with dusty AGB stars, symbiotic and eclipsing binaries being the most common. These stars can normally be reliably classified when given appropriate time sampling, however the two epochs of UGPS make their extraction more of a challenge. Colour based cuts (such as those used by Robitaille et al., 2008) can be used to isolate AGB stars, and it can be assumed that the MS eclipsing binaries will not be located in SFRs, hence a lack of nearby star formation tracers (YSOs, infrared-dark clouds, outflows etc) can also identify MS variables. Difficulties can arise within the Galactic plane, through projection effects; an evolved star at a significant distance can be seen through SFRs, which will change the observed colours. Additionally certain phenomena involving ejection of material can cause stellar variability with an associated IR excess, making a classification a challenge. A sample of ten stars remained of uncertain nature (see Table 6.1), these seemingly fall into 3 more distinct groups, which will each be discussed further. One additional star, GPSV13 is additionally included, owing to to the similarity between itself and 6 other stars in the sample.

6.2 Non-YSO High Amplitude Variable Stars

The most common group is the 6 prospective Be stars, and the one (GPSV13) confirmed as a classical Be star (Contreras Peña et al., 2014a). The other six lacked photometric confirmation of Hα emission with IPHAS. This is owing to the degeneracy between spectral type, interstellar extinction and Hα excess in the IPHAS two colour diagram (Drew et al. (2005); Raddi et al. (2018)). The data available for each of these stars suggests some form of early-type star, that possesses either a disk or shell of thin circumstellar material, hence an IR flux higher than a normal B-type star. Thus the most likely classifications are (i) classical Be stars with unusually high amplitude and unusually long bursts and (ii) some type of B[e] star, a broad class of variables that includes FS CMa stars (binary systems that have a compact dust envelope), B[e] supergiants, symbiotic B[e] stars and the central stars of compact PNe. B[e] stars are characterised by low excitation forbidden lines such as [SII] and [FeII] as well as HI lines. The various types of B[e] star are poorly understood (e.g. their evolutionary status; see recent review by Oudmaijer and Miroshnickenko (2017)), whilst classical Be discs offer an excellent laboratory for understanding the viscous evolution of accretion discs in general, including the more complex YSO discs.

Source 363 is also included in this sample (of 11, as mentioned above), although for discussion of this object please refer to chapter 5, wherein its nature as a CV, and further as an IP, established. Note that this source will not be further discussed in detail in this chapter.

The final 3 stars are all now suspected of being evolved stars, in large part because of the approximately sinusoidal nature of their variability, seen in NEOWISE light curves (see Figures 6.5, 6.10 & 6.11). Two were originally thought to be young stellar objects; in part because one (source 143) was projected onto a known star-forming region, and the other (source 239) had a YSO like colour and spectrum. Source 507 was observed to have an AGB-like spectrum after initial classification, but its $W1-W2$ colours were far bluer tha expected for an AGB star. The colour was closer to the MIR colours displayed by YSOs, thus making a case for investigating further.

A later spectrum (Figure 6.9) for Source 507 displayed absorption features associated with 13CO, which would make the evolved star classification more probable. This was suspected in (Contreras Peña, 2015), although not expanded upon owing to the unusual distance measurements for the object.

Source Number	Other Name	Possible Star Type	RA	Dec	Kc	Ko	ΔK(*Inc.2MASS*)	W1	W2
130	TYC 5408-965-1	Possible Be Star	112.6448	-14.2543	12.04724121	10.99499989	1.066000114	12.014	12.046
143	GPSV3	Unusual AGB Star	274.6864	-11.6144	12.472745	13.750602	1.277857	9.264	7.014
234	GPSV13	Classical Be Star	285.3438	11.8676	12.920371	11.896123	1.024248	13.168	13.151
239	GPSV15	Unusual AGB Star	285.8838	12.0992	11.211374	12.2408495	1.0294755	8.412	6.434
310		Possible Be Star	291.4171	17.5630	12.440638	11.01275	1.43225	12.216	12.18
363		Intermediate Polar	295.7930	18.6477	17.691833	15.717914	1.973919	-	-
400		Possible Be Star	300.3896	27.8867	12.88952351	11.74499989	1.144523621	12.552	12.484
507	GPSV34	Unusual AGB Star	308.6130	42.2315	11.4592495	13.24400043	2.107000168	9.423	8.472
577		Possible Be Star	318.5037	52.8627	12.430016	11.37899971	1.05101629	12.25	12.194
593		Possible Be Star	323.4509	51.8189	12.79123306	11.29500008	1.496232986	12.333	12.232
607		Possible Be Star	334.7112	57.8001	12.08006668	13.26200008	1.211999527	12.979	12.935

TABLE 6.1: Target list for the non-YSO variable star sample

Source 143 has been selected for further study (see Section 6.3), in part due to it's Gemini/NIFS spectrum showing very cool temperatures (1200K) and the presence of numerous low excitation metal emission lines, giving the first major indication that it was an evolved object. Emission lines are rare in dusty AGB stars, especially the Mira type pulsating variables, but they have been known to display hydrogen excitation when in symbiotic systems (Whitelock (1988) - see also section 3.3.4). These systems also show large amplitude variability over similar timescales to traditional Miras, with periods of between 280 and 580 days. Metal lines are not traditionally seen in emission, but have been noted in absorption in dusty carbon or barium type AGB stars (Matsunaga et al., 2017), due to atmospheric pollution from a companion star passing through the AGB's Roche-lobe. Given the low excitation energies seen in Source 143, the emission of the metals could be caused by shock excitation of a dusty shell around the star (possibly from a newer, faster moving shell). Sources 143 and 507 have both been checked against the Ishihara et al. (2011a) Colour-Colour relation, which compares J-K NIR colour to AKARI [9]-[18] micron colour, which serves to distinguish C and O rich AGB stars, and both stars appear slightly off the expected distribution, but on the side of an O-rich star, although this could be due to the average J-K colour not being comparable to single epoch WISE MIR data. With no one method available to prove these objects as either YSOs or AGBs, We set out to analyse the kinematics of source 143, in order to place it at a distance that would be conducive to one of these classifications.

6.3 Analysis of Source 143 (GPSV3)

Leading the case for IR bright stars being possibly mis-identified as YSOs is GPSV3 (source 138), which displayed a 1.28 magnitude change in K, and was projected against the Serpens OB2 star formation region. It's J-H versus H-K colours also placed it between the regions occupied by YSOs and AGB stars, leading to its nature being ambiguous. The combined near

and mid-IR colours don't fit however, as to be a traditional AGB star it's distance would have to be at approximately 37kpc, using the AGB-distance relation Ishihara et al. (2011a). Whereas a preliminary RV check by Contreras-Peña (private comm.) indicated a nearby distance solution in-line with a membership of Serpens OB2.

A NIR spectrum was obtained in 2012 with Gemini/NIFS, previously published in Contreras Peña et al. (2014a), and is reproduced in Figure 6.1. This spectrum is noteworthy for the presence in emission of numerous excited metals, including Fe, Si, Mg and Al. Cool gas can be identified from multiple bandheads of 12CO absorption, which is best fit with a temperature of 1200 K, although the fainter 2-1 (2.29μm) bandhead is not as well fit by the model (see Figure 6.2). This fit makes use of a series of `idl` scripts to create a grid of 8000 model 12CO molecular lines, at range of temperatures and column densities. These models are set to the spectral resolution of the instrument used to obtain the observed spectra, and manually adjusted to account for the central wavelength shift associated with radial velocity. A `python` code then computes a reduced χ^2 value for each model from the grid. A final best fitting model is then selected by eye from the ten models with the lowest reduced χ^2 (checking too many of the models by eye would be inefficient). A faint line with a possible inverse P Cygni-like profile can be seen at 2.16μm, which might be associated with Brackett γ emission from infalling material. Multiple features at differing strengths indicates that this is a complex system, most likely with several individual components, including cool circumstellar material, and a hotter central source which is exciting material through shocks.

6.3.1 Infrared Light Curves

While Serpens was not covered by the initial VVV survey, it did feature in the extended follow up (VVV/X), and `python` code was used to generate a light-curve for source 143 (see Figure 6.3) from the individual photometric catalogues for each VVV/X tile. This had to be used instead of the VIRAC2 light curve because much of data is not fully available yet. The produced curve shows some evidence for a 660 day period (this can be seen in the phase folded light curve of Figure 6.4) with an amplitude of 1.2 mag. This is backed up by the data from NEOWISE (Figure 6.5), which reveals similar behaviours, although the reddening between the near and mid-IR is not as high as one might expect for an AGB star. The MIR light curve has a shorter best-fit period, at 596 days, which might be the result of the wider sampling of NEOWISE when compared to VVV/X. It is worth noting however, that the fit on the period from the VVV/X

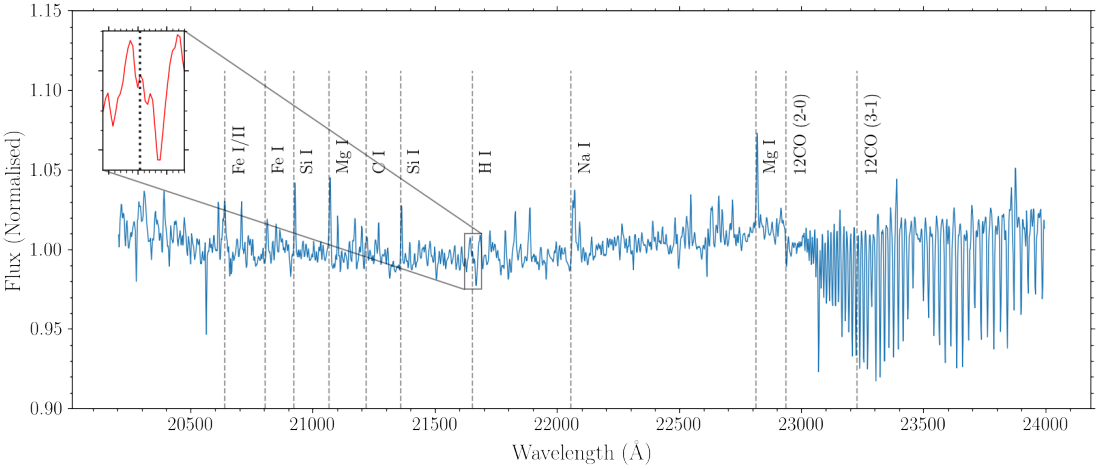

FIGURE 6.1: Gemini/NIFS *Ks* spectrum for Source 143, First published in Contreras-Peña et al. (2014a). There is some uncertainty in the line identification, due to the large number of metal lines within the wavelength coverage, notably with Si and Fe. It is worth noting that the 2.28μm Mg I feature, is likely lower in flux than it appears, as it was seen again in YSOs which had spectra from the same set of observations, albeit to a lower extent than seen here, some flux is considered to be real however, owing to the detection of additional Mg I at 2.11μm. Magellan/FIRE spectra of similar targets, at similar resolution, found no detection of this line. The inset part of the spectrum shows a possible inverse p-cygni line profile of the red shifted Br γ line, the dotted line shows the rest frame wavelength.

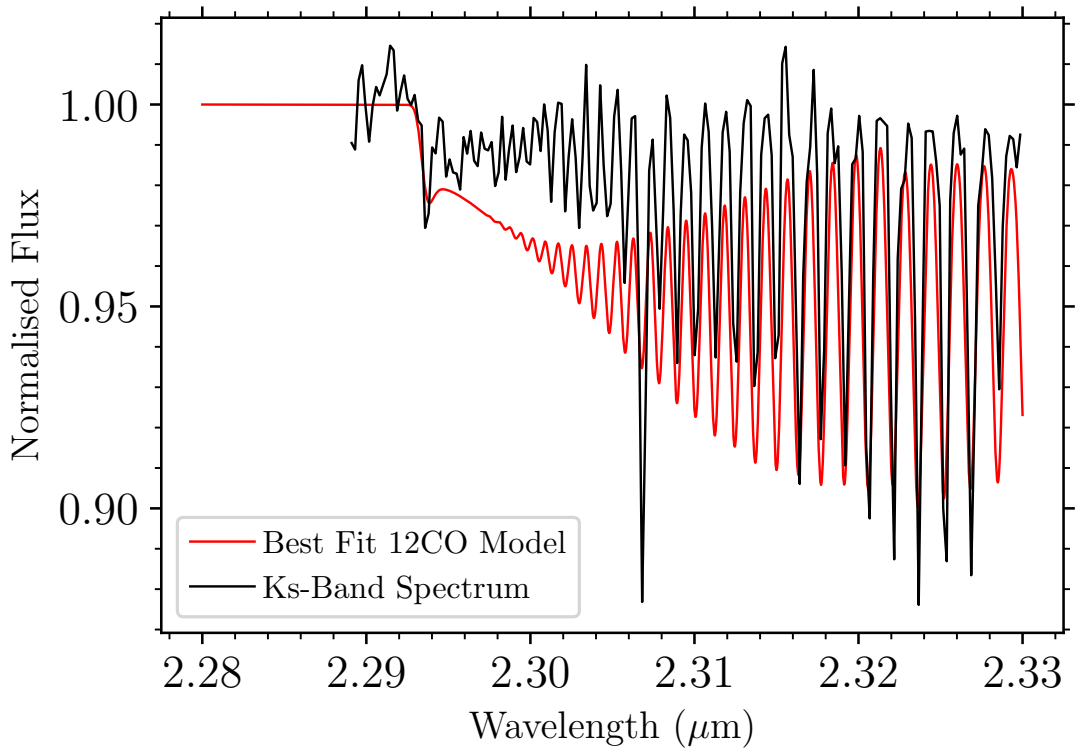

FIGURE 6.2: Section of Source 143's *Ks* spectrum displaying 12CO, best fit by a 1200K model (with a CO column density of 1×10^{20}cm^{-2}. Fitting was carried out by minimising the reduced χ^2 value across a grid of temperatures and column densities, for CO molecular line list.

data could be slightly dubious, as there is only one point after the first complete cycle. Given the difficulty in providing a reliable uncertainty to a fitted period (beyond taking half of the sampling rate as a additional upper and lower bounds), I will simply state that the NEOWISE LC would have an error of $\pm$150 days, following the above method, well within the $\sim$70 day discrepancy between the NIR and MIR periods.

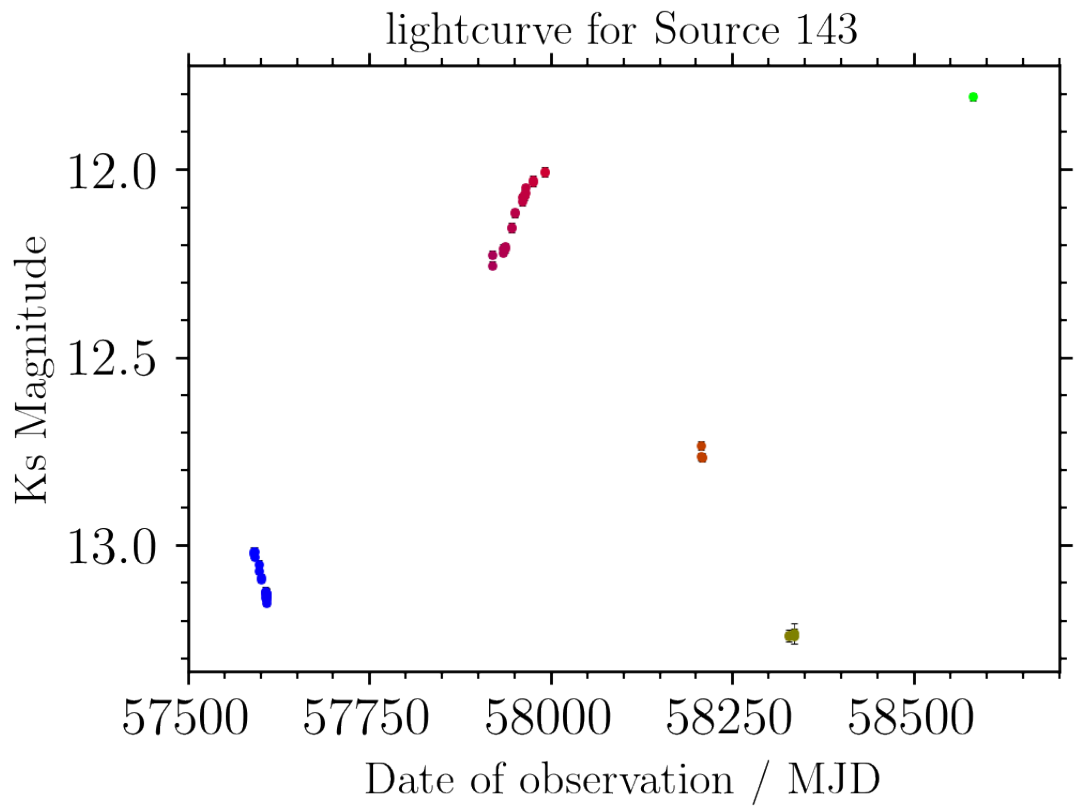

FIGURE 6.3: VVVX *Ks*-band light curve for Source 143, covering 2.7 years with 50 epochs. The peak amplitude is over 1.2 mag, which is consistent with the change seen in UKIDSS. The colours are an aid to better understand figure 6.4, by providing each epoch with a colour.

6.3.2 Proper Motion Analysis

This star lacks any pm data from Gaia (up to and including DR3) (Gaia Collaboration et al. (2018b),Brown et al. (2016)), so a system to gain a tangent plane proper motion was devised. This would use the multiple epochs of images of the star and it's local region, to map a 1' circle centred on GPSV3, onto the tangent plane, using Gaia astrometry for other stars within the circle as a reference point for measuring the motion of our star. A Python script carried out this task, which was built by Leigh Smith (private comm.) to work with UKIDSS data, so

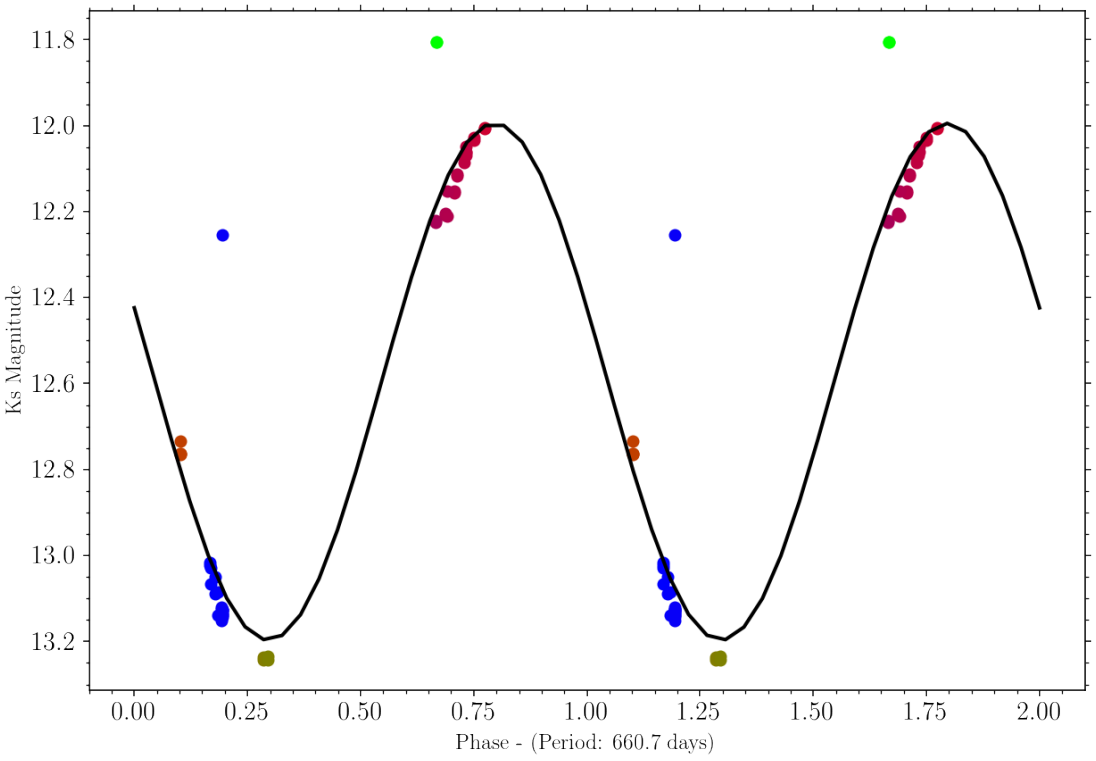

FIGURE 6.4: Phase fold of the VVV/X light curve. A best fit period was found using `astropy`'s generalised Lomb-Scargle fitter, at 660.7 days. Two cycles are featured to aid visualisation of the period. The colours on the plot represent the observation date, see 6.3.

I adapted it to work simultaneously with catalogues from VVV/X. The resulting tangent plane offsets for GPSV3 were plotted in both RA and Dec, and from there a weighted least squares fit was performed, see figure 6.6 for details.

The proper motions that were measured (see Table 6.2) call into question the initially perceived membership of Serpens OB2. An average proper motion for 79 known Serpens OB2 members was calculated from Gaia DR3 astrometry resulting in values of -1.695 ± 0.078mas/yr & -0.6542 ± 0.082mas/yr in l & b respectively. This contrasts to Source 143 with a difference of 1.8 ± 0.4mas/yr in l & 0.79 ± 0.12mas/yr in b.

Finding an estimate for the distance of this star can be accomplished kinematically (which produces two distances, one nearby and another at long distance), either through the use of a spectroscopically determined radial velocity, or via astrometric measurements of the stars position and proper motion. The first method was tested with the tool provided from Wenger et al. (2018) gives a far distance of 16.4±0.7kpc, see Table 6.2 for the value used. It should be noted there is a caveat that this calculation does not cover objects that are part of the galactic halo. In this

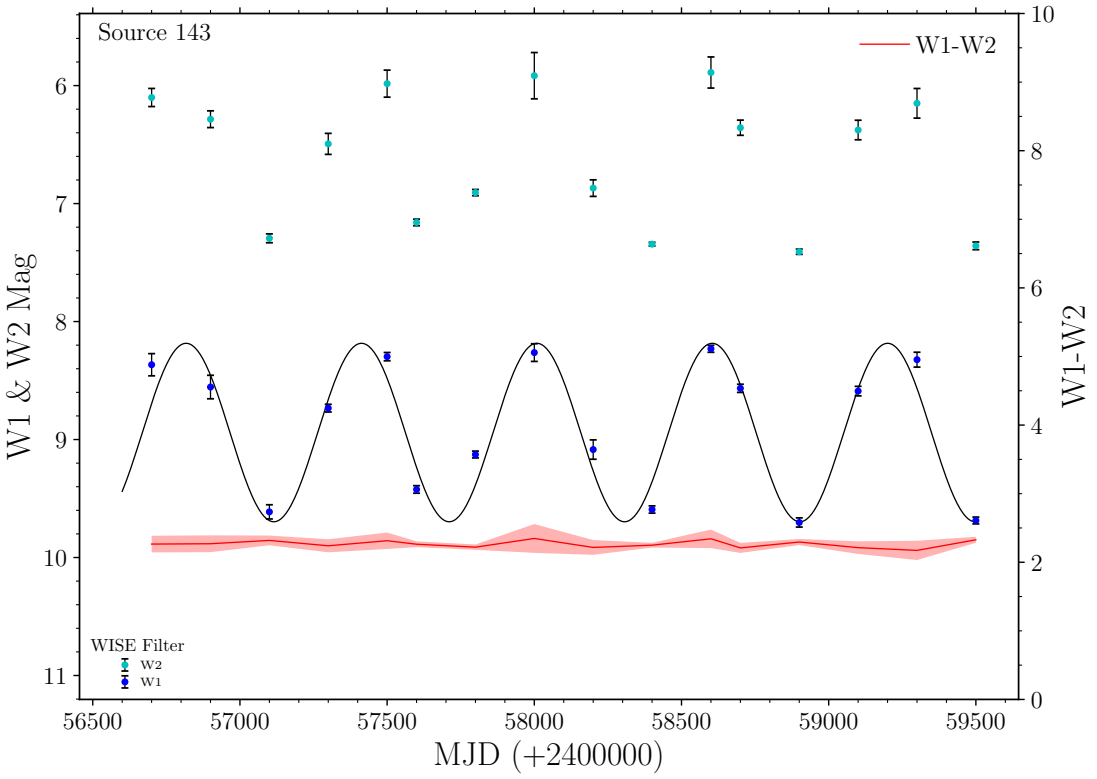

FIGURE 6.5: NEOWISE light curve covering 7.5 years of observation. Comparable periodicity to VVV/X is visible, with a best fit period of 596 days (∼10% difference from VVV/X). Peak amplitudes of 1.6 mag and 1.7 mag in *W1* & *W2* respectively, are in line with results in *Ks*.

case we will take the galactic disk to be of a 14kpc radius about the galactic centre Minniti et al. (2011).

To carry out the second method, I have run a modified `Python` program, originally produced for Smith et al. (2018), which computes a probability density grid for distance (from a preset array between 0.1pc & 4×10^5pc) against the tangential velocity for both the galactic disk (as a function of radius *R*), and the individual target. The former is produced from combining the tangential velocity with respect to the local standard of rest for the sun (this data from Schönrich et al. (2010)), with measurements of its peculiar velocity. The values for the target star are sampled from distributions that allow for a range velocities (both tangential and peculiar), for stars of different populations within the galactic thin disk. These velocity spreads are taken from Bensby (2013), and use distributions for young stars in the thin disk, as well as the mature thin disk population, which in this case represent the two competing potential classifications for Source 143: as a nearby YSO, or of a more distant evolved AGB star. In the case that Source 143 is a YSO,it would have to be at either 0.8kpc or 6kpc (see Figure 6.7), and given that Serpens OB2 is at ∼2kpc (Forbes, 2000), this would seem unlikely. There could be the

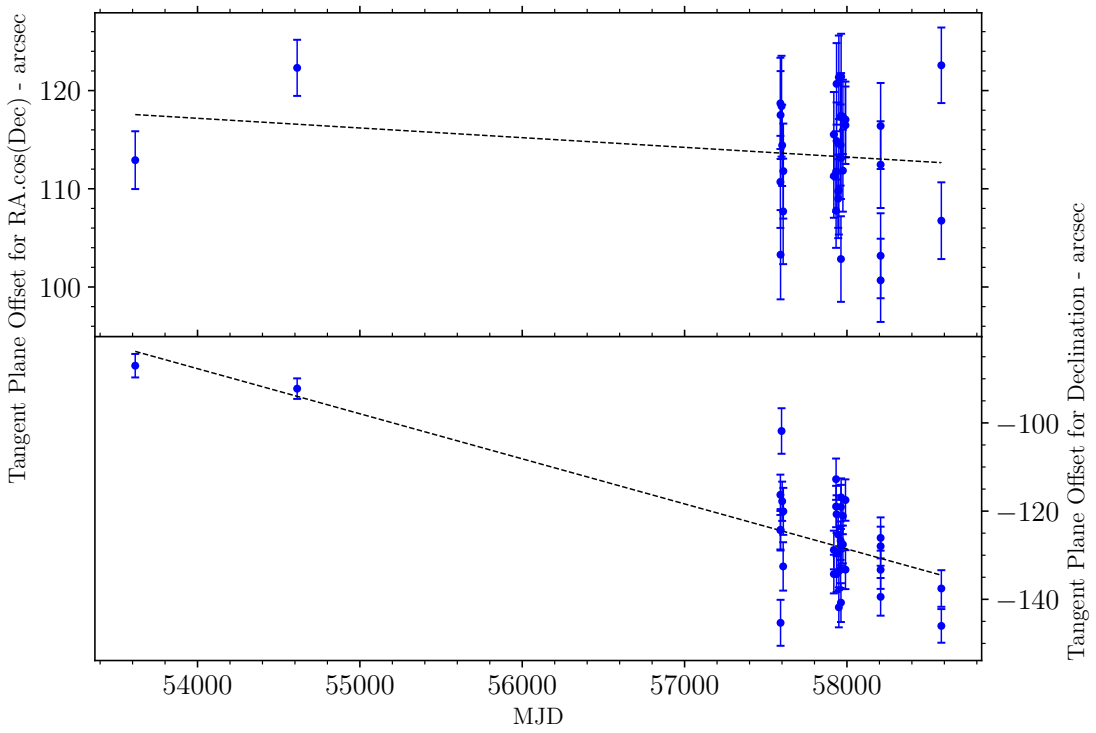

FIGURE 6.6: Proper motion fit for RA (lower) and declination (upper), carried out with the `python` package `lmfit`. Fitting utilised a Markov-chain Monte Carlo, comprising 10000 runs. The best fit proper motions are -0.38 ± 0.41mas/yr & -3.67 ± 0.39mas/yr in RA and Dec respectively.

Measured & Best Fit Astrometric Parameters for Source 143		
Parameter	Value	Error
Radial Velocity	-4.906 kms^{-1}	$\pm$3.648kms^{-1}
Proper Motion (RA)	-0.38 mas.yr^{-1}	$\pm$0.41mas.yr^{-1}
Proper Motion (Dec)	-3.70 mas.yr^{-1}	$\pm$0.39mas.yr^{-1}
Proper Motion (l)	-3.40 mas.yr^{-1}	$\pm$0.54mas.yr^{-1}
Proper Motion (b)	-1.40 mas.yr^{-1}	$\pm$0.17mas.yr^{-1}
Tangential Velocity W component	-199kms^{-1}	$\pm$66.2kms^{-1}

TABLE 6.2

case that the star is a YSO projected against Serpens at the shorter of these distances, but the 5kpc case would lead to the star (and an associated SFR) being too high above the galactic disk to be reasonable. Looking at Figure 6.8, the case that GPSV3 is a halo AGB star is made stronger as this classification would lead to a likely distance of between 20kpc and 35kpc (from the aforementioned code's galactic disk rotation model), similar to the distance from Ishihara 2011, discussed later. An additional factor to consider is the fact that the proper motion is higher in the latitude direction than the longitude direction (see Table 6.2), which would be appropriate for a halo object given the velocities involved, furthered by the fact that at an extended distance, the star would be well outside the galactic disk (although note that in the halo object case, both RV-based and PM-based distance measurements will not be accurate).

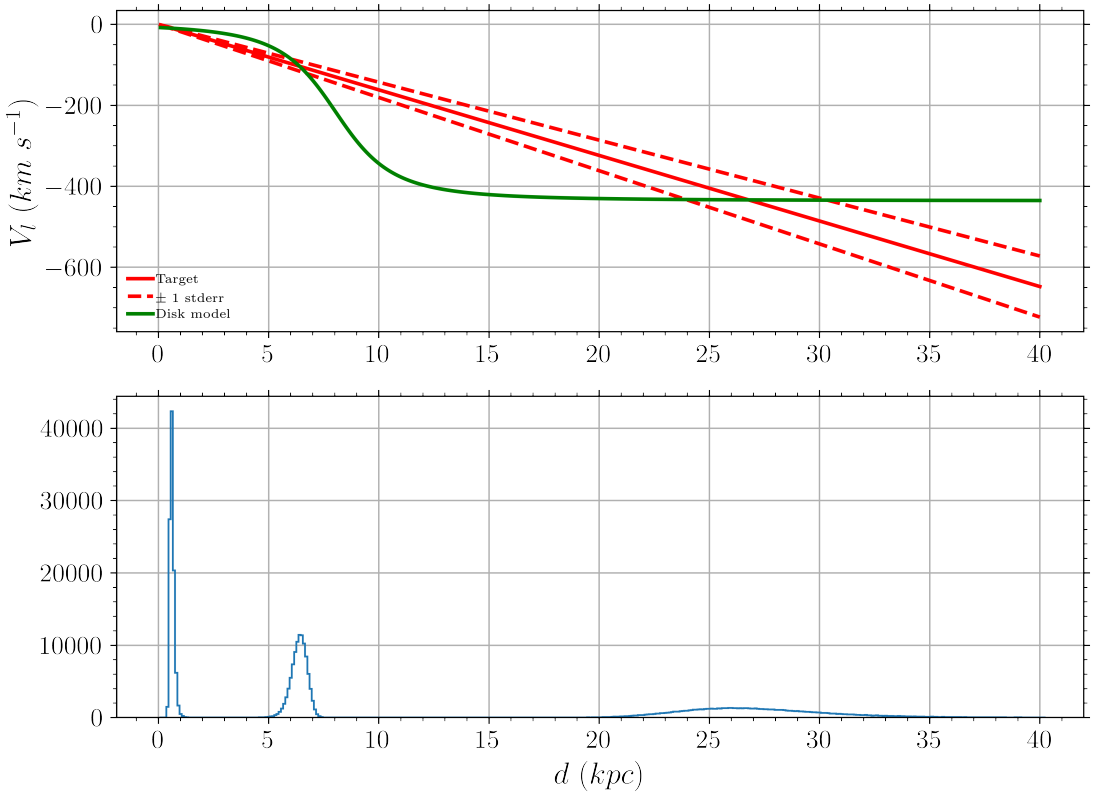

FIGURE 6.7: Velocity/distance plot and probability histogram for Source 143, using the assumption that the star is a YSO, by using radial velocity models associated with young thin disk objects. Results from this put the star at either 0.5pc or 6pc, neither of which fit with the projection onto Serpens OB2.

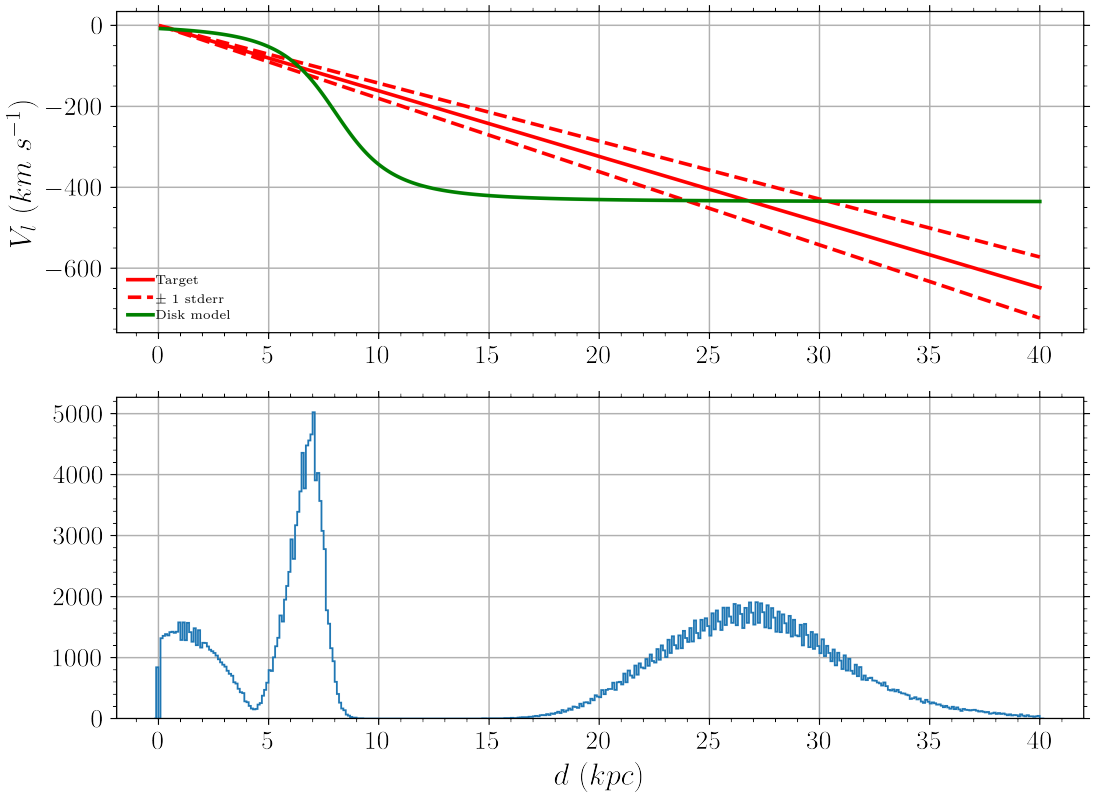

FIGURE 6.8: Velocity/distance plot and probability histogram for Source 143, using a broader radial velocity range, associated with the mature thin disk population. This provided a broader range of distances, allowing a far distance between 20pc and 30+pc to be more likely.

6.4 Other AGB Star Candidates

Two further variable stars can be investigated in a similar vein, sources 239 and 507 (Named as GPSV15 and GPSV34 in Contreras Peña et al. (2014a) respectively), certain details of which can be seen in Table 6.1. Their MIR colours are provided in Table 6.3, wherein sources 143 and 239 satisfy the criterion of Lucas et al. (2017) for dust-rich AGB stars: $W3 - W4 < 0.7 \times (W1 - W2) \& W1 - W2 > 1.5$. Both of these also meet the criteria for an 'extreme' dusty AGB star, with $W2 < 7.8$. These criteria were modified from those used by Robitaille et al. (2008), who substitute Wise $W2$ for Spitzer $I2$ (which have similar bandpasses).

It should be noted here that the likely reason that source 507 does not meet these thresholds is that it appears to have had it's WISE photometry measured at the systems photometric maximum (see Figure 6.11), which would also coincide with the system's bluest colour due to the reduction in the observed optical depth.

Source	$J-H$	$H-K$	$W1-W2$	$W3-W4$
143	-	3.56	2.25	1.35
239	3.31	2.93	1.98	1.21
507	2.74	1.82	0.951	1.15

TABLE 6.3: Selected near and mid-infrared colours for the three candidate post-main sequence variable stars from the earlier sample. All colours are given in magnitudes, and are taken from contemporaneous measurements. It should be noted however that during the epoch of these measurements the stars are not at the same point in their various periodic cycles, with sources 143 and 239 at a faint state but 507 at near peak brightness.

Gemini/NIFS *Ks* spectra for these two stars can be seen in Fig. 6.9, These were originally published in Contreras Peña et al. (2014a). Source 239 (GPSV15) displays several prominent absorption features beyond the ubiquitous 12CO, with Fe I the most likely cause, as the three deepest features are all at wavelengths that correspond with iron lines (there are Si I lines at similar wavelengths, but in this instance they would have to have a significant red-shifted component to fit). Source 507 (GPSV34) has a similar spectrum, but without the atomic absorption lines, although additional components at 2.345μm and 2.374μm from 13CO are clearly visible. Both spectra lack the traditional absorption associated with water at the red end of the spectrum, which is more common among AGB stars, owing to extinction from circumstellar matter.

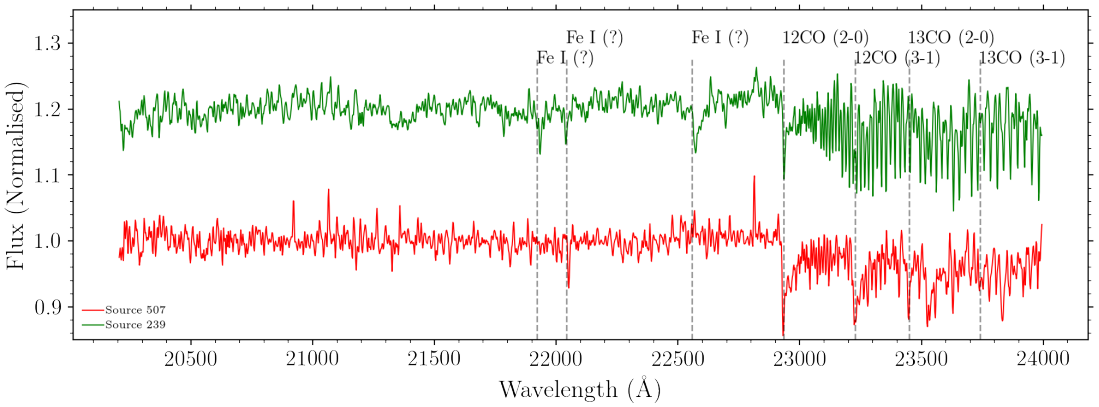

FIGURE 6.9: Gemini/NIFS *Ks* spectra for sources 239 (green) and 507 (red).

Both targets display very similar behaviour in their MIR light curves; NEOWISE data (displayed in Figures 6.10 & 6.11) indicates clear periodic features, that are sinusoidal, with some aperiodic variation. The periods are fitted with the usual `astropy LombScargle` procedure, but in these instances the best-fitting periods were selected from the peaks in the power spectrum by eye (see figure 6.12). The frequencies with a higher power seem to be shorter aliases (factors of the true period), that are capable of fitting more of the points via higher frequencies. The likely physical reason that certain points do not fit is interaction between the first and second pulsation states of

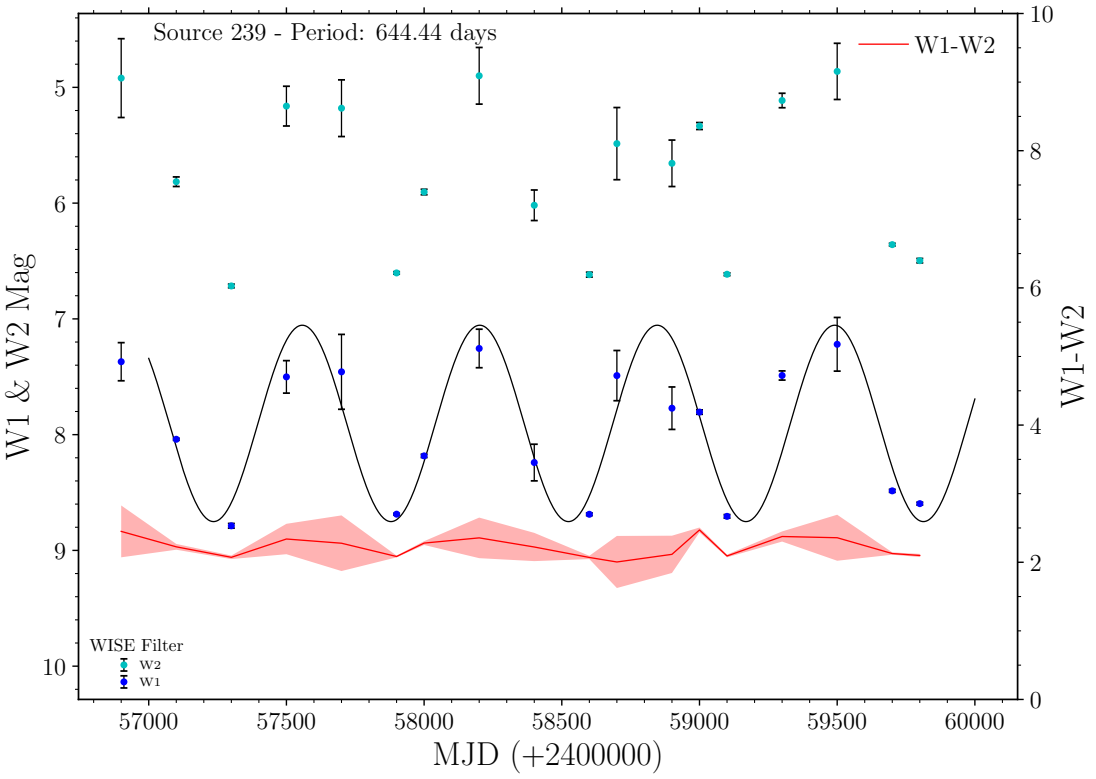

FIGURE 6.10: NEOWISE light curve covering 8+ years of observation for Source 239 (GPSV15). The long term behaviour is loosely periodic (or quasi-periodic) and can be reasonably well fit by a 644 day period via `astropy` Lomb-Scargle. This period is inline with dusty-AGB stars, such as a Mira-type.

Source	$\Delta W1$	$\Delta W2$	Maximum W1 - W2	Minimum W1 - W2
143	1.47	1.52	2.35	2.17
239	1.57	1.85	2.47	2.00
507	1.67	1.20	1.38	0.900

TABLE 6.4: Photometric information for the Evolved star candidates. Source 239 has the highest amplitudes in $W2$ and is also the star that shows the largest change in line-of-sight reddening, thus implying a higher mass loss rate. It is notable that Source 507 has the lowest $W2$ amplitude but the highest in $W1$, this trend continues into the NIR with this star also having the highest K-band amplitude (2.1 mag).

the star, which can cause aperiodic slight increases in flux shortly after the photometric minima. Source 239 has the larger amplitude in $W2$, but Source 507 has the larger in $W1$, see Table 6.4.

6.4.1 Possible Classifications

Given the above results it can be assumed that source 143 is a post main-sequence object, and thus established methods can be used to refine any classification. In that vein, a separate distance estimate can be calculated from the object's MIR flux. Using the work of Ishihara et al. (2011b)

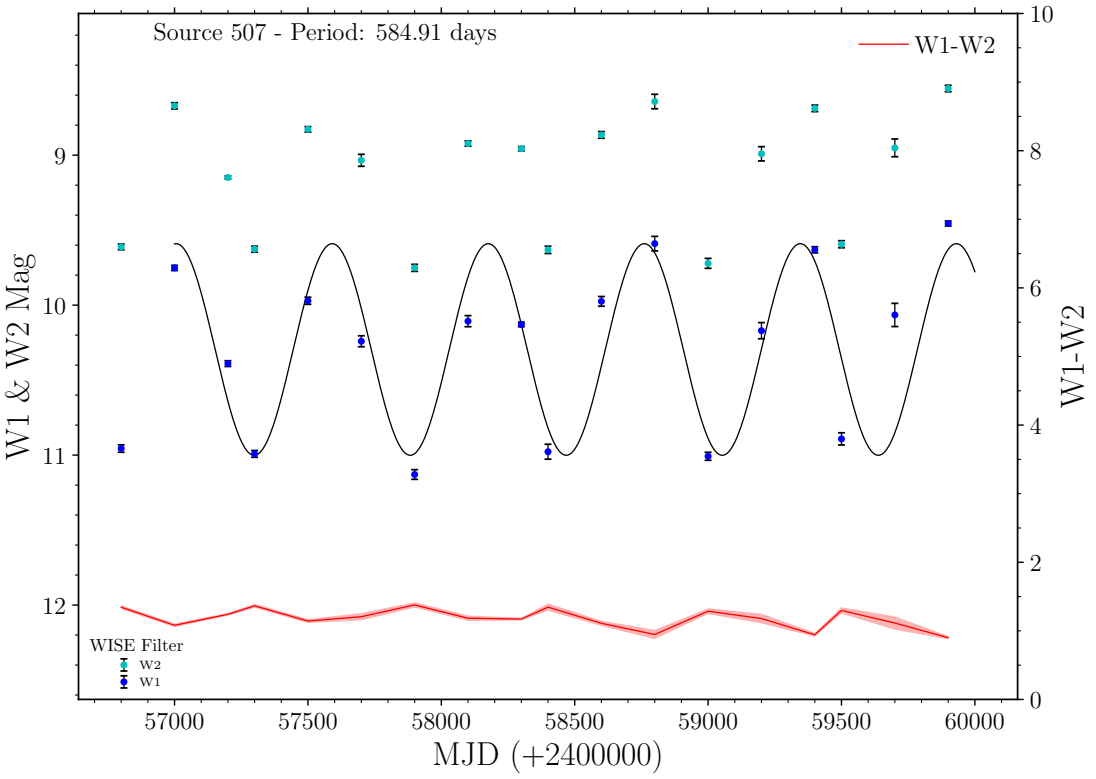

FIGURE 6.11: NEOWISE light curve covering 8+ years of observation for Source 507 (GPSV34). The long term behaviour is loosely periodic (or quasi-periodic) and can be reasonably well fit by a 585 day period via `astropy` Lomb-Scargle. This period is inline with dusty-AGB stars, such as a Mira-type.

the following equation can be used:

$$d = 10^{C1+(C2\times ln(\dot{M}))} - 0.5log([9]) \tag{6.1}$$

Where $C1$ & $C2$ are constants (6.1 ± 0.06 & 0.35 ± 0.01 respectively), and [9] is the flux for the AKARI 9μm band. The mass loss rate is noted as $\dot{M}$, and given by:

$$\dot{M} = ln(3.8 \times (K - [9]) - 0.4) - 8.0 \tag{6.2}$$

Where K is the apparent magnitude in 2MASS K. It can be seen in Figure 6.13 that the flux estimate provides a distance of 35.72 ± 2.417kpc, which tallies with the proper motion based distance estimated earlier. This distance is likely more precise than is accurate, owing to a stipulated scatter of $\pm 50\%$. With that in mind, the star's separation from the dust rich line is still more associated with O-rich stars than C-rich ones (see figure A.1 Ishihara et al. (2010)).

Source 143 lacks a traditional AGB spectrum, with a large number of metal emission lines (see

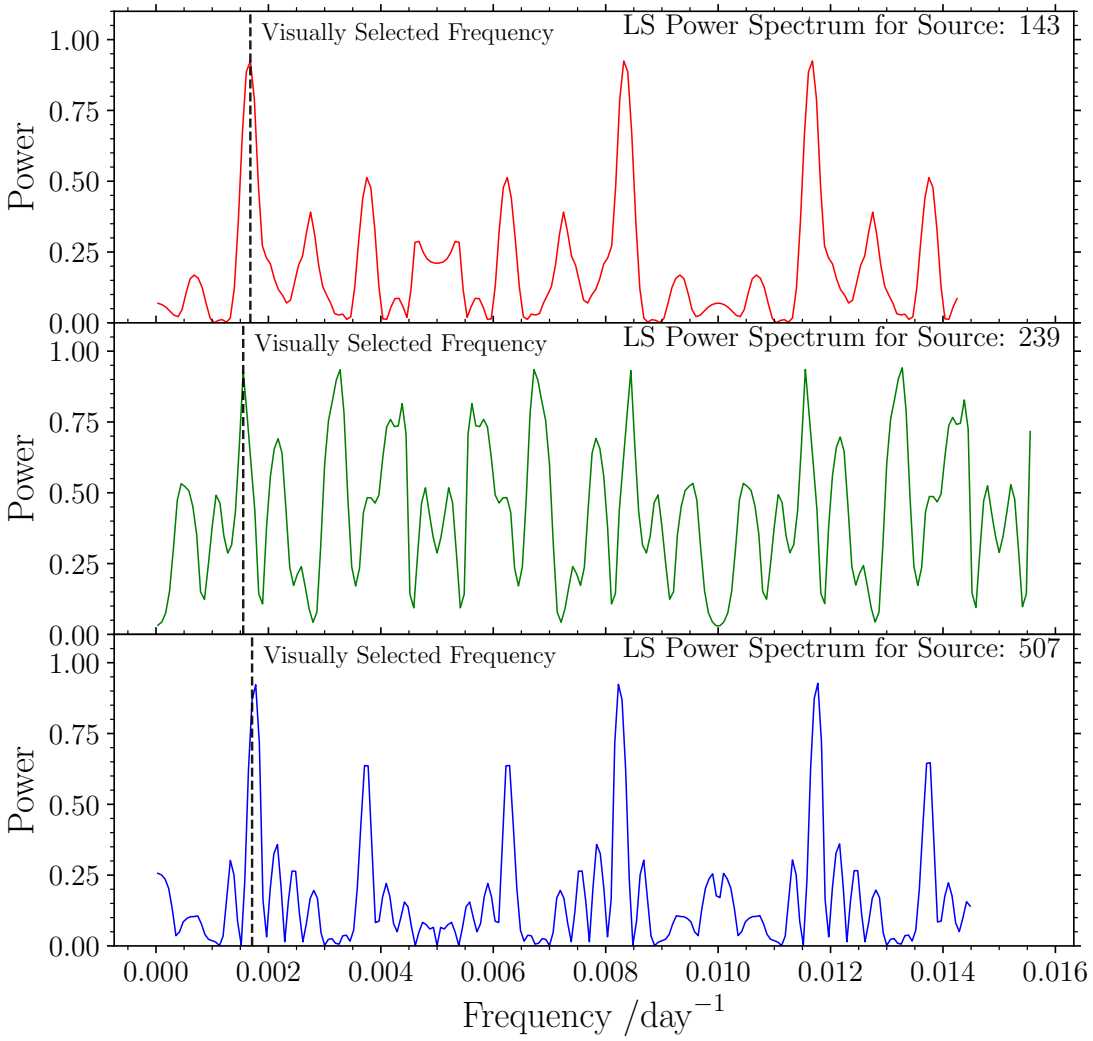

FIGURE 6.12: Lomb-Scargle power spectra for each of the three candidate AGB stars in this chapter. Each spectrum is output from `astropy.timeseries.LombScargle`, applied to the star's associated NEOWISE W1 light curve. Marked on each (dashed line) is the frequency that has been visually selected to be the best fit of the obvious peaks in the data.

figure 6.1) present alongside the more typical absorption features associated with 12CO. Given this, and the very red colours of the source it can be anticipated that the star has a loosely bound outer envelope, with a combination of high winds and interaction with previously ejected material, as indicated by the shock excitation of the metals found in the star's photosphere. Features such as this could (but do not necessarily) indicate the star is evolving off the asymptotic giant branch, towards the post-AGB phase. Post-AGB stars (PAGB), also known as proto-planetary nebulae, are end-of-life AGB stars characterised by reduced mass loss, and high extinction from ejected circumstellar matter (see Oudmaijer et al. (1995) & Raman and Anandarao (2008) for

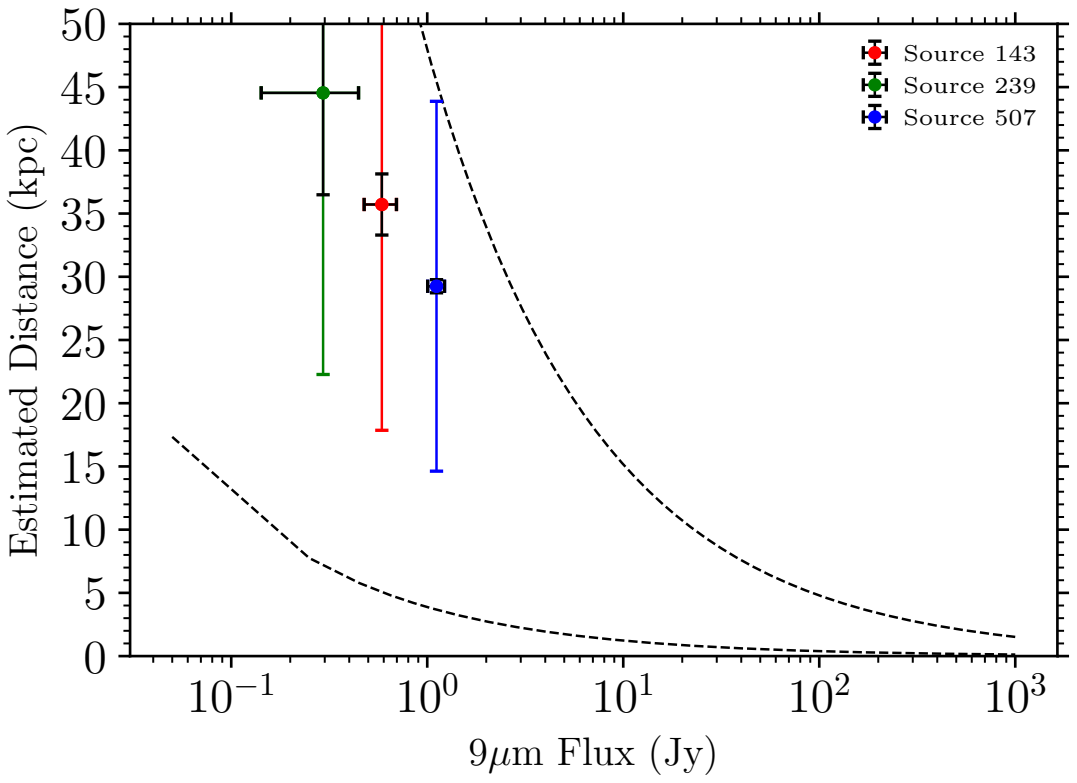

FIGURE 6.13: Flux-distance plot showing Sources 143, 239, 507 in relation to tracks representing typical AGB stars with $K-[9]=1mag$ & $K-[9]=14mag$ for the most dust poor and dust rich cases respectively. The $[9]\mu$m flux is from the AKARI mid-infrared all-sky survey.

an in-depth look at PAGB spectra in the NIR). Whilst spectroscopically similar (although lacking in the characteristic Brackett γ emission), the time-series behaviour of Source 143 displays high amplitude variability, which is not seen in PAGB stars, and thus a different classification is warranted.

With high-amplitude, long-period variation seen in both NIR and MIR it might be convenient to consider a Mira-type classification for source 143, this however has some uncertainty. First while Miras have established long periods and Source 143's $\approx 596-660$ day period is within the 80-1000 day range expected, the range of periodicities between near and mid-infrared observations implies that the variation is possibly semi-regular, or perhaps the differing wavebands are being influenced by variable emission/extinction withing the expanding dust shell. Secondly the spectrum is seemingly devoid of 13CO, which is unexpected for dusty AGB stars. It should be noted however that given the low temperature estimated for the CO bandheads, that 13CO simply may not be excited, and may still be present in the system. Carbon-rich Mira variables

do show more scatter in their lightcurves, often caused by obscuration from circumstellar matter, which is aperiodic. This would make for a compelling argument for these three red sources, however C-rich Miras are most associated with low metallicities, and as such are most often found in either the LMC or the galactic bulge. Taking account of the above discussions, the case of the OH/IR star becomes available for consideration.

OH/IR stars were first described by Wilson and Barrett (1971), Noting the existence of narrow band OH sources associated with long-period IR variables. These Mira-like objects were posited by Wood (1982) (amongst others) to be stars at the end of the AGB, undergoing a 'super-wind' type mass loss phase. These had previously been theorised to explain the dichotomy between the observed low WD masses as compared the measured mass loss rates of 'normal' AGB stars (Iben and Renzini, 1983). This change in mass loss rate is driven by thermal pulsations, which occur more frequently in lower mass ($M \leq 2M_{\odot}$) stars (Vassiliadis and Wood, 1993), although some high mass OH/IR stars are known (described as the 'high-luminosity group' by Jiménez-Esteban and Engels (2015)). As standard, an OH/IR star is O-rich, thermally pulsing Mira-type AGB star, characterised by OH maser emission at 1.6 GHz and high amplitude, long-period light curves. The periods tend to be longer than those of a classical Mira. They feature spectra with variable line strengths, which are loosely dependant on phase. The lines in question are a mix of metals, silicates and and hydrogen recombination, although cold CO is present in absorption like many dusty AGB stars.

A subset of candidate OH/IR sources lack the characteristic OH maser emission, but have features that are otherwise consistent with that classification are known as 'OH/IR Mimics' Lewis (1992); Seaquist and Ivison (1994). It is posited that the Maser emission is prevented by the presence of a degenerate companion (a WD), which heats the cool dust shell from the evolved companion. This heating dissociates the OH molecules, thus preventing the maser emission.

The various types of thermally pulsing AGB stars (TP-AGB) can be fitted to empirical period-luminosity tracks, as seen in Whitelock et al. (2008), and De Beck et al. (2010). Within figure 6.14, the three AGB star candidates from this chapter are are shown against tracks from Feast et al. (1989), representing the relation for oxygen rich stars, both of Mira and OH/IR types. Sources 143 and 239 are better fit by this relation than Source 507, which could be over luminous in the Akari 9μm bandpass, and thus have an inaccurate distance. Using AKARI [9] fluxes and the distance distributions from Figure 6.13, the luminosities ranging from $16950 \pm 6279 L_{\odot}$ for Source 239, to $22320 \pm 786.9 L_{\odot}$ for Source 507. All three luminosities place closer to the

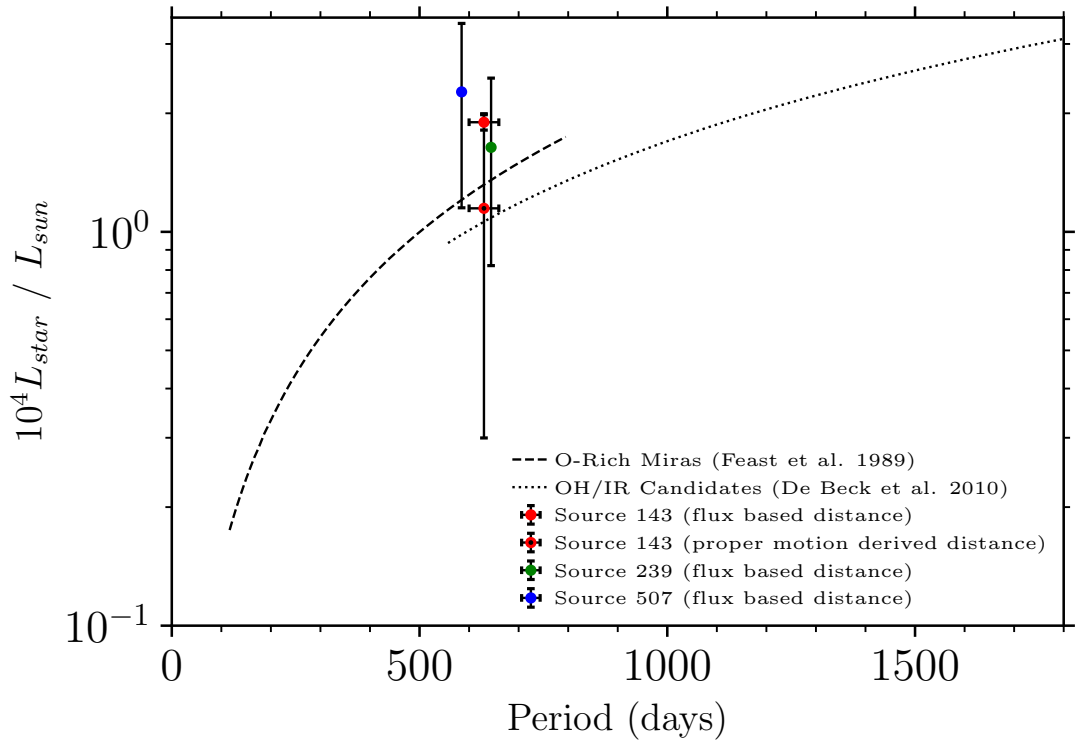

FIGURE 6.14: Period-Luminosity plot for O-rich variable AGB stars. The blue line represents the relation for O-rich Mira-type stars, and the yellow line illustrates an extended relationship for OH/IR stars. Source 143 is shown twice, for both the flux based distance (red) and the value derived from the star's relative motion, as in section 6.3.2 (red & black). Sources 239 and 507 are also plotted, just using their flux based distances from Figure 6.13 (green & blue respectively). The flux based distances lead to luminosities that more closely resemble Mira-type objects, whereas the lower distance estimated from our kinematic method places source 143 closer to the relationship for OH/IR stars. All luminosities are the mean value taken from sampling both distance and flux distributions, with 10000 runs.

relation for Miras, than to that of OH/IR stars. Source 143 has two points on the plot, with the additional point using the distance distribution from Figure 6.8 for the luminosity calculation, providing a lower luminosity of $11630 \pm 8556 L_{\odot}$ (the large errors are a by product of the 10kpc spread used in the distance distribution). This lower value nominally falls closer to the OH/IR relation, but the 1σ errors place it within the same range as the flux based distances. This plot does provide an additional check on the best fit photometric periods, with any shorter alias of true period (which had a slightly lower error on the Lomb-Scargle power spectrum for sources 239 and 507) falling a large distance away from the expected trends for AGB stars.

At this juncture it is a challenge to confirm one classification specifically, with the period not being long enough to rule out Mira-like behaviour.

6.5 Conclusions

With widely separated observing windows, variability in the infrared can be easily identified, but classification can be challenging given the limitations posed by the observing methods used in UGPS-UKIDSS. Without multi-epoch colour information the method driving an objects variability is more difficult to determine, and the wide spacing often means it is not possible to place meaningful upper limits on the timescales of individual instances of variability/variability events. Whilst the recent VVV/X survey Minniti et al. (2010) alleviates some of the above drawbacks from the varied cadencing of its observations, and the implementation of multiple epochs of multi-colour images, it is inevitably still the case that the that the clearest picture of any system comes from multi-wavelength studies, and by combining both time-series and spectroscopic monitoring. To that end, there are several further tasks that would be of benefit to better understand these variables, so as to more efficiently extract them from samples of YSOs:

- Given the spectral variability of these pulsating stars, obtaining additional K-band spectra would be a priority. This would provide an indication of how the emission lines in Source 143 change over the course of its pulsation cycle, in addition to providing an opportunity to see if those same features become visible in sources 239 and 507. If these spectra are of higher resolution, then the ability to measure the metalicity and mass loss rates for the stars will become available (through accurate measures of line radial velocities), further informing the true nature of the sources.

- The identification of other candidates will better constrain the range of periods and IR colours that this grouping occupies. Utilising the well sampled VVV survey (in the southern hemisphere) will provide the greatest concentration of similar stars to the three discussed here. Selection would entail using the Virac2b (Smith et al. In Prep.) catalog, with stars of greater than 1 magnitude variability in Ks, whose interquartile range would be on the order of 50% of the peak amplitude (to select sinusoid-like variables), and with similar median NIR colours to Sources 143, 239 & 507. This sample could then be matched to a NEOWISE sample with similar conditions, designed to find AGB stars at the edge of the NIR/MIR colour space closest to YSOs.

Chapter 7

Future Work and Concluding Remarks

We have thoroughly investigated a wide range of variable stars from a single selection of high-amplitude NIR sources, and present findings relevant to numerous aspects of the infrared variable sky. We first built on the work of Contreras Peña (2015) to provide clear indications of two new FUors in the W48 and Cygnus-X regions, utilising calculated upper limits from 2MASS, as well as their continued MIR behaviour as seen by NEOWISE. Further to this we also report on seven other candidate eruptive variables, of an emission-line type, either classical EXors, or of the understudied long-duration type. From the sample of 'likely' YSOs with large NIR outbursts, we utilise time domain photometry and single-epoch spectroscopy to examine the demographics of high amplitude variable YSOs. Analysis of the sample with a Bayesian approach finds that EVs have expectation values of between 11% and 30% of the sample.

To place these findings into broader context we leveraged the crossover between the UKIDSS UGPS and the Spitzer Cygnus-X Legacy Survey, to examine both the rates of eruptive variability for YSOs within Cygnus-X and viability of using non-detections to trace candidate eruptive YSOs. The former objective has found results that are broadly consistent with previous research, noting that the expectation value found of $10.7^{1.8}_{0.9}\%$ is comparable with the $\approx 9\%$ found in Contreras Peña (2015). The latter aim was achieved, finding 6 further candidate eruptive sources from a sample of 15 stars with real variability (although there exists a caveat that 216 stars had to be manually inspected to find this sample, which will not scale well to larger or deeper surveys). We also present the serendipitous result of a possible new class of slowly erupting variable, with rise times of $>$10 years.

We also report on a collection of unusual variable stars found within the wider sample of 618 high-amplitude NIR variable stars from Lucas et al. (2017). Principally we discuss Source 363, an IP of novel character, which is suspected to have a thicker accretion disk and longer spin period than others in the class. A wide range of methods were used to determine the true nature of the system, including multiple optical light curves, optical spectroscopy, narrow-band photometry and targeted x-ray observations. Newly developed machine learning methods (detailed in Miller et. al. Submitted to RASTI, 2023) were trialed, fitting a likely 63 minute spin period using PDM.

Finally we present a brief study of three likely evolved stars with slightly unexpected NIR & MIR colours for normal Mira-like AGB stars. This entailed examining multiple infrared light curves, as well as NIR parallaxes, to fit proper motions, and thus work out distances. These can be compared to RV distances measured from 12CO absorption lines, and empirically derived distances from MIR fluxes. The combined information has led this author to infer that the stars are oxygen-rich Mira-type stars within the Galactic halo with colours that are are possibly affected by line-of-sight reddening. This would likely have been observed as a result of projection behind galactic plane star forming regions.

There are still unanswered questions from this body of work, which can be further investigated in the coming months and years. These include:

- Does our 10% EV rate hold across the entire Kryukova et al. (2014) sample of YSOs in Cygnus-X, as compared to the original NIR non-detection sample? In so doing more insight can be gained into the prevalence of 'dippers' within this sample, which were curiously absent from the 123 stars examined so far.

- What can we learn about the slowly rising EV YSOs, and can we identify more (in addition to the five found in this work)? Follow-up observations of the five long-duration sources are being undertaken, First determining the current photometric state in NIR bands, and using the results to acquire spectra for the brightest targets. Ideally the follow-up will be undertaken with either Gemini North, or IRTF, and the results will be able to determine the current accretion state and method of the systems.

- Further understanding the optically faint IPs (as discussed in chapter 5) is important when trying to consider the number density (and thus rarity) of these objects. To that end, a follow-up investigation into the classification of additional candidates using the periodic

variable catalogue PRIMVS (Miller et. al. in prep.), has been started, utilising both manual inspection and ML based hierarchical clustering methods. Once a selection of high-confidence targets has been selected, a combined telescope proposal for both optical and soft X-ray bands will be written. Results could indicate the number density of these star systems, with respect to traditional IPs.

- Finally, understanding the prevalence of evolved objects within samples of YSO candidates will be useful in improving the accuracy of the next generation of galactic plane surveys (such as those by Rubin & WEAVE). To explore this a final piece of future work will be to use VIRAC-2β (Smith et al., 2018) to locate more objects similar to those discussed in chapter 6 or the candidate D-type symbiotes found in section 3.3.4. Providing a idea into whether or not these stars are a distinct group or purely a result of projection onto areas of the galactic plane with high reddening in the line-of-sight.

Bibliography

Andre, P., Ward-Thompson, D., and Barsony, M., 1993. Submillimeter Continuum Observations of rho Ophiuchi A: The Candidate Protostar VLA 1623 and Prestellar Clumps. *ApJ*, 406:122.

Andronov, I.L. and Breus, V.V., 2013. Variability of the Rotation Period of the White Dwarf in the Magnetic Cataclysmic Binary System EX Hya. *Astrophysics*, 56(4):518.

Antoniucci, S., Giannini, T., Li Causi, G., et al., 2014. On the Mid-infrared Variability of Candidate Eruptive Variables (EXors): A Comparison between Spitzer and WISE Data. *ApJ*, 782(1):51.

Arnaud, K.A., 1996. XSPEC: The First Ten Years. In G.H. Jacoby and J. Barnes, editors, *Astronomical Data Analysis Software and Systems V*, volume 101 of *Astronomical Society of the Pacific Conference Series*, page 17.

Aspin, C., Reipurth, B., Beck, T.L., et al., 2009. V1647 Orionis: Reinvigorated Accretion and the Re-Appearance of McNeil's Nebula. *ApJ*, 692(2):L67.

Aspin, C., Reipurth, B., Herczeg, G.J., et al., 2010. The 2008 Extreme Outburst of the Young Eruptive Variable Star EX Lupi. *ApJ*, 719(1):L50.

Astropy Collaboration, Price-Whelan, A.M., Sipőcz, B.M., et al., 2018. The Astropy Project: Building an Open-science Project and Status of the v2.0 Core Package. *AJ*, 156(3):123.

Astropy Collaboration, Robitaille, T.P., Tollerud, E.J., et al., 2013. Astropy: A community Python package for astronomy. *A&A*, 558:A33.

Atwood, W.B., Abdo, A.A., Ackermann, M., et al., 2009. The Large Area Telescope on the Fermi Gamma-Ray Space Telescope Mission. *ApJ*, 697(2):1071.

Audard, M., Péter´abrahám, P.P., Dunham, M.M., et al., 2014. Episodic Accretion in Young Stars. Technical report.

Bailer-Jones, C.A.L., Rybizki, J., Fouesneau, M., et al., 2021. Estimating Distances from Parallaxes. V. Geometric and Photogeometric Distances to 1.47 Billion Stars in Gaia Early Data Release 3. *The Astronomical Journal*, 161(3):147.

Bailer-Jones, C.A.L., Rybizki, J., Fouesneau, M., et al., 2021. VizieR Online Data Catalog: Distances to 1.47 billion stars in Gaia EDR3 (Bailer-Jones+, 2021). *VizieR Online Data Catalog*, I/352.

Barentsen, G., Farnhill, H.J., Drew, J.E., et al., 2014. The second data release of the INT Photometric Hα Survey of the Northern Galactic Plane (IPHAS DR2). *MNRAS*, 444(4):3230.

Beerer, I.M., Koenig, X.P., Hora, J.L., et al., 2010. A Spitzer View of Star Formation in the Cygnus X North Complex. *ApJ*, 720(1):679.

Benjamin, R.A., Churchwell, E., Babler, B.L., et al., 2003. GLIMPSE. I. An SIRTF Legacy Project to Map the Inner Galaxy. *PASP*, 115(810):953.

Bensby, T., 2013. Characterisation of the Galactic thick disk. *Proceedings of the International Astronomical Union*, 9(S298):17.

Beuther, H., Klessen, R., Dullemond, C., et al., 2014. Protostars and Planets VI. In *Protostars and Planets VI*.

Bonnardeau, M., 2015. AO Psc time keeping. *Information Bulletin on Variable Stars*, 6146:1.

Bonnell, I. and Bastien, P., 1992. A Binary Origin for FU Orionis Stars. *ApJ*, 401:L31.

Borchert, E.M.A., Price, D.J., Pinte, C., et al., 2022. Sustained FU Orionis-type outbursts from colliding discs in stellar flybys. *MNRAS*, 517(3):4436.

Bouvier, J., Alencar, S.H.P., Boutelier, T., et al., 2007a. Magnetospheric accretion-ejection processes in the classical T Tauri star AA Tauri. *A&A*, 463(3):1017.

Bouvier, J., Alencar, S.H.P., Boutelier, T., et al., 2007b. Magnetospheric accretion-ejection processes in the classical T Tauri star AA Tauri. *A&A*, 463(3):1017.

Bouvier, J., Grankin, K., Ellerbroek, L.E., et al., 2013a. AA Tauri's sudden and long-lasting deepening: enhanced extinction by its circumstellar disk. *A&A*, 557:A77.

Bouvier, J., Grankin, K., Ellerbroek, L.E., et al., 2013b. AA Tauri's sudden and long-lasting deepening: enhanced extinction by its circumstellar disk. *A&A*, 557:A77.

Bradley, L., Sipőcz, B., Robitaille, T., et al., 2023. astropy/photutils: 1.8.0.

Bradley, L., Sipőcz, B., Robitaille, T., et al., 2021. astropy/photutils: 1.2.0.

Braithwaite, J. and Spruit, H.C., 2004. A fossil origin for the magnetic field in A stars and white dwarfs. *Nature*, 431(7010):819.

Brown, A.G., Vallenari, A., Prusti, T., et al., 2016. Gaia Data Release 1: Summary of the astrometric, photometric, and survey properties. *Astronomy and Astrophysics*, 595.

Bruch, A., 2021. A comparative study of the strength of flickering in cataclysmic variables. *MNRAS*, 503(1):953.

Buckley, D.A.H., Cropper, M., Ramsay, G., et al., 1998. The new intermediate polar RX J1238-38: a system below the period gap? *MNRAS*, 299(1):83.

Buckley, D.A.H. and Tuohy, I.R., 1989. A Spectroscopic, Photometric, and X-Ray Study of the DQ Herculis System 1H0542-407. *ApJ*, 344:376.

Burwitz, V., Reinsch, K., Beuermann, K., et al., 1996. A new soft intermediate polar: RX J0512.2-3241 in Columba. *A&A*, 310:L25.

Campello, R.J.G.B., Moulavi, D., and Sander, J., 2013. Density-based clustering based on hierarchical density estimates. In J. Pei, V.S. Tseng, L. Cao, H. Motoda, and G. Xu, editors, *Advances in Knowledge Discovery and Data Mining*, pages 160–172. Springer Berlin Heidelberg, Berlin, Heidelberg.

Carey, S.J., Noriega-Crespo, A., Mizuno, D.R., et al., 2009. MIPSGAL: A Survey of the Inner Galactic Plane at 24 and 70 μm. *PASP*, 121(875):76.

Chambers, K.C., Magnier, E.A., Metcalfe, N., et al., 2016. The Pan-STARRS1 Surveys. *arXiv e-prints*, arXiv:1612.05560.

Churchwell, E., Babler, B.L., Meade, M.R., et al., 2009. The Spitzer/GLIMPSE Surveys: A New View of the Milky Way. *PASP*, 121(877):213.

Cieza, L.A., Casassus, S., Tobin, J., et al., 2016. Imaging the water snow-line during a protostellar outburst. *Nature*, 535(7611):258.

Clemens, J.C., Crain, J.A., and Anderson, R., 2004. The Goodman spectrograph. *SPIE*, 5492:331.

Cody, A.M. and Hillenbrand, L.A., 2010. Precision Photometric Monitoring of Very Low Mass σ Orionis Cluster Members: Variability and Rotation at a Few Myr. *ApJ*, 191(2):389.

Connelley, M.S. and Reipurth, B., 2018. A Near-infrared Spectroscopic Survey of FU Orionis Objects. *The Astrophysical Journal*, 861:145.

Contreras Peña, C., Lucas, P.W., Froebrich, D., et al., 2014a. Extreme infrared variables from UKIDSS - I. A concentration in star-forming regions. *MNRAS*, 439(2):1829.

Contreras Peña, C., Lucas, P.W., Froebrich, D., et al., 2014b. Extreme infrared variables from UKIDSS - I. A concentration in star-forming regions. *MNRAS*, 439(2):1829.

Contreras Peña, C., Lucas, P.W., Minniti, D., et al., 2017. A population of eruptive variable protostars in VVV. *MNRAS*, 465(3):3011.

Contreras Peña, C.E., 2015. *Extreme Variables in Star Forming Regions*. Ph.D. thesis, University of Hertfordshire, UK.

Contreras Peña, C., Lucas, P.W., Kurtev, R., et al., 2017. Infrared spectroscopy of eruptive variable protostars from VVV. *Monthly Notices of the Royal Astronomical Society*, 465(3):3039.

Contreras Peña, C., Johnstone, D., Baek, G., et al., 2020. The relationship between mid-infrared and sub-millimetre variability of deeply embedded protostars. *Monthly Notices of the Royal Astronomical Society*, 495(4):3614.

Covey, K.R., Larson, K.A., Herczeg, G.J., et al., 2021. A Differential Measurement of Circumstellar Extinction for AA Tau's 2011 Dimming Event. *AJ*, 161(2):61.

Cuello, N., Ménard, F., and Price, D.J., 2023. Close encounters: How stellar flybys shape planet-forming discs. *European Physical Journal Plus*, 138(1):11.

De Beck, E., Decin, L., de Koter, A., et al., 2010. Probing the mass-loss history of AGB and red supergiant stars from CO rotational line profiles. II. CO line survey of evolved stars: derivation of mass-loss rate formulae. *A&A*, 523:A18.

Dekany, R., Smith, R.M., Riddle, R., et al., 2020. The Zwicky Transient Facility: Observing System. *PASP*, 132(1009):038001.

Dong, R., Liu, H.B., Cuello, N., et al., 2022. A likely flyby of binary protostar Z CMa caught in action. *Nature Astronomy*, 6:331.

Drew, J.E., Gonzalez-Solares, E., Greimel, R., et al., 2014a. The VST Photometric Hα Survey of the Southern Galactic Plane and Bulge (VPHAS+). *MNRAS*, 440(3):2036.

Drew, J.E., Gonzalez-Solares, E., Greimel, R., et al., 2014b. The VST Photometric Hα Survey of the Southern Galactic Plane and Bulge (VPHAS+). *MNRAS*, 440(3):2036.

Drew, J.E., Greimel, R., Irwin, M.J., et al., 2005. The INT Photometric Hα Survey of the Northern Galactic Plane (IPHAS). *MNRAS*, 362(3):753.

Drew, J.E., Greimel, R., Irwin, M.J., et al., 2005. The INT Photometric H Survey of the Northern Galactic Plane (IPHAS). *Monthly Notices of the Royal Astronomical Society*, 362(3):753.

Evans, P.A., Beardmore, A.P., Page, K.L., et al., 2009. Methods and results of an automatic analysis of a complete sample of Swift-XRT observations of GRBs. *MNRAS*, 397(3):1177.

Evans, P.A., Hellier, C., and Ramsay, G., 2006. XMM-Newton observations of the complex spin pulse of the intermediate polar PQ Geminorum. *MNRAS*, 369(3):1229.

Evans, P.A., Osborne, J.P., Beardmore, A.P., et al., 2014. 1SXPS: A Deep Swift X-Ray Telescope Point Source Catalog with Light Curves and Spectra. *ApJ*, 210(1):8.

Evans, P.A., Page, K.L., Osborne, J.P., et al., 2020. 2SXPS: An Improved and Expanded Swift X-Ray Telescope Point-source Catalog. *ApJ*, 247(2):54.

Feast, M.W., Glass, I.S., Whitelock, P.A., et al., 1989. A period-luminosity-colour relation for Mira variables. *MNRAS*, 241:375.

Fehér, O., Kóspál, Á., Ábrahám, P., et al., 2017. Interferometric view of the circumstellar envelopes of northern FU Orionis-type stars. *A&A*, 607:A39.

Fischer, W.J., Hillenbrand, L.A., Herczeg, G.J., et al., 2022. Accretion Variability as a Guide to Stellar Mass Assembly. *arXiv e-prints*, arXiv:2203.11257.

Fischer, W.J., Megeath, S.T., Furlan, E., et al., 2017. The Herschel Orion Protostar Survey: Luminosity and Envelope Evolution. *ApJ*, 840(2):69.

Flewelling, H., 2017. Pan-STARRS Data Release 1. In *American Astronomical Society Meeting Abstracts #229*, volume 229 of *American Astronomical Society Meeting Abstracts*, page 237.07.

Forbes, D., 2000. The Serpens OB2 Association and Its Thermal “Chimney”. *AJ*, 120(5):2594.

Gaia Collaboration, Brown, A.G.A., Vallenari, A., et al., 2018a. Gaia Data Release 2. Summary of the contents and survey properties. *A&A*, 616:A1.

Gaia Collaboration, Brown, A.G.A., Vallenari, A., et al., 2018b. Gaia Data Release 2. Summary of the contents and survey properties.

Gaia Collaboration, Brown, A.G.A., Vallenari, A., et al., 2021. Gaia Early Data Release 3. Summary of the contents and survey properties. *A&A*, 649:A1.

Gaia Collaboration, Prusti, T., de Bruijne, J.H.J., et al., 2016a. The Gaia mission. *A&A*, 595:A1.

Gaia Collaboration, Prusti, T., de Bruijne, J.H.J., et al., 2016b. The Gaia mission. *A&A*, 595:A1.

Graham, M.J., Drake, A.J., Djorgovski, S.G., et al., 2013. Using conditional entropy to identify periodicity. *MNRAS*, 434(3):2629.

Green, G.M., Schlafly, E., Zucker, C., et al., 2019. A 3D Dust Map Based on Gaia, Pan-STARRS 1, and 2MASS. *ApJ*, 887(1):93.

Green, J.D., Evans, N.J., Ágnes Kóspál, et al., 2013. An analysis of the environments of fu orionis objects with herschel*. *The Astrophysical Journal*, 772(2):117.

Greene, T.P., Barsony, M., and Weintraub, D.A., 2010. Near-IR H_2 Emission of Protostars: Probing Circumstellar Environments. *ApJ*, 725(1):1100.

Greene, T.P. and Lada, C.J., 1996. Near-Infrared Spectra and the Evolutionary Status of Young Stellar Objects: Results of a 1.1-2.4 (??) Survey. *AJ*, 112:2184.

Greene, T.P., Wilking, B.A., Andre, P., et al., 1994. Further Mid-Infrared Study of the rho Ophiuchi Cloud Young Stellar Population: Luminosities and Masses of Pre–Main-Sequence Stars. *ApJ*, 434:614.

Groot, P.J., Verbeek, K., Greimel, R., et al., 2009. The UV-Excess survey of the northern Galactic plane. *MNRAS*, 399(1):323.

Guo, Z., Lucas, P.W., Contreras Peña, C., et al., 2020. Short- and long-term near-infrared spectroscopic variability of eruptive protostars from VVV. *MNRAS*, 492(1):294.

Guo, Z., Lucas, P.W., Contreras Peña, C., et al., 2021. Analysis of physical processes in eruptive YSOs with near-infrared spectra and multiwavelength light curves. *MNRAS*, 504(1):830.

Guo, Z., Lucas, P.W., Smith, L.C., et al., 2022. Large-amplitude periodic outbursts and long-period variables in the VVV VIRAC2-β data base. *MNRAS*, 513(1):1015.

Gutermuth, R.A. and Heyer, M., 2015. A 24 μm Point Source Catalog of the Galactic Plane from Spitzer/MIPSGAL. *AJ*, 149(2):64.

Hailey, C.J., Mori, K., Perez, K., et al., 2016. Evidence for Intermediate Polars as the Origin of the Galactic Center Hard X-ray Emission. *ApJ*, 826(2):160.

Hartmann, L., Herczeg, G., and Calvet, N., 2016. Accretion onto Pre-Main-Sequence Stars. *Annual Review of Astronomy and Astrophysics*, 54(1):135.

Hellier, C., 1993. The four periodicities of the cataclysmic variable TV Columbae. *MNRAS*, 264:132.

Hellier, C., 1997. Spectroscopy of the intermediate polars BG Canis Minoris and PQ Geminorum. *MNRAS*, 288(4):817.

Hellier, C. and Beardmore, A.P., 2002. The accretion flow in the discless intermediate polar V2400 Ophiuchi. *MNRAS*, 331(2):407.

Herbig, G.H., ???? THE SPECTRA OF Be-AND Ae-TYPE STARS ASSO-CIATED WITH NEBULOSITY*. Technical report.

Herbig, G.H., 1977. ERUPTIVE PHENOMENA IN EARLY STELLAR EVOLUTION*! Technical report.

Herbig, G.H., 1989. European Southern Observatory Conference and Workshop Proceedings. In *European Southern Observatory Conference and Workshop Proceedings*.

Hillenbrand, L.A., 1997. On the Stellar Population and Star-Forming History of the Orion Nebula Cluster. *AJ*, 113:1733.

Hillenbrand, L.A., Contreras Peña, C., Morrell, S., et al., 2018. Gaia 17bpi: An FU Ori-type Outburst. *ApJ*, 869(2):146.

Hillenbrand, L.A., De, K., Hankins, M., et al., 2021. Outbursting Young Stellar Object PGIR 20dci in the Perseus Arm. *AJ*, 161(5):220.

Hillenbrand, L.A., Isaacson, H., Rodriguez, A.C., et al., 2022. LkHα 225 (V1318 Cyg) South in Outburst. *AJ*, 163(3):115.

Hilton, E.J., Szkody, P., Mukadam, A., et al., 2009. XMM-Newton and Optical Observations of Cataclysmic Variables from the Sloan Digital Sky Survey. *AJ*, 137(3):3606.

Hodapp, K.W., Denneau, L., Tucker, M., et al., 2020. The Outburst of the Young Star Gaia19bey. *AJ*, 160(4):164.

Höfner, S. and Olofsson, H., 2018. Mass loss of stars on the asymptotic giant branch. Mechanisms, models and measurements. , 26(1):1.

Hora, J., Bontemps, S., Megeath, T., et al., 2007. A Spitzer Legacy Survey of the Cygnus-X Complex. Spitzer Proposal ID #40184.

Iben, I., J. and Renzini, A., 1983. Asymptotic giant branch evolution and beyond. *Annual Review of Astronomy and Astrophysics*, 21:271.

Ishihara, D., Kaneda, H., Onaka, T., et al., 2011a. Galactic distributions of carbon- and oxygen-rich AGB stars revealed by the AKARI mid-infrared all-sky survey. *A&A*, 534:A79.

Ishihara, D., Kaneda, H., Onaka, T., et al., 2011b. Galactic distributions of carbon- and oxygen-rich AGB stars revealed by the AKARI mid-infrared all-sky survey. *A&A*, 534:A79.

Ishihara, D., Onaka, T., Kataza, H., et al., 2010. The AKARI/IRC Mid-Infrared All-Sky Survey. Technical report.

Ivanova, N., Justham, S., Chen, X., et al., 2012. Common envelope evolution: Where we stand and how we can move forward. *The Astronomy and Astrophysics Review*, 21.

Jiménez-Esteban, F.M. and Engels, D., 2015. Study of extremely reddened AGB stars in the Galactic bulge. *A&A*, 579:A76.

Joshi, V.H., Ashok, N.M., and Banerjee, D.P.K., 2011. A study of the near-infrared modulation at spin and orbital periods in the intermediate polar WX Pyx. *Bulletin of the Astronomical Society of India*, 39:259.

Joy, A.H., 1945. T Tauri Variable Stars. *The Astrophysical Journal*, 102:168.

Kaluzny, J. and Semeniuk, I., 1988. Photometric Observations of the Intermediate Polar AO Piscium. *Information Bulletin on Variable Stars*, 3145:1.

Karakas, A.I. and Lattanzio, J.C., 2014. The Dawes Review 2: Nucleosynthesis and Stellar Yields of Low- and Intermediate-Mass Single Stars. , 31:e030.

Karambelkar, V.R., Kasliwal, M.M., Tisserand, P., et al., 2021. Census of R Coronae Borealis Stars. I. Infrared Light Curves from Palomar Gattini IR. *ApJ*, 910(2):132.

Kemp, J., Patterson, J., Thorstensen, J.R., et al., 2002. Rapid Oscillations in Cataclysmic Variables. XV. HT Camelopardalis (=RX J0757.0+6306). *PASP*, 114(796):623.

Kenyon, S.J. and Hartmann, L., 1995. Pre-Main-Sequence Evolution in the Taurus-Auriga Molecular Cloud. *ApJ*, 101:117.

Kenyon, S.J., Hartmann, L.W., Strom, K.M., et al., 1990. An IRAS Survey of the Taurus-Auriga Molecular Cloud. *AJ*, 99:869.

Kim, Y.G., Andronov, I.L., Park, S.S., et al., 2005. Orbital and spin variability of the intermediate polar BG CMi. *A&A*, 441(2):663.

Knigge, C., Baraffe, I., and Patterson, J., 2011. THE EVOLUTION OF CATACLYSMIC VARIABLES AS REVEALED BY THEIR DONOR STARS. *The Astrophysical Journal Supplement Series*, 194(48pp):28.

Koenig, X.P. and Leisawitz, D.T., 2014. A CLASSIFICATION SCHEME FOR YOUNG STELLAR OBJECTS USING THE WIDE-FIELD INFRARED SURVEY EXPLORER AllWISE CATALOG: REVEALING LOW-DENSITY STAR FORMATION IN THE OUTER GALAXY. *The Astrophysical Journal*, 791(2):131.

Kóspál, Á., Ábrahám, P., Acosta-Pulido, J.A., et al., 2013a. Exploring the circumstellar environment of the young eruptive star V2492 Cygni. *A&A*, 551:A62.

Kóspál, Á., Ábrahám, P., Acosta-Pulido, J.A., et al., 2013b. Exploring the circumstellar environment of the young eruptive star V2492 Cygni. *A&A*, 551:A62.

Kóspál, Á., Ábrahám, P., Goto, M., et al., 2011. Near-infrared Spectroscopy of EX Lupi in Outburst. *ApJ*, 736(1):72.

Kryukova, E., Megeath, S.T., Gutermuth, R.A., et al., 2012. Luminosity Functions of Spitzer-identified Protostars in Nine Nearby Molecular Clouds. *AJ*, 144(2):31.

Kryukova, E., Megeath, S.T., Hora, J.L., et al., 2014. The Dependence of Protostellar Luminosity on Environment in the Cygnus-X Star-forming Complex. *AJ*, 148(1):11.

Kryukova, E., Megeath, S.T., Hora, J.L., et al., 2014. THE DEPENDENCE OF PROTOSTELLAR LUMINOSITY ON ENVIRONMENT IN THE CYGNUS-X STAR-FORMING COMPLEX. *The Astronomical Journal*, 148(18pp):11.

Kóspál, , Szabó, Z.M., Ábrahám, P., et al., 2020. V346 nor: The post-outburst life of a peculiar young eruptive star. *The Astrophysical Journal*, 889(2):148.

Lacy, M., Baum, S.A., Chandler, C.J., et al., 2020. The Karl G. Jansky Very Large Array Sky Survey (VLASS). Science Case and Survey Design. *PASP*, 132(1009):035001.

Lada, C.J., 1987. Star formation: from OB associations to protostars. In M. Peimbert and J. Jugaku, editors, *Star Forming Regions*, volume 115, page 1.

Lamers, H.J.G.L.M., Zickgraf, F.J., de Winter, D., et al., 1998. An improved classification of B[e]-type stars. *A&A*, 340:117.

Lewis, B.M., 1992. Miras Without Masers are Symbiotic Stars. In H.A. McAlister and W.I. Hartkopf, editors, *IAU Colloq. 135: Complementary Approaches to Double and Multiple Star Research*, volume 32 of *Astronomical Society of the Pacific Conference Series*, page 241.

Littlefield, C., Garnavich, P., Kennedy, M.R., et al., 2020. The Rise and Fall of the King: The Correlation between FO Aquarii's Low States and the White Dwarf's Spin-down. *The Astrophysical Journal*, 896(16pp):116.

Littlefield, C., Scaringi, S., Garnavich, P., et al., 2021. Quasi-periodic Oscillations in the TESS Light Curve of TX Col, a Diskless Intermediate Polar on the Precipice of Forming an Accretion Disk. *The Astronomical Journal*, 162(2):49.

Lomb, N.R., 1976. Least-Squares Frequency Analysis of Unequally Spaced Data. , 39(2):447.

Lorenzetti, D., Antoniucci, S., Giannini, T., et al., 2012. On the nature of exor accretion events: An infrequent manifestation of a common phenomenology?*. *The Astrophysical Journal*, 749(2):188.

Lucas, P.W., Elias, J., Points, S., et al., 2020a. Discovery of a mid-infrared protostellar outburst of exceptional amplitude. *MNRAS*, 499(2):1805.

Lucas, P.W., Hoare, M.G., Longmore, A., et al., 2008. The UKIDSS galactic plane survey. *Monthly Notices of the Royal Astronomical Society*, 391(1):136.

Lucas, P.W., Hoare, M.G., Longmore, A., et al., 2008. The UKIDSS Galactic Plane Survey. *MNRAS*, 391(1):136.

Lucas, P.W., Minniti, D., Kamble, A., et al., 2020b. VVV-WIT-01: highly obscured classical nova or protostellar collision? *MNRAS*, 492(4):4847.

Lucas, P.W., Smith, L.C., Contreras Peña, C., et al., 2017. Extreme infrared variables from UKIDSS - II. An end-of-survey catalogue of eruptive YSOs and unusual stars. *Monthly Notices of the Royal Astronomical Society*, 472(3):2990.

Mainzer, A., Bauer, J., Cutri, R.M., et al., 2014. Initial Performance of the NEOWISE Reactivation Mission. *ApJ*, 792(1):30.

Makin, S.V. and Froebrich, D., 2018. VizieR Online Data Catalog: YSO jets from UWISH2. IV. Cygnus-X outflows (Makin+, 2018). *VizieR Online Data Catalog*, page J/ApJS/234/8.

Manara, C.F., Ansdell, M., Rosotti, G.P., et al., 2022. Demographics of young stars and their protoplanetary disks: lessons learned on disk evolution and its connection to planet formation. *arXiv e-prints*, arXiv:2203.09930.

Masetti, N., Nucita, A.A., and Parisi, P., 2012. Optical identification of X-ray source 1RXS J180431.1-273932 as a magnetic cataclysmic variable. *A&A*, 544:A114.

Mateo, M., Szkody, P., and Garnavich, P., 1991. Near-Infrared Time-resolved Spectroscopy of the Cataclysmic Variable YY Draconis. *ApJ*, 370:370.

Matsunaga, N., Menzies, J.W., Feast, M.W., et al., 2017. Discovery of carbon-rich Miras in the Galactic bulge. Technical report.

Mayne, N.J. and Naylor, T., 2008. Fitting the young main-sequence: distances, ages and age spreads. *MNRAS*, 386(1):261.

McInnes, L., Healy, J., and Melville, J., 2018. UMAP: Uniform Manifold Approximation and Projection for Dimension Reduction. *arXiv e-prints*, arXiv:1802.03426.

Meisner, A.M., Caselden, D., Schlafly, E.F., et al., 2023. unTimely: a Full-sky, Time-domain unWISE Catalog. *AJ*, 165(2):36.

Merrill, P.W. and Humason, M.L., 1932. A Bright Line of Ionized Helium, λ4686, in Three Stellar Spectra with Titanium Bands. *PASP*, 44(257):56.

Minniti, D., Lucas, P., Emerson, J., et al., 2010. VISTA Variables in the Via Lactea (VVV): The public ESO near-IR variability survey of the Milky Way. *New Astronomy*, 15(5):433.

Minniti, D., Saito, R.K., Alonso-García, J., et al., 2011. The Edge of the Milky Way Stellar Disk Revealed Using Clump Giant Stars as Distance Indicators. *ApJ*, 733(2):L43.

Miroshnichenko, A.S., Gray, R.O., Bjorkman, K.S., et al., 2008. Infrared Spectroscopy of Galactic FS CMa Stars with the Spitzer Space Telescope. In *American Astronomical Society Meeting Abstracts #212*, volume 212 of *American Astronomical Society Meeting Abstracts*, page 9.01.

Miroshnichenko, A.S. and Zharikov, S.V., 2015. FS CMa Type Binaries. In *EAS Publications Series*, volume 71-72 of *EAS Publications Series*, pages 181–186.

Molnar, T.A., Sanders, J.L., Smith, L.C., et al., 2022. VizieR Online Data Catalog: VIVACE, VIrac VAriable Classification Ensemble (Molnar+, 2022). *VizieR Online Data Catalog*, J/MNRAS/509/2566.

Monguió, M., Greimel, R., Drew, J.E., et al., 2020. IGAPS: the merged IPHAS and UVEX optical surveys of the northern Galactic plane. *A&A*, 638:A18.

Morales-Calderón, M., Stauffer, J.R., Hillenbrand, L.A., et al., 2011a. Ysovar: The First Sensitive, Wide-area, Mid-infrared Photometric Monitoring of the Orion Nebula Cluster. *ApJ*, 733(1):50.

Morales-Calderón, M., Stauffer, J.R., Hillenbrand, L.A., et al., 2011b. Ysovar: The First Sensitive, Wide-area, Mid-infrared Photometric Monitoring of the Orion Nebula Cluster. *ApJ*, 733(1):50.

Morris, C., Maccarone, T.J., Lucas, P.W., et al., 2022. UGPS J194310+183851: an unusual optical and X-ray faint cataclysmic variable? *MNRAS*, 514(4):6002.

Munari, U., 2019. The Symbiotic Stars. *arXiv e-prints*, arXiv:1909.01389.

Norton, A.J., Butters, O.W., Parker, T.L., et al., 2008. The Accretion Flows and Evolution of Magnetic Cataclysmic Variables. *ApJ*, 672(1):524.

Norton, A.J., Quaintrell, H., Katajainen, S., et al., 2002. Pulsations and orbital modulation of the intermediate polar 1WGA J1958.2+3232. *A&A*, 384:195.

Norton, A.J., Wynn, G.A., and Somerscales, R.V., 2004. The Spin Periods and Magnetic Moments of White Dwarfs in Magnetic Cataclysmic Variables. *ApJ*, 614(1):349.

Offner, S.S.R. and McKee, C.F., 2011. The Protostellar Luminosity Function. *ApJ*, 736(1):53.

Oliveira, A.S., Rodrigues, C.V., Cieslinski, D., et al., 2017. Exploratory Spectroscopy of Magnetic Cataclysmic Variables Candidates and Other Variable Objects *. *The Astronomical Journal*, 153:144.

Oliveira, J., van Loon, J., Sewiło, M., et al., 2019. Herschel spectroscopy of Massive Young Stellar Objects in the Magellanic Clouds . Technical report.

Oudmaijer, R. and Miroshnickenko, A., 2017. Introduction to the B[e] Phenomenon. In *ASP Conference Series*.

Oudmaijer, R.D., Waters, L.B.F.M., van der Veen, W.E.C.J., et al., 1995. Near-infrared spectroscopy of post-AGB stars. *A&A*, 299:69.

Pecaut, M.J. and Mamajek, E.E., 2013. Intrinsic Colors, Temperatures, and Bolometric Corrections of Pre-main-sequence Stars. *ApJ*, 208(1):9.

Pérez, S., Hales, A., Liu, H.B., et al., 2020. Resolving the FU Orionis System with ALMA: Interacting Twin Disks? *ApJ*, 889(1):59.

Predehl, P., Andritschke, R., Arefiev, V., et al., 2021. The eROSITA X-ray telescope on SRG. *A&A*, 647:A1.

Pretorius, M.L., 2009. Time-resolved optical observations of five cataclysmic variables detected by INTEGRAL. *MNRAS*, 395(1):386.

Pretorius, M.L., Knigge, C., Schwope, A.D., et al., 2013. The space density of magnetic cataclysmic variables. *MNRAS*, 432(1):570.

Pretorius, M.L. and Mukai, K., 2014. Constraints on the space density of intermediate polars from the Swift-BAT survey. *MNRAS*, 442(3):2580.

Raddi, R., Drew, J.E., Fabregat, J., et al., 2018. First results of an Hα based search of classical Be stars in the Perseus Arm and beyond. Technical report.

Raman, V.V. and Anandarao, B.G., 2008. Infrared spectroscopic study of a selection of AGB and post-AGB stars. *Monthly Notices of the Royal Astronomical Society*, 385(2):1076.

Rappaport, S., Joss, P.C., and Webbink, R.F., 1982. The evolution of highly compact binary stellar systems. *ApJ*, 254:616.

Rappaport, S., Verbunt, F., and Joss, P.C., 1983. A new technique for calculations of binary stellar evolution application to magnetic braking. *ApJ*, 275:713.

Rebull, L.M., Cody, A.M., Covey, K.R., et al., 2014. Young stellar object variability (ysovar): Long timescale variations in the mid-infrared. *The Astronomical Journal*, 148(5):92.

Rice, T.S., Reipurth, B., Wolk, S.J., et al., 2015. Near-infrared Variability in the Orion Nebula Cluster. *AJ*, 150(4):132.

Rieke, G.H., Young, E.T., Engelbracht, C.W., et al., 2004. The Multiband Imaging Photometer for Spitzer (MIPS). *ApJ*, 154(1):25.

Rivinius, T., Carciofi, A.C., and Martayan, C., 2013. Classical Be stars. Rapidly rotating B stars with viscous Keplerian decretion disks. , 21:69.

Robitaille, T.P., Meade, M.R., Babler, B.L., et al., 2008. INTRINSICALLY RED SOURCES OBSERVED BY SPITZER IN THE GALACTIC MIDPLANE. *The Astronomical Journal*, 136(6):2413.

Rodríguez-Gil, P., Gänsicke, B.T., Araujo-Betancor, S., et al., 2004. DW Cancri: a magnetic VY Scl star with an orbital period of 86 min. *Monthly Notices of the Royal Astronomical Society*, 349(1):367.

Samus, N.N., Kazarovets, E.V., Kireeva, N.N., et al., 2010. General Catalogue of Variable Stars: Current Status and New Name-Lists. *Odessa Astronomical Publications*, 23:102.

Sazonov, S., Revnivtsev, M., Burenin, R., et al., 2008. Discovery of heavily-obscured AGN among seven INTEGRAL hard X-ray sources observed by Chandra. *A&A*, 487(2):509.

Scargle, J.D., 1982. Studies in astronomical time series analysis. II. Statistical aspects of spectral analysis of unevenly spaced data. *ApJ*, 263:835.

Scholz, A., Froebrich, D., and Wood, K., 2013. A systematic survey for eruptive young stellar objects using mid-infrared photometry. *MNRAS*, 430(4):2910.

Schönrich, R., Binney, J., and Dehnen, W., 2010. Local kinematics and the local standard of rest. *MNRAS*, 403(4):1829.

Schreiber, M.R., Belloni, D., Gänsicke, B.T., et al., 2021. The origin and evolution of magnetic white dwarfs in close binary stars. *Nature Astronomy 2021 5:7*, 5(7):648.

Seaquist, E.R. and Ivison, R.J., 1994. A search for symbiotic behaviour amongst OH/IR colour mimics. *MNRAS*, 269:512.

Shu, F., Najita, J., Ostriker, E., et al., 1994. Magnetocentrifugally Driven Flows from Young Stars and Disks. I. A Generalized Model. *ApJ*, 429:781.

Shu, F.H., Adams, F.C., and Lizano, S., 1987. Star formation in molecular clouds: observation and theory. *Annual Review of Astronomy and Astrophysics*, 25:23.

Silber, A.D., 1992. Phd thesis. *PhD Thesis, MIT*.

Sipos, N., Ábrahám, P., Acosta-Pulido, J., et al., 2009. EX Lupi in quiescence. *A&A*, 507(2):881.

Skrutskie, M.F., Cutri, R.M., Stiening, R., et al., 2006a. The Two Micron All Sky Survey (2MASS). *AJ*, 131(2):1163.

Skrutskie, M.F., Cutri, R.M., Stiening, R., et al., 2006b. The Two Micron All Sky Survey (2MASS). *AJ*, 131(2):1163.

Smith, L.C., Lucas, P.W., Kurtev, R., et al., 2018. VIRAC: the VVV Infrared Astrometric Catalogue. *MNRAS*, 474(2):1826.

Southworth, J., Gänsicke, B.T., Marsh, T.R., et al., 2007. SDSSJ233325.92+152222.1 and the evolution of intermediate polars. *MNRAS*, 378(2):635.

Staude, A., Schwope, A.D., Krumpe, M., et al., 2003. 1RXS J062518.2+733433: A bright, soft intermediate polar. *A&A*, 406:253.

Stellingwerf, R.F., 1978. Period determination using phase dispersion minimization. *ApJ*, 224:953.

Stetson, P.B., 1996. On the Automatic Determination of Light-Curve Parameters for Cepheid Variables. *PASP*, 108:851.

Szkody, P., Henden, A., Fraser, O.J., et al., 2005. Cataclysmic Variables from Sloan Digital Sky Survey. IV. The Fourth Year (2003). *AJ*, 129(5):2386.

Tody, D., 1986. The IRAF Data Reduction and Analysis System. In D.L. Crawford, editor, *Instrumentation in astronomy VI*, volume 627 of *Society of Photo-Optical Instrumentation Engineers (SPIE) Conference Series*, page 733.

UKIDSS Consortium, 2012. VizieR Online Data Catalog: UKIDSS-DR6 Galactic Plane Survey (Lucas+ 2012). *VizieR Online Data Catalog*, II/316.

Vassiliadis, E. and Wood, P.R., 1993. Evolution of Low- and Intermediate-Mass Stars to the End of the Asymptotic Giant Branch with Mass Loss. *ApJ*, 413:641.

Virtanen, P., Gommers, R., Oliphant, T.E., et al., 2020. SciPy 1.0: Fundamental Algorithms for Scientific Computing in Python. *Nature Methods*, 17:261.

Voges, W., Aschenbach, B., Boller, T., et al., 1999a. The ROSAT all-sky survey bright source catalogue. *A&A*, 349:389.

Voges, W., Aschenbach, B., Boller, T., et al., 1999b. The ROSAT all-sky survey bright source catalogue. *A&A*, 349:389.

Vollmann, K. and Eversberg, T., 2006. Remarks on statistical errors in equivalent widths. 327(9):789.

von Neumann, J., 1941. Distribution of the Ratio of the Mean Square Successive Difference to the Variance. *The Annals of Mathematical Statistics*, 12(4):367 .

Wang, S. and Chen, X., 2019. The Optical to Mid-infrared Extinction Law Based on the APOGEE, Gaia DR2, Pan-STARRS1, SDSS, APASS, 2MASS, and WISE Surveys. *ApJ*, 877(2):116.

Warner, B., 1995. *Cataclysmic Variable Stars*. Cambridge Astrophysics. Cambridge University Press.

Webbink, R.F. and Wickramasinghe, D.T., 2002. Cataclysmic variable evolution: AM Her binaries and the period gap. *MNRAS*, 335(1):1.

Wenger, T.V., Balser, D.S., Anderson, L.D., et al., 2018. Kinematic Distances: A Monte Carlo Method. *The Astrophysical Journal*, 856(1):52.

Whitelock, P., 1988. INFRARED OBSERVATIONS OF SYMBIOTIC MIRAS.

Whitelock, P.A., 2003. A Comparison of Symbiotic and Normal Miras (invited review talks). In R.L.M. Corradi, J. Mikolajewska, and T.J. Mahoney, editors, *Symbiotic Stars Probing Stellar Evolution*, volume 303 of *Astronomical Society of the Pacific Conference Series*, page 41.

Whitelock, P.A., Feast, M.W., and Van Leeuwen, F., 2008. AGB variables and the Mira period–luminosity relation. *Monthly Notices of the Royal Astronomical Society*, 386(1):313.

Whitney, B., Benjamin, R., Meade, M., et al., 2011. Glimpse360: Observing The Outback Of The Galaxy. In *American Astronomical Society Meeting Abstracts #217*, volume 217 of *American Astronomical Society Meeting Abstracts*, page 241.16.

Wilking, B.A., 1989. The Formation of Low-Mass Stars. *PASP*, 101:229.

Wilson, W.J. and Barrett, A.H., 1971. . Conference on late Type Stars, Kitt Peak, Arizona.

Wood, P.R., 1982. . volume 103 of *IAU Symposium on Planetary Nebulae*.

Woudt, P.A. and Warner, B., 2003. RX J1039.7-0507: a new intermediate polar and probable recent nova, possessing a large reflection effect. *MNRAS*, 339(3):731.

Woudt, P.A., Warner, B., Gulbis, A., et al., 2012. CC Sculptoris: a superhumping intermediate polar. *MNRAS*, 427(2):1004.

Wright, E.L., Eisenhardt, P.R.M., Mainzer, A.K., et al., 2010. The Wide-field Infrared Survey Explorer (WISE): Mission Description and Initial On-orbit Performance. *AJ*, 140(6):1868.